Study of metal- and metalloid-bearing nanoparticles in shallow hydrothermal systems

Vicente María Durán Toro

This doctoral thesis project was performed in the Hydrothermal Geomicrobiology group of MARUM research institute between March 2016 and January 2020.

Study of metal- or metalloid-bearing nanoparticles in shallow hydrothermal systems

Author: Vicente María Durán Toro

This dissertation is submitted to obtain a doctoral degree from the Faculty of Geosciences of The University of Bremen in Germany.

Dissertation zur Erlangung des Doktorgrades der Naturwissenschaften (Dr. rer. nat.) am Fachbereich Geowissenschafen.

Contact: vduran-toro@marum.de

Reviewer 1: Dr. Solveig I. Bühring (MARUM – University of Bremen, Germany)

Reviewer 2: Associate Professor, Dr. Eoghan P. Reeves (University of Bergen, Norway)

Doctoral Colloquium: May 11th, 2020

TABLE OF CONTENTS

Abstract

Nanomaterials are structures with at least one of their dimensions in the nanometer scale, conventionally between 1 and 100 nm. The size confinement effect of materials can generate unique physical properties i.e. higher solubility, acute antimicrobial effects, UV-VIS absorbance etc. Nanomaterials can naturally occur in the environment, for instance, hydrothermal systems have been described as a source of amorphous metal (Fe, Cu, Zn) bearing nanoparticles to the ocean. Elements with detrimental effects, like arsenic (As), are also enriched in hydrothermal fluids, yet, As bearing nanoparticles have not been considered. The aim of this doctoral dissertation is to identify and characterize As based nanomaterials present in a hydrothermal system (Chapter 3), evaluate environmental parameters controlling the formation and stability of the colloids (Chapter 4) and the possible toxic implications of the material to the marine microbial communities (Chapter 5).

The study site corresponds to the island of Milos (Greece), where the shallow hydrothermal systems with hot fluids rich in As represent an ideal environment to understand the formation, stability and toxicity of As based colloidal material under a gradient of parameters (temperature, pH or organic matter: OM). Hydrothermal fluids, porewater and seawater collected (Paleochori and Spathi bay, Milos) showed a significant percentage of As in the size fraction between 200 and 20 nm, suggesting the presence of As bearing nanoparticles. Further characterizations, revealed the presence of nanospheres with a size diameter distribution between 250 and 50 nm, an elemental composition rich in As, S and O; and the absence of a crystal phase, which classifies it as an amorphous material. The particles where observed in samples with the highest As content, elevated temperatures and the lowest pH values, suggesting a critical role of environmental parameters in the formation and stability of the colloids. Therefore, synthesis of As colloidal particles was evaluated under environmental hydrothermal conditions. The results indicated precipitation of amorphous As and S rich nanospheres as a natural phenomenon occurring in marine environments at low pH. During As and S precipitation, temperature and OM (thiol rich additives; cysteine and glutathione) can dictate the morphology, size and As content of the particles. At high temperatures and in the absence of additives, the morphology, size and As content of the material highly resemble the particles described in the hydrothermal system off Milos. The results indicate the formation of colloids being favored within the first 24 hours of incubation at high temperatures and with a distinctive S and As ratio, confirming hydrothermal systems as a source of As bearing nanoparticles to the ocean. However, stability of the material was further evaluated, establishing a total dissolution of the particles at high temperature after 72 hours. No dissolution was observed when temperatures of incubation where below 75°C, suggesting stabilization of the material once mixed with seawater.

The toxicity of synthetic As bearing nanoparticles was evaluated in marine bacterial cultures (*Shewanella oneidensis* MR1). A decrease in cell density and growth rate after cultivation with the colloids was observed. Furthermore, the bacteriostatic effect, was characterized by variations of intact polar lipids, specifically, changes in abundance of aminolipids and aminophospholipids. When compared to soluble forms of As, the bacteriostatic and the lipid response found within treatments of dissolved As^{+3} species was very similar to those observed with the nanoparticles. The outcomes suggest the release of dissolved As^{+3} species from the colloidal structure as a mechanism of toxicity.

In conclusion, this thesis reveals the existence of amorphous arsenic bearing nanoparticles in a hydrothermal system. The formation and stability of the colloids strictly depends on environmental parameters like pH, temperature and organic matter (additives rich in -SH groups), and finally, this study suggests a bacteriostatic effect of the nanoparticles, characterized by changes in aminolipids and aminophosholipid abundance. The results and discussions highlight the importance of a deeper understanding in colloidal chemistry of harmful elements, like As, present in hydrothermal fluids (e.g., Hg, Sb). A greater comprehension of nanomaterial behavior in the ocean will further contribute in the conservation of the marine ecosystems.

Keywords

Marine hydrothermal systems
Arsenic nanoparticles
Arsenic colloidal particles
Milos
Arsenic

Zusammenfassung

Nanomaterialen sind Strukturen, deren Größenordnung in mindestens einer ihrer Dimensionen im Nanometerbereich, üblicherweise zwischen 1 und 100 nm, liegt. Durch die Größe der Materialien können sich einzigartige physikalische Eigenschaften entwickeln, ~~so~~wie höhere Löslichkeit, akute anti-mikrobielle Effekte, Absorption von US-VIS Strahlung und andere. Nanomaterialien können natürlich in der Umwelt vorkommen, zum Beispiel hydrothermale Systeme wurden als ozeanische Quelle für amorphe, metall (Fe, Cu, Zn)-haltige Nanopartikel beschrieben. Elemente mit schädlicher Wirkung, wie Arsen (As) sind ebenfalls angereichert in hydrothermalen Fluiden, dennoch wurden arsenhaltige Nanopartikel bisher nicht beobachtet. Das Ziel dieser Doktorarbeit ist es arsenhaltige Nanomaterialien eines hydrothermalen Systems zu identifizieren und zu charakterisieren (Kapitel 3) sowie Umweltfaktoren zu indentifizieren, welche die Bildung und Stabilität der Kolloide kontrollieren (Kapitel 4) und mögliche toxische Auswirkungen des Materials auf die marine mikrobielle Gemeinschaft (Kapitel 5), zu bewerten.

Das Untersuchungsgebiet ist die Insel Milos (Griechenland), welche dank Flachwasser-Hydrothermalsystemen mit heißen Fluiden, reich an As, ideale Rahmenbedingungen bietet, um die Bildung, Stabilität und Toxizität von As-basierten kolloidalen Materialien entlang eines Gradienten verschiedenster Parameter (Temperatur, pH-Wert, Organisches Material: OM), zu verstehen. Proben hydrothermaler Fluide, von Porenwässern und Meerwasser (Paleochori and Spathi bay, Milos), zeigten einen signifikanten prozentualen Anteil an As in der Größenfraktion zwischen 200 und 20 nm, was das Vorliegen von As-Nanopartikeln vermuten lässt. Weiterführende Charakterisierung zeigte die Präsenz von Nanosphären mit einer Durchmesserverteilung zwischen 250 und 50 nm, einer elementaren Zusammensetzung reich in As, S und O; und das Fehlen einer kristallinen Phase, die sie als amorphes Material klassifiziert. Die Partikel wurden beobachtet in Proben mit höchsten As-Gehalten, bei erhöhter Temperatur und niedrigstem pH-Wert, was eine entscheidende Rolle von Umweltparametern für die Entstehung und Stabilität der Kolloide vermuten lässt. Daher, wurde die Synthese von kolloidalen As-Partikeln unter hydrothermalen Bedingungen untersucht. Die Ergebnisse deuten auf eine Präzipitation von amorphen As- und S-reichen Nanosphären als natürlich vorkommendes Phänomen hin, welches in der Meeresumwelt bei niedrigem pH-Wert vorkommt. Während der Ausfällung von As und S, können Temperatur und OM-Gehalt (thiol-reiche Zusatzstoffe, Cystein und Glutathionin), über Morphologie, Größe und den As-Gehalt der Partikel bestimmen. Bei hohen Temperaturen und ohne Zusatzstoffe, gleichen die Morphologie, Größe und der As-Gehalt des Materials stark den im Hydrothermalsystem vor Milos beschriebenen Partikeln. Die Ergebnisse zeigen eine bevorzugte Bildung der Kolloide innerhalb der ersten 24 Stunden der Inkubation bei hohen Temperaturen und mit markantem Verhältnis von S zu As, was hydrothermale Systeme als ozeanische Quelle für As-haltige Nanopartikel bestätigt. Allerdings wurde, nach weitergehender Untersuchung der Stabilität des Materials, eine komplette Auflösung der Partikel nach 72 Stunden bei hohen Temperaturen, festgestellt. Keine Zersetzung war zu beobachten, bei Inkubationstemperaturen unter 75°C, was eine Stabilisierung des Materials nach der Durchmischung der Fluide mit Seewasser nahelegt.

Die Toxizität der synthetisierten As-haltigen Nanopartikel wurde bewertet in einer marinen Bakterienkultur (*Shewanella oneidensis* MR1). Eine Abnahme der Zelldichte und der Wachstumsrate nach Kultivierung mit den Kolloiden war zu beobachten. Desweiteren wurde der bakteriostatische Effekt charakterisiert anhand der Variation der intakten polaren Membranlipide, insbesondere, anhand der Veränderungen in der Abundanz von Aminolipiden und Aminophospholipiden. Im Vergleich mit löslichen Formen von As, war der bakteriostatische Effekt und die Anpassung der Lipide in den Experimenten mit gelöstem As^{3+} Formen, und mit Nanopartikeln sehr ähnlich. Die Resultate zeigen eine mögliche Freisetzung von gelöstem As^{3+} aus den kolloidalen Strukturen als Mechanismus der Toxizität.

Zusammenfassend zeigt diese Arbeit erstmalig die Existenz amorpher arsenhaltiger Nanopartikel in hydrothermalen Systemen. Die Entstehung und Stabilität der Kolloide ist streng abhängig von Umweltparametern, wie pH-Wert, Temperatur und organischem Material (Zusatzstoffe reich an -SH-Gruppen) und diese Studie zeigt einen bakteriostatischen Effekt der Nanopartikel, welcher charakterisiert werden kann anhand der Veränderungen in der Menge an Aminolipiden und Aminophospholipiden. Die Ergebnisse und deren Diskussionen beleuchten die Relevanz eines vertieften Verständnisses der Kolloidchemie schädlicher Elemente, wie As oder anderer hydrothermal verfügbarer Elemente (z.B. Hg, Sb). Ein erweitertes Verständnis über das Verhalten von Nanomaterialien im Ozean wird außerdem dazu beitragen, unsere Meeresumwelt und deren Ökosysteme zu schützen und zu erhalten.

Schlüsselbegriffe

Marine hydrothermale Systeme
Arsen-Nanopartikel
Arsen-Kolloidpartikel
Milos
Arsen

List of Manuscripts and Contributions of Authors

Manuscript #1 – Chapter 3

Amorphous arsenic sulfide nanoparticles in a shallow water hydrothermal system

V.M. Durán-Toro*, R.E. Price, M. Maas, C.-C. Brombach, T. Pichler, K. Rezwan, S.I. Bühring.

V.M.D.T, M.M., K.R. and S.I.B. designed the research, R.E.P. and T.P. carried out field sampling. V.M.D.T and C.C.B. performed laboratory work. V.M.D.T analyzed the data with the help from R.E.P., M.M., T.P., K.R. and S.I.B; V.M.D.T wrote the manuscript with input from all co-authors. *, corresponding author.

Published in Feb., 2019. Journal Marine Chemistry
(https://doi.org/10.1016/j.marchem.2019.03.008)

Manuscript #2 – Chapter 4

Synthesis of As and S colloidal particles under environmental hydrothermal conditions

V. Duran-Toro,*, K. Rezwan, S.I. Bühring & M. Maas.

V.M.D.T, K.R., S.I.B and M.M. designed the research. V.M.D.T performed laboratory work. V.M.D.T analyzed the data with the help from K.R. and M.M.; V.M.D.T wrote the manuscript with input from all co-authors. *, corresponding author.

In preparation (Journal Environmental Science and Technology)

Manuscript #3 – Chapter 5

Lipid response of *Shewanella oneidensis* MR1 to arsenic colloidal particles

V. Duran-Toro* and S. I. Bühring.

V.M.D.T and S.I.B designed the research. V.M.D.T performed laboratory work. V.M.D.T analyzed the data with the help from S.I.B.; V.M.D.T wrote the manuscript with input from all co-authors. *, corresponding author.

In preparation (Journal Science of The Total Environment)

List of Abbreviations and Symbols

AEG, Acyl/Ether Glycerol
ATP, Adenosyl Tri-Phosphate
BAB, Back-arc Basin
BL, Betaine Lipid
DAG, Diacylglycerol
DGTS, Di-Acyl-Glyceryl-Tri-Methyl-Homoserine
DLS, Dynamic Light Scattering
DMA, Di-Methyl Arsinite
DMAA, Di-Methyl Arsinic Acid
DOC, Dissolved Organic Carbon
DOM, Dissolved Organic Matter
DPG, Di-phosphatidylglycerol
DNA, Deoxyribonucleic Acid
EDX, Energy Dispersive X-ray Spectroscopy
EPA, US Environmental Protection Agency
EM, End Member
ESI, Electro Spray Ionization
G-DAG, Glycosyl Diacylglycerol
GSH, Glutathione
HF, Hydrothermal Fluid
HG-AFS, Hydride Generation – Atomic Fluorescence Spectrometry
HILIC, Hydrophilic Interaction Liquid Chromatography
HPLC, High Pressure Liquid Chromatography
ICP, Inductively Coupled Plasma
IPL, Intact Polar Lipid
Ksp, Solubility Product Constant
MMA, Mono-Methyl Arsonate
MMAA, Mono-Methyl Arsonic Acid
MTA, Mono-Thio-Arsenate
MOR, Mid Ocean Ridge
MS, Mass Spectrometry
NP, Nanoparticle
OD, Optical Density
OL, Ornithine Lipid
OM, Organic Matter
OES, Optical Emission Spectroscopy
PC, Polycarbonate
PDI, Poly-Dispersity Index
PE, Phosphatidylethanolamine
PG, Phosphatidylglycerol
POC, Particulate Organic Carbon
ppm, Part Per Million
ppb, Part Per Billion

PW, Porewater
ROS, Reactive Oxygen Species
RP, Rocky Point
rRNA, Ribosomal Ribonucleic Acid
R-SH, Reduced Thiol
SAED, Selected Area Electron Diffraction
SB, Spathi Bay
SEM, Scattering Electron Microscopy
SGI, Syber Green I
SILAR, Successive Ionic Layer Adsorption and Reaction
SW, Seawater
TEM, Transmission Electron Microscopy
TLE, Total Lipid Extract
ToF, Time of Flight
UV, Ultraviolet
VIS, Visible
WHO, World Health Organization

Arsenic Colloidal Particles,	As_{CP}
Arsenic fraction below 200 nm,	As_{200}
Arsenic fraction below 20 nm,	As_{20}
Arsenic fraction between 200 and 20 nm,	As_{200-20}
Arsenic Nanoparticles,	As NP
Atomic weight percentage,	[Atom. %]
Gaseous phase,	(g)
Gram,	g
Growth rate,	μ
Hour,	h
Kilogram,	Kg
Kilovolt,	kV
Liquid phase	(l)
Liter,	L
Mass to Charge ratio,	m/z
Meter,	m
Microgram,	μg
Microliter,	μL
Micrometer,	μm
Micromolar,	μM
Milligram,	mg
Milliliter,	mL
Millimeter,	mm
Millimolar,	mM
Molar,	M
Nanogram,	ng
Nanometer,	nm
Nanomolar,	nM
Ohm,	Ω
Solid phase,	(s)
Seawater percentage,	%SW
Volume/Volume percentage,	v/v %
Wavelength,	λ
Weight percentage,	[Weight. %]
Weight/Volume percentage,	w/v %
Year,	yr

Chapter 1 - Introduction

1.1 Relevance of seawater chemical composition

Planet Earth has 71 % of its surface covered by liquid water ($H_2O(l)$) [1], where the most predominant waterbody corresponds to the ocean [1]. The different features of this water mass have developed and sustain life trough time [2], and hence, the understanding of its physical and chemical properties are of fundamental interest in several scientific fields [1]. Oceans are major contributors to global climate patterns, an important resource (tidal energy, commercial fishing or aquaculture, oil and gas exploration etc.) and host an invaluable biodiversity of the planet [1, 2]. Chemically, it represents a reservoir of nutrients required by diverse life forms, from unicellular organisms like algae, bacteria or archaea to higher organisms [2].

The stoichiometry of seawater has been reviewed previously, and shows presence of major inorganic components [3]. Table 1.1, summarizes the most relevant inorganic compounds found throughout the ocean, highlighting chloride (Cl^-), sodium (Na^+), sulfate (SO_4^{2-}), magnesium (Mg^{2+}) among others [3]. Even though, seawater stoichiometry appears constant, physical, geological or biological events can alter its composition [4-6]. Near surface seawater phenomena like density gradients, evaporation, or biological carbon fixation can dictate variations on its chemical composition, for example, sea surface carbon (C) enrichments by changes in total dissolved or particulate organic carbon (DOC and POC, respectively) [4]. Micronutrients, which correspond to elements with a nutritional value for organisms, play a key role in marine ecosystems [7]. Silicon (Si), phosphorous (P) or nitrogen (N), all classified as micronutrients, are found in seawater (Table 1.1) as key components when limiting primary productivity in the ocean, which represent ~50×10^{15} g C yr^{-1} or about half of the net primary production of the planet [8]. In a similar way, trace metals like manganese (Mn), iron (Fe), nickel (Ni), or zinc (Zn), with known biological role as cofactor or part of cofactors in proteins have an impact upon planktonic communities in the water column [7]. Concentration of trace metals, can vary along water masses, yet average values have been generated (Table 1.1) [9]. However, not every major or trace element detected in seawater has a beneficious effect on marine organisms. Arsenic (As), mercury (Hg) and lead (Pb) are also present in trace concentrations (Table 1.1) and their deleterious effects are well reviewed [9].

Table 1.1. Seawater chemical composition

Major solutes	**g per Kg of Seawater**
Chloride (Cl^-)	18.890
Sodium (Na^+)	10.556
Sulfate (SO_4^{2-})	2.649
Magnesium (Mg^{2+})	1.272
Calcium (Ca^{2+})	0.400
Potassium (K^+)	0.380
Bicarbonate (HCO_3^-)	0.140
Bromide (Br^-)	0.065
Boric acid (H_3BO_3)	0.026
Strontium (Sr^{2+})	0.013
Fluoride (F^-)	0.001
Near-surface nutrients	**part per million, ppm (mg L^{-1})**
Phosphorus (P)	0.07
Nitrogen (N)	0.5
Silicon (Si)	3
Trace elements	**part per billion, ppb (µg L^{-1})**
Lithium (Li)	170
Iodine (I)	60
Molybdenum (Mo)	10
Zinc (Zn)	10
Iron (Fe)	10
Aluminum (Al)	10
Copper (Cu)	3
Manganese (Mn)	2
Arsenic (As)	1.7
Cobalt (Co)	0.1
Lead (Pb)	0.03
Mercury (Hg)	0.03
Gold (Au)	0.004
Values obtained from [4, 5, 9]	

Between the different phenomena, which supply or remove dissolved constituents in seawater, contributions from rain or river water have an important impact on Ca^{2+}, HCO_3^- and SiO_2 [9]. In the case of Cl^-, an additional source can be addressed: volcanic gases containing HCl (g) in early Earth´s history are assumed to dispense large quantities of this soluble gas into the water column [9]. In a similar way, submarine hydrothermal activity, has been associated to play a role influencing the seawater composition of major and trace elements, due to plume discharges rich in H_2S, dissolved or particulate Fe, and the release of As and Hg [10-12]. Human activity cannot be decimated from factors influencing seawater, perhaps it is the most relevant in terms of spatial-temporal impacts [13].

Due to the complexity and global impact of seawater composition, the present doctoral dissertation was framed in the study of marine geochemical factors altering the stoichiometry of the ocean.

1.2 The Iron case

Iron is a metal, an element that belongs to group VIII of the periodic table, highly abundant in the Earth´s crust (5 % by weight) and present in different oxidation states (0, +2 and +3) [14]. However, abundance of Fe in the ocean is limited (~10 µg L^{-1}), which classifies it as a trace element [9, 14, 15]. During the last decades of Fe determination in water samples, three different fractions (sizes) have been established in order to understand its geochemical cycle in the ocean (Figure 1.1). These three fractions correspond to a particulate size near 0.4 µm, a colloidal fraction of particles between 0.4 and 0.02 µm, and a "truly" dissolved fraction, assuming no material suspended below the 0.02 µm [15, 16].

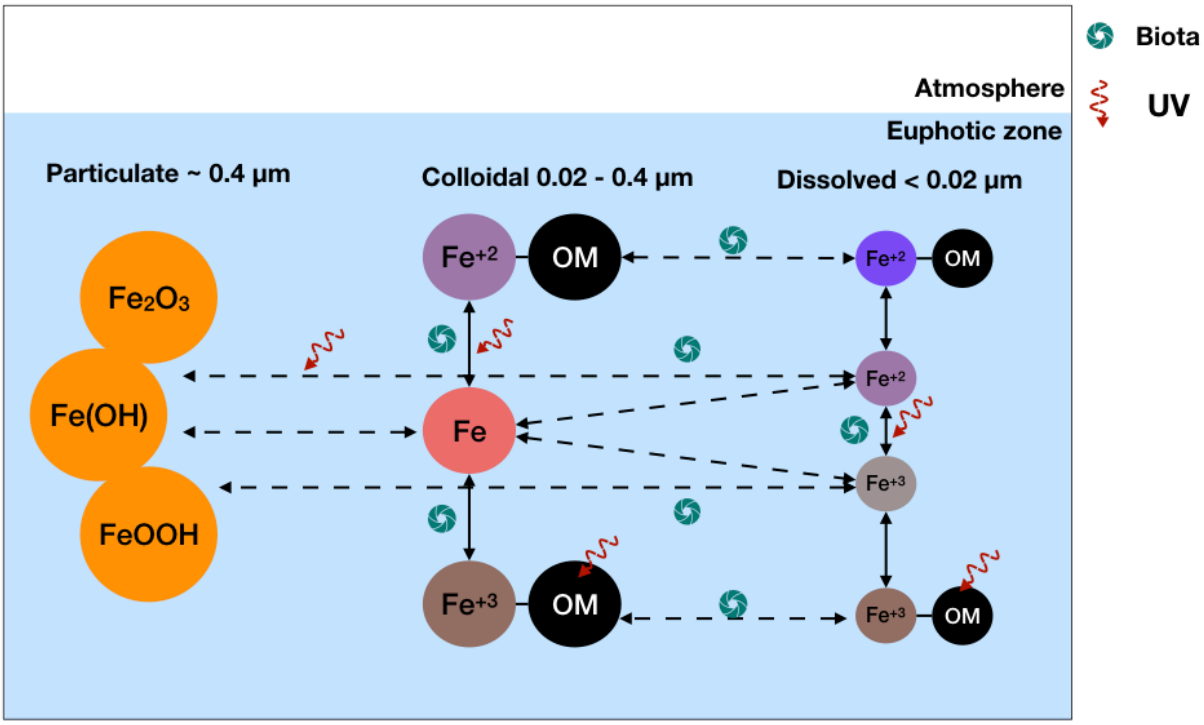

Figure 1.1. Modification of iron upon shallow seawaters. Dissolution (putative) process of iron particulate material occurs via wet oxidation (O_2 rich seawater), interaction with organic matter, photochemical mechanisms and biologically assisted reactions. The legend in the upper right corner indicates reactions assisted (directly or indirectly) by organisms and molecules or reactions sensitive to UV radiation. Scheme based on [15]. OM: Organic matter.

Size-partitioning profile studies of Fe in the water column have brought into discussion the role of physicochemical, biological or even geological phenomena controlling Fe-removal from water masses [15, 17-19]. For instance, dust, shallow sediments, sea ice and hydrothermal fluids can influence Fe distribution in shallow (above 200 m, meters) and deep (below 200 m) seawater [15, 20]. In 2011, hydrothermal systems were suggested for the first time as a source of Fe bearing colloidal particles to the deep ocean [21]. The stability of Fe colloidal particles in suspension, eluding aggregation, oxidation and sinking from the hydrothermal plume once in contact with cold and oxygen-rich seawater, was proposed as an explanation on how the particles remain suspended and travel longer distances [21-24]. Further explanations indicated a direct interaction, once the fluids are discharged into the ocean, between colloidal organic matter present in the plume and Fe [25].

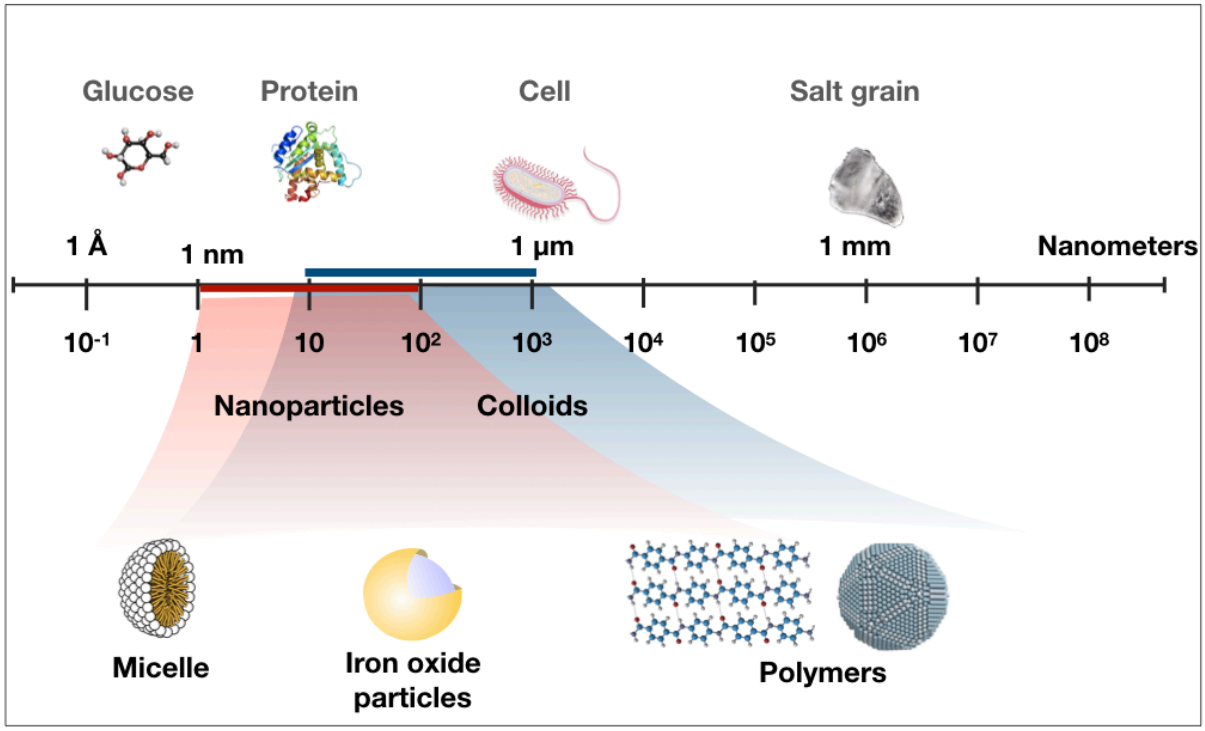

Figure 1.2. Interval scale of nano- and colloidal particles. The field of materials science defined nanoparticles as structures with at least one of their dimensions in the range of 1 to 100 nm. While colloidal particles are described as any material within a range of size between 10 nm to 1 µm. Chemical nature of nano- or colloidal particles can goes from organic nanoparticles like micelles to inorganic colloidal particles like iron particles. In the image, the red slot indicates nanoparticle size range and the blue slot the colloidal size interval, where both categories overlap as mentioned before. [26]

The novel or enhanced properties of Fe colloidal particles, with a size between 400 to 20 nm, correlate with modifications on material properties when confined to a nanometer scale, and represent an emerging cross-field of nano- and geosciences (Figure 1.2) [27]. Several Fe colloids, including Fe particles in hydrothermal systems, are characterized as nanoparticles or nanomaterials (1 to 100 nm) with interesting properties (Figure 1.2). For instance, pyrite (FeS_2), is a relevant mineral in the biogeochemical cycles of sulfur and iron in marine sediments, yet its anaerobic microbial oxidation has been established mainly for a putative nanosized particle fraction, which emphasizes the high reactivity of nanominerals in the environment [28]. Thus, the search for environmental hydrothermal systems and the generation of iron nanomaterials has gained attention in recent years [21, 29, 30]. Iron sulfide (FeS, FeS_2) colloidal particles (~ 100 nm) were found as a significant percentage (25 – 5 %) of the iron filterable fraction (below 200 nm) in deep-sea hydrothermal systems like Mid-Ocean Ridges or Back-arc Basins [21, 24, 29]. Furthermore, the rich geochemistry of hydrothermal fluids allowed the detection of Cu-Silicates and Zn colloidal aggregates in diverse systems like deep-sea vents or shallow water carbon dioxide (CO_2) rich cold seeps [29, 30]. Nonetheless, until date, no nanomineral or colloidal particle of a toxic element like As has been described to naturally occur in marine environments, not even in hydrothermal systems where As can be found in significant concentrations. Therefore, the identification of As bearing colloidal particles in a hydrothermal system represent an unexplored aspect of the metalloid chemistry in marine environments and constitute the third and a crucial chapter of this doctoral thesis, which is discussed in detail along the manuscript.

1.3 The Arsenic case

Arsenic is classified as a metalloid, an element from group XV, present in nature in different oxidation states (-3, 0, +3 or +5), major constituent of more than 240 mineral species and a minor (1.5 – 2 ppm) but ubiquitous element present in the Earth´s crust [31]. Its abundance in the ocean is orders of magnitudes lower than in the continental crust, between 0.5 to 3 $\mu g\ L^{-1}$ (ppb) with an average value of 1.7 $\mu g\ L^{-1}$ [32]. Arsenate (AsO_4^{3-}; As^{+5}) is the main arsenic species found in the water column (Figure 1.3), representing almost 80 % of the total arsenic detectable in open seawater [33].

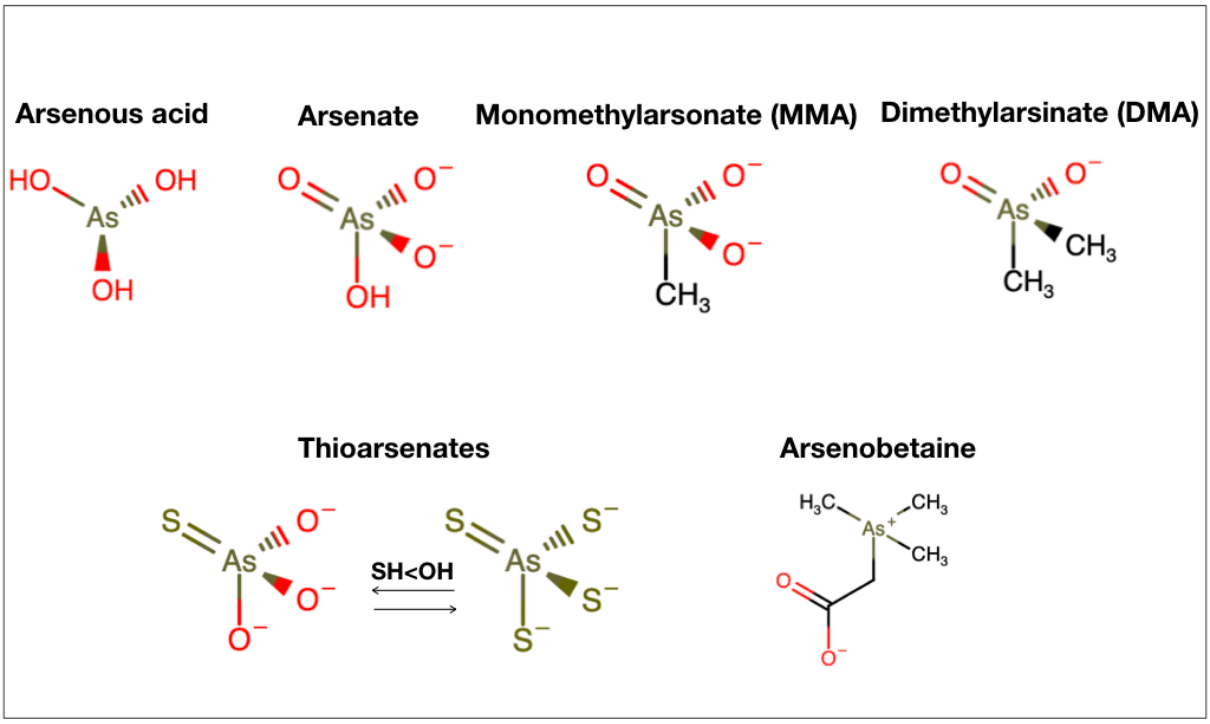

Figure 1.3. Common arsenic species in seawater. The oxidation state of arsenic in the water column is normally +5 (As^{+5}), with arsenate forms being the most abundant species in seawater. Regarding the pH-Eh and soluble sulfide content (HS^-, S^{2-}), stable thiolated forms of arsenate can be detected (thioarsenates). Under reducing conditions, oxidation state +3 (As^{+3}) can predominate and arsenous acid can be found. Finally, methylation or incorporation of arsenic into organic structures occur via enzymatic reactions, generating volatile compounds like MMA or DMA, or the liposoluble compound arsenobetaine.

Arsenic is a toxic element, and its abundance has been limited in aqueous solutions (including drinking water), to concentrations of total soluble forms (below 400 nm) lower than 10 µg L^{-1} [34]. Unfortunately, concentrations up to 50 µg L^{-1} are still being tolerated in developing countries [35]. The toxicity of As is associated to its oxidation state. In the case of arsenate (AsO_4^{3-}, As^{+5}) its chemical structure results very similar to phosphate (PO_4^{3-}), affecting metabolic reactions, by blocking catalytic, active or allosteric sites of enzymes and other proteins usually occupied by phosphorylated substrates, cofactor or co-enzymes (Figure 1.4) [36]. A common mechanism occurring in cells exposed to arsenate is the reduction from As^{+5} to As^{+3}, which, together with the metabolic block, has as major consequence: the accumulation of reactive oxygen species (ROS) due to a decrease in the enzymatic activity dealing with harmful reactive agents (Figure 1.4) [36, 37]. The accumulation of intracellular ROS generates the rapid oxidation of macromolecules like DNA, proteins and lipids, which results in damage or eventually cell death (Figure 1.4) [38, 39]. Other arsenic species, like arsenite (AsO_2^-, As^{+3}), can be found in the water column (Figure 1.3). As^{+3} species are associated to deep and shallow hydrothermal systems and represent the most deleterious form of the metalloid in the environment [10, 35]. The trivalent forms of arsenic (As^{+3}) have a great affinity for thiols or dithiol groups present in peptides and proteins with major biochemical roles inside of cells (Cysteine and Glutathione) (Figure 1.4) [36, 40, 41]. The direct consequences of As^{+3} is the

generation of oxidative damage (ROS-induction as described before) by deterioration of peptides and protein structures related to DNA reparation systems, and the alteration of the gene expression machinery and thiol-redox control system (Figure 1.4) [37]. Although, the toxicity of soluble arsenic in different oxidation states has been vastly reviewed, no differences in terms of particle size have been addressed so far. This is especially desired for As species in hydrothermal systems, where metallic based colloidal materials are described as significant components of hydrothermal fluids [21, 24, 29, 30].

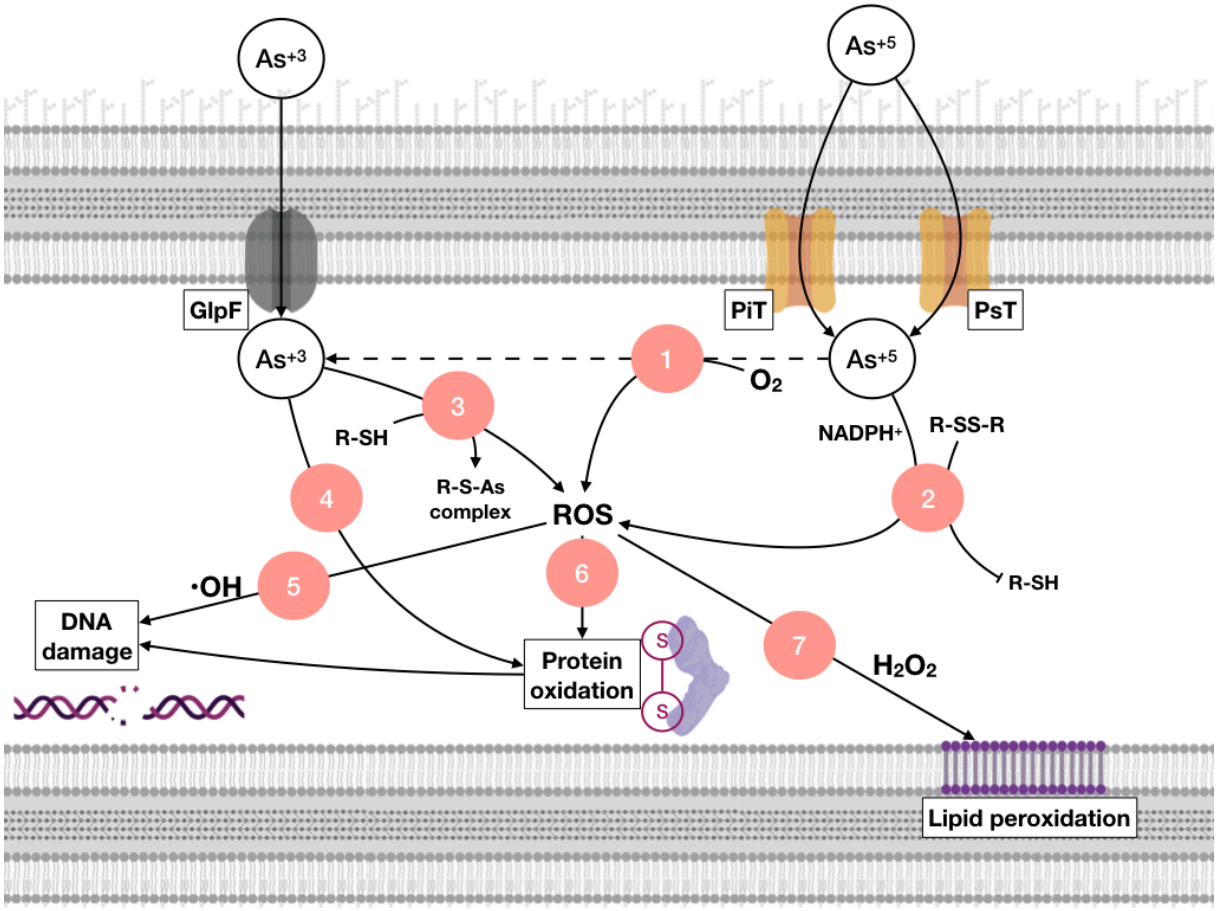

Figure 1.4. Arsenic effect upon cellular functions and macromolecules. Arsenic can enter the cell as As^{+3} via aquaglyceroporin type proteins (GlpF) or as As^{+5} through phosphate transporters (PiT, PsT). Once inside, (1), As^{+5} can be reduced to As^{+3} coupled to O_2 and reactive oxygen species (ROS) can be formed. (2), As^{+5} can also block phosphorylated enzymatic cofactors, as nicotinamide adenine dinucleotide phosphate ($NADPH^{+}$), and inactivate cellular functions as the redox thiol system with a crucial role during antioxidant activity, leading into ROS accumulation. (3), As^{+3}, can also lead to ROS accumulation by forming complexes with antioxidant reduced thiols (i.e. glutathione). (4), As^{+3} can disrupt di-sulfide bonds present in proteins by interacting with amino acid residues (Cysteine), leading to protein oxidation and loss of tertiary functions. Direct ROS oxidation of macromolecules occurs by interaction of nucleotides (5) with hydroxyl radical (•OH), amino acid residues (6), and peroxidation of membrane fatty acids (7) with hydrogen peroxide (H_2O_2). RSH, reduced thiol pool; RSSR, oxidized thiol pool.

1.4 Arsenic colloidal particles

Historically, environmental scientist, using particle filtration protocols have defined fractions of particulate (> 400 nm), colloidal (400-20 nm) and dissolved (< 20 nm) species of elements in aqueous samples (Figure 3.1) (i.e. Fe) [15, 23, 42, 43]. However, this has not always been the case, and it has changed through time when enabling technologies appeared [15, 42, 44]. This definition of colloidal particles (400 – 20 nm), represents a distant description from material sciences, where colloidal materials are designated as "… small solid particles that are suspended in a fluid phase. Their size range is typically between ~ 10 nm and several microns." (Figure 1.2) [26]. Therefore, constrains about colloidal fractions, materials or particles in environmental sciences raise ambiguously in many occasions. In the case of As, colloidal fractions have been poorly studied, and the designation of arsenic soluble forms can be attributed to operational limits below 400 nm and only in few reports below 200 nm (Figure 1.5) [10, 43, 45]. Every form of the metalloid above these references (400 or 200 nm) is considered to be a particulate material and therefore expected to sink in the water column. Generally, the presence of As in the colloidal fraction is assumed to happen because of the adsorption of soluble arsenic species to organic matter or iron particles (Figure 1.5) [46, 47].

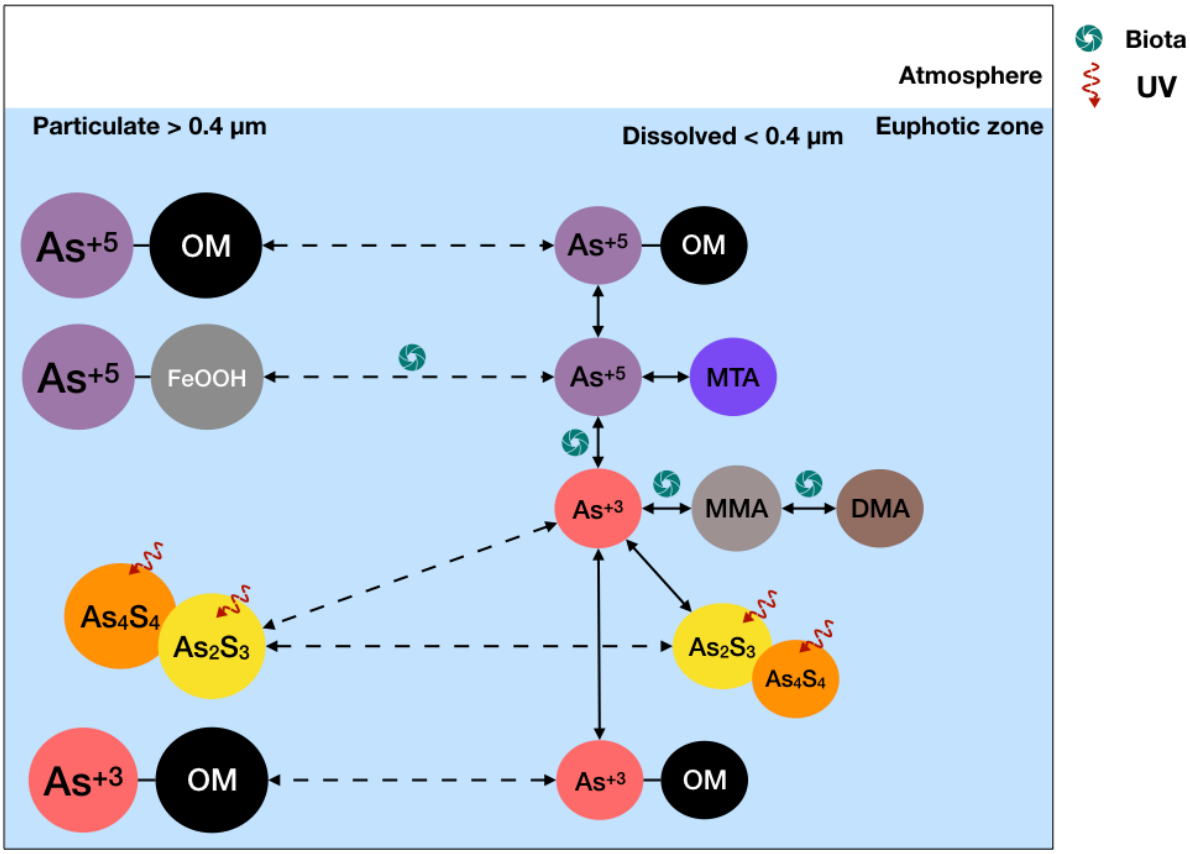

Figure 1.5. Modification of arsenic in seawater. Dissolution of arsenic particulate material induced by biological activity, wet oxidation (O_2 rich seawater) or photo-oxidation of particles can occur in seawaters. A predominant force of arsenic mobility in water column is driven by microbial oxidation-reduction and/or methylation of As^{+3} or As^{+5} present in the dissolved fraction as arsenous acid, arsenate, monothioarsenate (MTA), monomethylarsonate (MMA) or di-methylarsenite (DMA). The legend in the picture at the upper right corner indicates reactions assisted (directly or indirectly) by organisms and molecules or reactions sensitive to UV radiation.

In consequence, arsenic colloidal particles as a component of seawater, porewater or hydrothermal fluids have not been studied in the environment. Only synthetic protocols are available on the generation and characterization of this material (Table 1.2), using diverse mechanisms like chemical vapor deposition, milling of arsenic bearing minerals, chemical reduction or even biologically induced synthesis. The variety of As colloidal particles produced (Table 1.2), goes from simple zero-valent As particles (As^0), semiconductor materials like indium arsenide (InAs), to complex zirconium iron oxide covalent immobilizations (ZrAs-Fe_3O_4). The most frequently studied case is particles of arsenic sulfide (As_xS_y), which possess photoactive and potentially antitumoral effects (Table 1.2). The first report of As_xS_y colloidal synthesis was developed through stabilization of very small particles (1.5 – 15 nm) by pH reduction (2 – 6.8) and the use of additives like hexametaphosphate, SiO_2 or poly(vinyl alcohol) in a H_2S(g) saturated solution [48]. The parameters affecting colloids formation strictly depends on the mechanisms involved in the production of the material (Table 1.2). Among the mechanism described, highlights a resemble between As_xS_y synthesis parameters and natural hydrothermal systems. Features like aqueous reaction solutions rich in soluble sulfide (HS^-, S^{2-}), pH 4 - 7 and temperatures between 25 and 140 °C (Table 1.2), are comparable to hydrothermal conditions, where arsenic sulfide precipitates in the environment [45, 49]. As mentioned above, the size confinement, can confer unique properties to the materials, different to the analogous chemical compounds on larger scales [50]. Perhaps, the presence of similar As_xS_y colloidal particles (Table 1.2), will favor organisms-particle interaction, making a significant impact on the biology and chemistry of nearby systems where the particles are formed. Therefore, the understanding of As colloidal particle generation and stability in the environment, represent a relevant gap of knowledge in the biogeochemistry of this element, especially in hydrothermal ecosystems, and was further developed in the fourth chapter of this project.

Table 1.2. Main arsenic nanomaterial synthesis methods.

Method	Nanoparticle	Temperature	pH	Size/Morphology	References
Chemical vapor deposition/Thermal evaporation	GaAs/As_2S_3	~160°C;	n.s.	2-6nm/Dots ; ~1,2µm/micro-film	[51-55]
Electro-Chemical bath deposition/ SILAR	As_2S_3	6°C; 25°C	<7	185-520nm/Film 400-800nm/Film 200-380nm/Film	[56-60]
Laser ablation Laser irradiation	GaAs	n.s.	n.s.	9-13nm/Spheres; 30-80nm/nano-phases; 0,1-1,4µm/nano-lenslets	[61, 62]
Colloidal synthesis	InAs/As_2S_3	130-240 °C 25 °C	n.s. 3-6	2.5-6nm/Dots 1.5-15nm/spheres	[48, 63]
Covalent immobilization	ZrAs-Fe_3O_4/SiO_2	25-60°C	n.s.	30nm/Aggregates	[64]
Chemical reduction	As^0	25-60°C	7-9	67nm/Spheres	[65]

Grinding	As_4S_4	25 °C	~7	50nm/Spheres	[66]
Milling	As_4S_4	25 °C	~7	137-150nm/Grains	[67-71]
Co-precipitation	As_4S_4	40°C	<7	80nm/Spheres	[72, 73]
Cluster-mediate transformation	As_4S_4 / As_2S_3	25-140 °C	~8	3-9nm/Dots	[74, 75]
Biologically induced reduction	As_2S_3/AsS	~30 °C	~7	30-70nm/nanotubes; 50nm/Spheres	[76-78]
Chemical reduction	Orpiment (As_2S_3)	25 °C	4-7	n.s.	[79]*

*Precipitation of micro/macro crystals or bulk material. n.s. not specified. SILAR: Successive ionic layer adsorption and reaction.

1.5 The microbial response to arsenic in a hydrothermal system

Arsenic distribution has been studied in multiple environments, from acid mine drainage to shallow hydrothermal systems [45, 80-82]. In many cases, the dissolved fraction of arsenic (Figure 1.5), influences microbial biodiversity and the presence of detoxification mechanism in the environment [83-91]. In the case of hydrothermal systems, changes in biodiversity of bacterial communities and variations in distribution of arsenic resistance genes i.e. *ars*, *arr* or *aoi* have been documented [82, 87-89, 92]. The operons *ars*, and *arr* or *aoi* comprise common mechanisms of arsenic detoxification among bacteria (Figure 1.6) [93-95]. The operon *ars* encodes a detoxification system conserved in gram-negative organisms, and consists mainly of a transmembrane ATPase arsenite efflux pump (*ars*A and *ars*B sub-unites) and an arsenate reductase enzyme (*ars*C) (Figure 1.6) [95-97]. The *arr* genes, correspond to a dissimilatory reduction pathway of arsenate under anoxic conditions, where an [Fe-S] cluster, allocated in the enzyme ArrAB, mediates the use of arsenate as an electron acceptor couple to the metabolism of the microorganism (Figure 1.6) [98-102]. This mechanism is well documented among bacteria, in particular in marine sediment model organisms like *Shewanella spp.* [100, 101]. *Aoi* genes, encode arsenite oxidizing enzymes (AoxAB, AroAB or AsoAB), which in a similar way to ArrAB type proteins, have two subunits, with an [Fe-S] cluster and a molybdenum (Mo)- cofactor dependent site, catalyzing the oxidation of arsenite to arsenate (Figure 1.6) [102-104]. This mechanism is spread in different environments, among them geothermal and hydrothermal systems where As^{+3} species are abundant [88, 92, 105]. Arsenite oxidation is considered a potential pathway of chemolithotrophic metabolism, where the metalloid oxidation is coupled to O_2, NO_3 or ClO_4^- reduction [106-108]. Uptake of As^{+3} and As^{+5} also corresponds to a relevant response when dealing with arsenic toxicity (Figure 1.6). In the case of arsenate (As^{+5}), as an analogue of phosphate chemical structure, it gets transported inside of the cell through unspecific phosphate transporters like PitAB (Figure 1.6) [109]. On the other hand, As^{+3} species in aquatic environments with pH below 9.3 are mostly present as

$As(OH)_3$, which mimics the chemical structure of glycerol and allows its entrance via aquaglyceroporin channels (Figure 1.6) [109-111].

In marine ecosystems, many of these mechanisms are induced (affected) by hydrothermal activity, which generates As, S, P or pH gradients in the overlying water or within the porewater in the sediments [88, 92, 112]. Metagenomic analyses of the shallow water hydrothermal system off Milos (Greece), showed variations of the *ars*, *arr* and *aoi* genes together with changes in phosphate transporter gene expression along an As gradient in the porewater [88]. Even though, the results exhibited a series of response mechanisms to As, the main adaptation identified was the use of As detoxification genes (*ars*) and the expression of high specificity phosphate transporters, rather than the use of metabolic As cycling systems (*arr* or *aoi*) [88].

While, studies of gene and protein expression related to As uptake or oxidation-reduction systems represent a robust tool when understanding microbial adaptations, other macromolecules could play a role in the response to the biochemical stress triggered by the metalloid and deserve further attention (Figure 1.6). As described before, arsenic can induce oxidative stress (Figure 1.4), and together with other environmental stressors like the increase of salinity (NaCl % by weight), P deficiency, extreme pH values or temperatures; has an impact upon membrane lipids (Figure 1.4 and 1.6) [113-119]. Commonly, the effect of external parameters has been studied by following changes of intact polar lipids (IPLs) composition in environmental samples, batch cultures or microbial enrichments [113-118]. Due to the good stability of lipids over time, they constitute a well preserved record of environmental events, and represent a sensitive response to acute and chronic adaptations of organism to stress [120]. High NaCl concentrations for instance, result in a prominent abundance of anionic lipids like phosphatidylglycerol (PG) or di-phosphatidylglycerol (DPG) and a decrease of the aminophospholipid phosphatidylethanolamine (PE) [113, 119]. Glycolipids like monoglycosyl diacylglycerol (G-DAG) and aminolipids like diacylglyceryl trimethylhomoserine (DGTS) are found to replace phospholipids at low P concentration [115]. In the shallow water hydrothermal system off Milos a trend of decreasing aminolipids abundances (ornithine lipid and betaine lipid) could be observed together with multiple environmental stressors, among them high temperatures and As concentrations [117]. Nevertheless, only a few reports attributed modifications of lipids or lipid components in microorganism to arsenic stress [121, 122]. *Bacillus* sp. ORAs2 and a *Pseudomonas* sp. ORAs5 strains, for example, have shown an increase in their fatty acid saturation when exposed to increasing doses of As and in the presence of toluene [121]. Until date, no study has directly addressed a link between As stress and changes in microbial IPL composition. Perhaps, a direct interaction of As and IPLs, or between reactive agents derived from As stress and IPLs or even an effect upon lipid synthesis, can be evaluated under stress by soluble or colloidal forms of arsenic in microorganisms, representing a novel tool to monitor arsenic toxicity in aquatic environments, especially in hydrothermal systems like Milos. The fifth chapter of this thesis, describes the use of IPLs identification to understand the toxicity and mechanisms involved in the response of a bacterial model (*Shewanella oneidensis* MR1) to As colloidal particles.

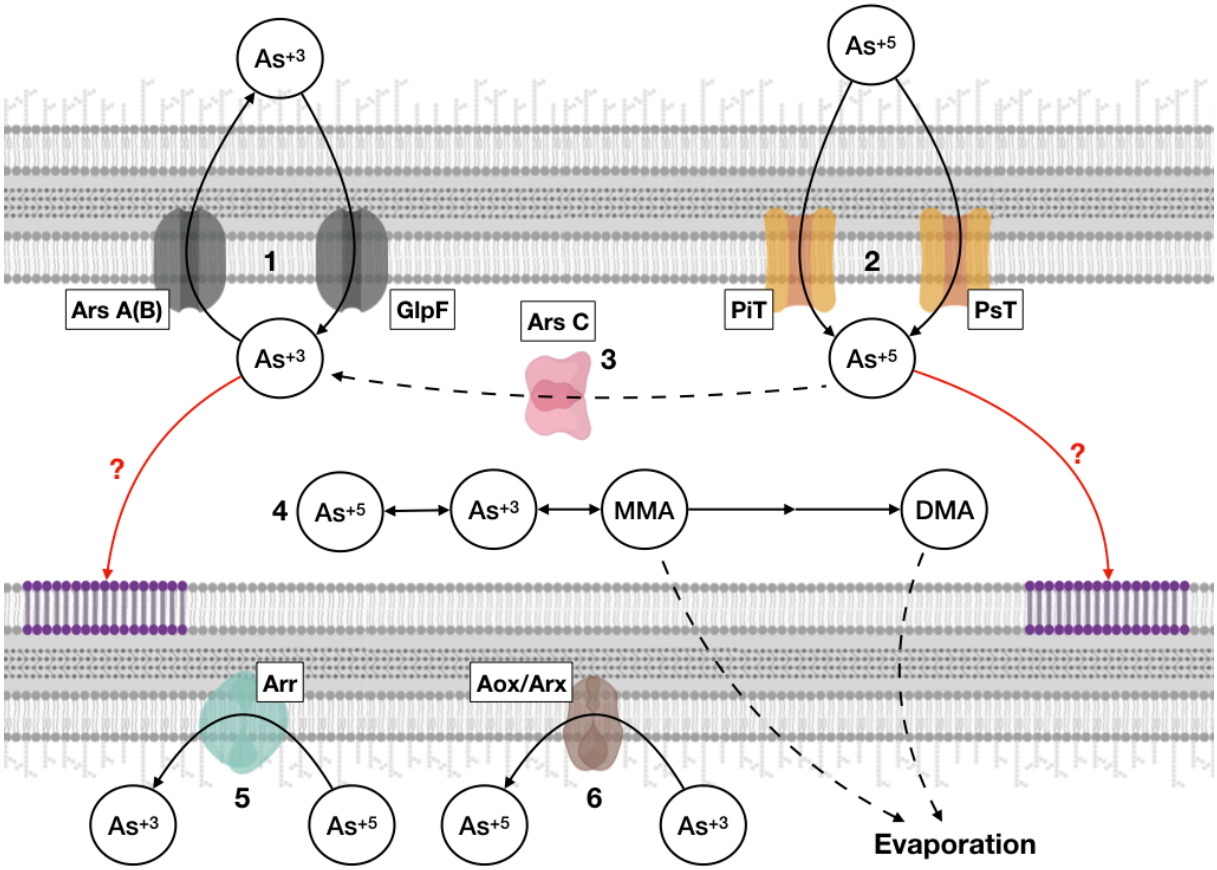

Figure 1.6. Arsenic detoxification mechanisms in prokaryotes cells. Transportation systems of arsenic account for, (1), uptake of As^{+3} by aquaglyceroporin type proteins (GlpF) and exporters like ArsAB. (2), As^{+5} is incorporated by two different phosphate affinity transporters, a low specificity, PiT, and a high phosphate affinity, PsT. (3), Once in the cytoplasm, As^{+5} is reduced by ArsC to As^{+3}, which can be expulsed from cells via ArsAB. (4), As^{+3} and As^{+5} pool in the cytoplasm can go through a series of reduction and oxidation by methylation steps via SAM (S-Adenosyl methionine) methylase activity, which leads to the generation of monomethylarsonate (MMA) or di-methylarsenite (DMA) which diffuses through the membrane and evaporates. (5), extracellular As^{+5} pool can be reduced by Arr type enzymes into As^{+3}, where arsenate is used as an electron acceptor, and can lead to precipitation of arsenic sulfide or other As^{+3} forms on the cell surface. (6), enzymatic oxidation (Aox, Arx) of extracellular arsenite (As^{+3}) coupled to cellular metabolism, leading to the formation of arsenate (As^{+5}). Red arrows indicate putative interaction between arsenic intracellular pool and membrane lipids as an unexplored mechanism of detoxification.

1.6 Milos, a natural laboratory for studying the generation and stability of arsenic sulfide colloidal particles

Hydrothermal systems can discharge As-rich hot fluids into the ocean, with one well-studied example being the island of Milos (Greece) (Figure 1.7).

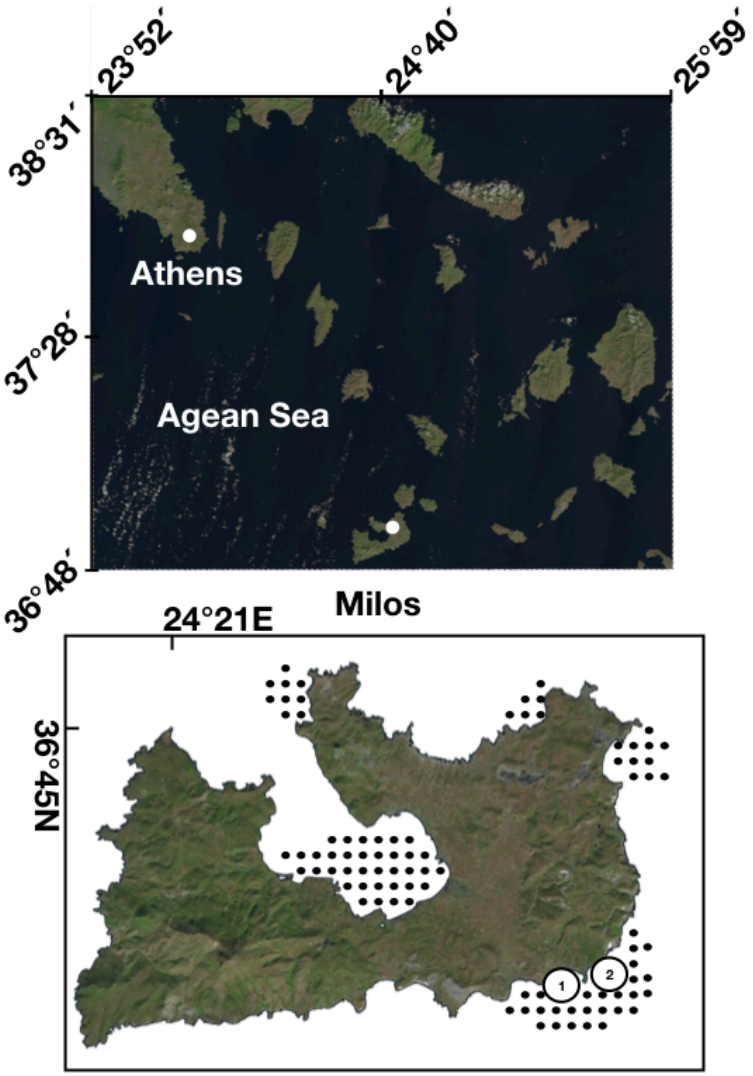

Figure 1.7. Geo-localization of the hydrothermal system off Milos. Top, regional map of Milos island located in the Aegean Sea. Bottom, Milos island map, with hydrothermal active zones (dots) discovered by [123]. Two locations were marked, (1), Paleochori and (2) Spathi bay, based on their characteristic and well-studied geochemical parameters (Table 1.3).

Among the different hydrothermal systems of the island, Paleochori and Spathi bay have soluble concentrations of As up to 78 μM (Table 1.3) [45]. These hydrothermal systems, can discharge fluids with a high content of soluble sulfide (HS^-, S^{2-}), reaching concentrations of 3 mM in porewater (Table 1.3) [45]. As a consequence, different arsenic sulfide species (As_xS_y) can be found, between them orpiment (As_2S_3) and thioarsenate [45]. The solubility of arsenic sulfide species is very low, with a solubility product constant of 10^{-16} (Ksp, As_2S_3), which classifies them as poorly soluble in aqueous solutions and explains the formation of arsenic sulfide mineral phases (Orpiment or amorphous minerals) in the sediments influenced by the hydrothermal activity (Figure 1.8) [49, 124]. The phase stability of arsenic sulfide minerals is strictly controlled by changes in pH and temperature [125]. In Milos, hydrothermal fluids or porewater can present pH values below 5 (Table 1.3 and Figure 1.8), where stability is high, and precipitation of arsenic sulfide is favored [125]. While the temperature, which results in a key factor due to the strong gradients in the sediments off the island (Table 1.3 and Figure 1.8) [112], decreases the phase stability at values near 90 °C, triggering the dissolution of crystalline minerals (i.e. orpiment or realgar). Yet, amorphous forms (without any crystalline structure) are known to remain stable under such conditions [125], which correlate with amorphous arsenic sulfide precipitates detected in Milos (Figure 1.8) [49]. However, temperature and pH are not the only important parameters present in a hydrothermal system. Organic matter (OM) could also play a role in arsenic sulfide mobility and crystal phase stabilization [126, 127]. In wet peat systems, the high content of soluble sulfide (HS^-, S^{2-}) results in S-rich OM, which can interact with soluble arsenic species, favoring the generation of amorphous arsenic forms at temperature around 25 °C [126, 127]. The interaction of OM and As was rather explained by a covalent bond between As and S atoms found in the OM [127]. Although a similar phenomenon can occur between dissolved OM present in hydrothermal fluids or porewater in hydrothermal systems, scarce reports have focused on OM-As interaction at high temperatures. The presence of highly specific organic ligands of Cu in Paleochori bay hydrothermal systems, indicated mobilization of metallic species in Milos driven by OM [128]. Thus, comparable events can be expected within the dispersion and availability of different dissolved metallic species, or metalloids like As, with direct implications in the chemistry of colloidal particles.

Table 1.3. Environmental parameters of porewater in venting areas off Milos Island.

	Location	pH	T (°C)	H_2S (mM)	As (μM)
1	Paleochori bay	3 – 7	26 – 95	3.1	39
2	Spathi bay	4 – 6	65 – 82	2.9	78

1 & 2 correspond to locations marked in Figure 7. Values obtained from references [45, 134]

Many of the parameters mentioned above are crucial to understand the formation and stability of colloidal particles, therefore, Milos represent a suitable natural laboratory for identification and characterization of these materials (Figure 1.8). To understand the influence of pH, temperature or OM on the stability of arsenic colloidal particles, further field and laboratory studies are required. Therefore, the main field work and analyses of parameters influencing generation of As colloidal particles, were focused in the shallow hydrothermal systems off Milos.

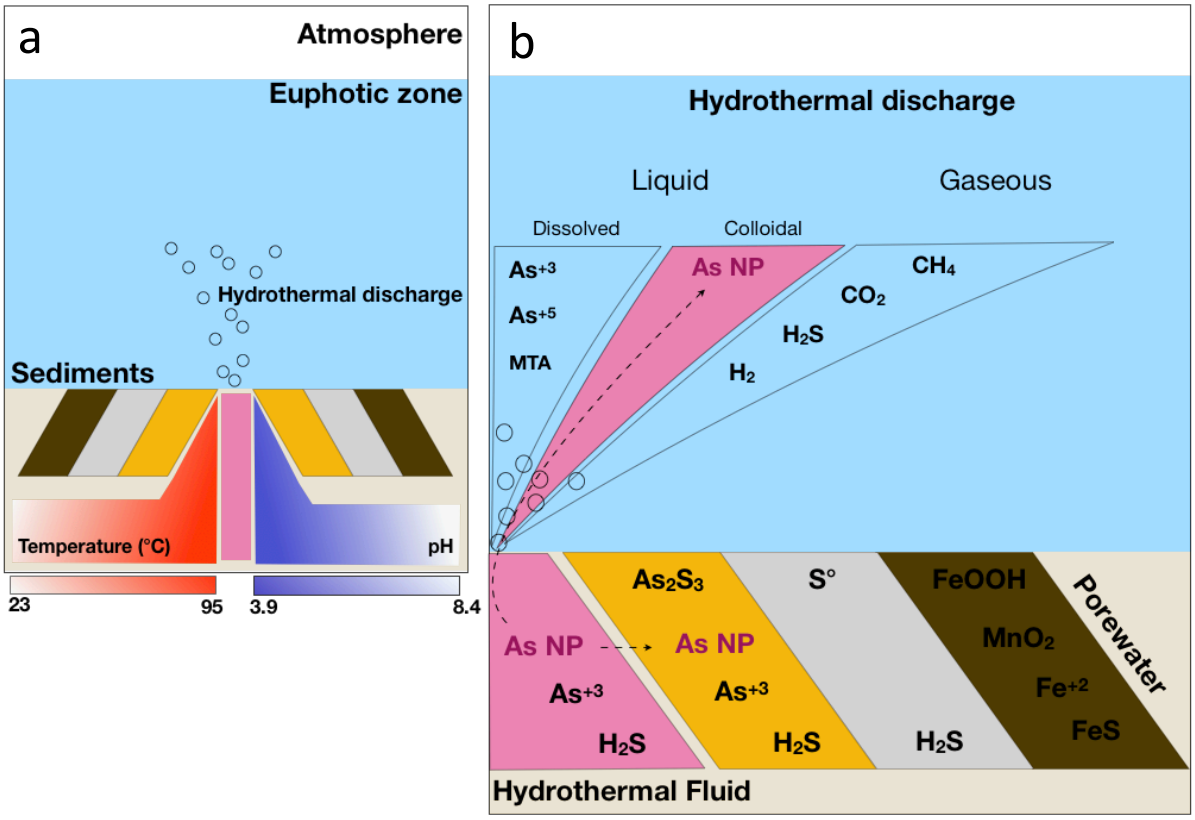

Figure 1.8. Model of a shallow hydrothermal vent in Milos. a, sediments surrounding the vents are greatly influenced in their temperature and pH along sagittal and axial sections of the seafloor. A hydrothermal discharge, consisting of fluids and gases, emerging from the center of the vent, where distinctive sediment profiles can be visually observed. b, major, putative or confirmed, chemical species present in the hydrothermal discharge corresponded to dissolved arsenic species (arsenite, arsenate, mono-thioarsenate, MTA) and gases of H_2S, H_2 or CO_2, among others. Proposed and detected chemical species present in sediments around the vents are characterized by yellow arsenic sulfide minerals, abundant white elemental sulfur, and finally, further from the vent, accumulation of brownish iron sulfide/oxide and manganese oxide particles. As NP, correspond to potential arsenic nanoparticles, present in hydrothermal fluids (pink), the colloidal fraction in the liquid phase of the hydrothermal discharge or in the sediments (porewater).

Chapter 2 - Hypothesis and Objectives

2. Hypothesis and Objectives

The aim of this dissertation was to identify the presence and influence of As nanoparticles on the biogeochemistry of marine environments, specifically in hydrothermal systems. Chapter 3 discusses the chemical characterization of As nanoparticles in environmental samples, followed (Chapter 4) by the understanding of chemical parameters like temperature or OM (additives) in the stability of synthetic colloidal As material. Finally, the toxicity of synthesized As nanoparticles was evaluated through studies of intact polar lipids (IPLs) variations in the marine microbial model *Shewanella oneidensis* MR1 (Chapter 5).

Hypothesis 1:

Arsenic rich nanoparticles can naturally occur in a shallow hydrothermal system, representing a significant percentage of the filterable fraction (< 200 nm) of the metalloid present in hydrothermal fluids.

Objective: Identify and characterize As rich nanoparticles in environmental samples from a shallow hydrothermal system.

Approach: In Chapter 3, general geochemical data and trace quantification of As by hydride generation – atomic fluorescence spectroscopy (HG-AFS) were used to show the relevance of a colloidal arsenic fraction in environmental samples of the shallow hydrothermal systems off Milos (hydrothermal fluids, porewater and seawater). In a second step, scattering and transmission electron microscopy (SEM and TEM) coupled to energy dispersive x-ray spectroscopy (EDX) and selected area electron diffraction (SAED), were used to identify and chemically characterize suspended particles present in environmental samples rich in colloidal arsenic fractions.

Hypothesis 2:

Temperature and sulfur rich organic matter (OM) play a key role in phase stability during synthesis of As nanoparticle under environmental hydrothermal conditions.

Objective: Characterize As rich nanoparticles synthesized at different reaction temperatures and in the presence of thiol rich additives.

Approach: In Chapter 4, aqueous synthesis of colloidal As rich particles was achieved using different reaction temperatures and in the presence or absence of thiol rich additives with a biological origin (cysteine and glutathione). Particles size, morphology, chemical composition and crystal phase were determined by SEM-EDX and TEM-SAED.

Hypothesis 3:

Arsenic colloidal particles have a toxic effect upon *Shewanella oneidensis* MR1, characterized by an alteration of intact polar lipid composition in a membrane of the marine microbial model.

Objective: Evaluate the toxicity of As colloidal particles in cultures of *Shewanella oneidensis* MR1.

Approach: In Chapter 5, evaluation of As colloidal particles toxicity in *Shewanella oneidensis* MR1 cultures was performed by determination of growth inhibition, changes in growth rates and variations of membrane lipid composition. Intact polar lipids relative abundance was established by high performance liquid chromatography coupled to quadrupole time of flight mass spectrometry (HPLC–qToF-MS).

Chapter 3- Identification of As bearing nanoparticles in a shallow hydrothermal system

Manuscript title, authors and publication status:

Amorphous arsenic sulfide nanoparticles in a shallow water hydrothermal system

V.M. Durán-Toro[1*], R.E. Price[2], M. Maas[3,4], C.-C. Brombach[5], T. Pichler[5], K. Rezwan[3,4], S.I. Bühring[1]

1Hydrothermal Geomicrobiology Group, MARUM Center for Marine Environmental Sciences, University of Bremen, Bremen, Germany
2Stony Brook University, School of Marine and Atmospheric Sciences (SoMAS), Stony Brook, New York 11794, USA
3Advanced Ceramics, University of Bremen, Bremen, Germany
4MAPEX - Center for Materials and Processes, University of Bremen, Bremen, Germany
5Dept. of Geochemistry and Hydrogeology, University of Bremen, Bremen, Germany
* Corresponding author: vduran-toro@marum.de

Marine Chemistry (published in Feb., 2019)

https://doi.org/10.1016/j.marchem.2019.03.008

Chapter 3 – Abstract

Hydrothermal fluids can contain trace elements such as arsenic (As), which are toxic to surrounding biota. In these kind of fluids, the bioavailability and biotransformation of As have been investigated but so far the ratio of total soluble As (< 200 nm) versus the amount of As contained in a nanoparticulate phase has not been reported. Here, for the first time, the presence of As in the nanoparticulate fraction (between 200 and 20 nm) is described for arsenic-rich hydrothermal fluids in a marine shallow-water hydrothermal system. Samples of diffusively venting hydrothermal fluids, porewater and seawater were collected in the hydrothermal system located in Paleochori Bay, Milos Island (Greece), and the fraction between 200 and 20 nm (As_{200-20}) was studied. Up to 38 % of the soluble arsenic was present within the As_{200-20} fraction in pore fluids, 10 to 20 % in hydrothermal fluids and 5 % in seawater. Identification and characterization of particles in hydrothermal fluid, porewater and seawater was performed by scanning electron microscopy coupled to energy dispersive X-ray spectroscopy (SEM-EDX), transmission electron microscopy (TEM) with selected area electron diffraction (SAED) and dynamic light scattering (DLS). The particles are of spherical morphology with a polydisperse size distribution (PDI: 0.37) and diameters close to 100 nm. EDX studies confirmed a chemical composition rich in As and S. The SAED pattern revealed absence of a crystal phase indicating the presence of an amorphous arsenic sulfide material. These results bring into discussion the role of the nanoparticulate fraction for As dispersion, bioavailability, and potentially harmful effects in marine coastal ecosystems.

Key words:

Arsenic, nanoparticles, hydrothermal vents, Milos.

3.1 Introduction

Naturally occurring nanoparticles (NPs) (i.e., sulfides, oxides or zero valent particles), can feature different physical properties compared to bulk materials [129, 130]. In the case of a marine environment these properties could significantly impact the transportation of elements within the water column, their bioavailability and potential toxicity [15]. For example, in 2011, the hydrothermal activity of deep-sea vents was established as a source of iron (Fe) sulfide NPs to the ocean [21]. The hydrothermal fluids described by Yücel et al. (2011) were rich in nano-structures of FeS_2 (nano-pyrite), a structure associated with an increased active surface area, a lower oxidation rate and a lower settling rate, when compared to macro-particles of the mineral [21]. These properties have direct implications for the biogeochemical cycling of Fe in deep-ocean ecosystems, and it was suggested as an explanation of how Fe, released due to hydrothermal activity, avoids sedimentation and thus remains longer in the water column [15, 21].

Subsequently, research on NP fractions in hydrothermal fluids was expanded to different marine ecosystems [29, 30, 131]. Gartman et al. (2014) reported Cu and Zn pyrite-containing nano-aggregates as a widespread component in black smoker emissions from hydrothermal vents, and Kadar et al. (2012) described nano-clusters rich in Fe and Mn that aggregated into larger colloids when mixed with seawater along a pH gradient in a shallow water vent system. Thus, most of the research on NPs in hydrothermal vents to date describes the generation of metallic enrichments, forming amorphous and highly polydisperse metallic NPs, rich in Fe, Mn, Si, S or O [30, 131]. However, to the best of our knowledge, no NP fraction of potentially toxic elements such as arsenic has been investigated in hydrothermal fluids.

Arsenic is a trace element present in many hydrothermal fluids, classified as a metalloid with extremely harmful biological effects at high concentrations [36, 82, 132-134]. It is an element widely spread in the environment, being present in different oxidation states (typically +3 and +5 and -3), as inorganic (i.e. hydrides, AsH_3; sulfides, As_4S_4; oxides, As_2O_3) or organo-arsenic (i.e. dimethylarsenic acid, $(CH_3)_2AsOOH$ cacodylic acid, etc.) compounds [135, 136]. The toxicity of arsenic has been reviewed extensively and differs on a biochemical level according to its oxidation state [36, 132]. The two main inorganic forms of soluble arsenic are arsenate, As^{+5}, and arsenite, As^{+3}. Arsenate is found mainly in oxygen-rich fluids and due to chemical similarities with phosphate (PO_4^{3-}) both molecules compete by affinity for specific union sites of enzymes, resulting for example, in blocked coenzymes or substrates like adenosine tri-phosphate (ATP) [36, 132]. As^{+3} on the other hand, has a high affinity for thiol groups present in cell macromolecules (i.e., proteins), where it can alter their structure and function [36, 132]. The main cellular effect of As is upon cell proliferation by damaging the DNA replication and reparation system and oxidative stress by decreasing the concentration of low-molecular-weight thiols (i.e. glutathione) used in the cell redox-system [36, 137].

Arsenic is elevated relative to background seawater in many submarine hydrothermal fluids [92, 134, 138-140], which provides an opportunity to study the cycling and particulate phases of this element in the marine environment. The shallow-water hydrothermal system in Milos (Greece), in particular, is a natural laboratory for studying As release. There, vent fluid

concentrations as high as 78 µM were determined, comparable to values found in fluids of deep-sea hydrothermal systems, like mid-ocean ridge (MOR) or back-arc basins (BAB) (0.7 to 10 µM) [134, 141]. In general, reducing hydrothermal fluids have mainly As^{+3}, which is also the case in the Milos system [45]. In Paleochori Bay a strong hydrothermal influence is manifested by a yellow-orange (arsenic sulfide) precipitate on the sediment surface [49, 142], together with high temperature (> 85 °C) and low pH values (~5) [143]. Surrounding the yellow areas, white microbial mats are present at midrange temperatures (~45 to 85 °C), covering the most extensive areas of the bay characterized by sulfur and silica mineralogy [123, 143, 144]. In the outer rim of the hydrothermally influenced sediment, lower temperatures (~30 - 35°C) and the accumulation of Fe- and Mn-oxides are manifested as brown surface structures. Arsenic sulfide precipitation in Palaeochori Bay can be explained by the high concentration of soluble sulfide (HS^-, S^{2-}) present in the fluids (~3 mM) [49, 134], which, together with the low pH, and reducing conditions, can trigger the generation of several insoluble arsenic sulfide species [79]. Interestingly, the arsenic sulfide precipitate that accumulated on top of and within the sediments had a size 10^4 times larger than any As-S artificially produced nano-material (Table 1.2) [49], including As_2S_3 quantum dots formed by cluster mediated transformation from orpiment bulk material or As_2S_3 nano-film generation through chemical bath deposition (Table 1.2) [59, 75]. Among the different arsenic forms described to date, it was never found as a nanomaterial occurring in nature (Table 1.2) [131]. So far, As had been widely studied regarding its distribution as soluble species, complexation or adsorption into the particulate (> 400 nm), colloidal (< 400 nm) or truly dissolved (< 20 nm) fractions of organic matter and Fe in the water column [15, 46, 47, 145-147], without considering individual As NPs. The World Health Organization (WHO) guideline value for As in drinking water was established at 10 µg L^{-1}, although many countries operate with a limit of 50 µg L^{-1} [148]. In a similar way, the aquatic life ambient water quality criteria provided by the US-Environmental Protection Agency (EPA) limited the presence of As (in any oxidation state) to 69 and 36 µg L^{-1} for acute and chronic exposure, respectively, in saltwater systems. These criteria for As regulation in aqueous environments only consider soluble As (< 400 nm), and do not consider particle size variables, e.g., nanoparticles, as being part of the soluble As concentrations and with a potential different toxic impact than the "truly" dissolved species (< 20 nm) [149-152]. Thus, the identification of As in a nanoparticulate fraction (200-20 nm) could be crucial for the understanding of As dispersion and bioavailability.

Milos is a promising natural model site to study arsenic in the nanoparticulate form, and provides an opportunity to understand the formation of As NPs and their potential impact on marine organisms. The present work describes, for the first time, the identification and chemical characterization of As- and S-rich NPs found in seawater, porewater and hydrothermal fluid in Palaeochori and Spathi Bay and discusses the potential influence of As NP emissions to the coastal ocean biogeochemistry. With the present study, we want to contribute to the generation of an expanded vision of arsenic transport and toxicity, taking the unexplored but potentially significant fraction of As NP into account.

3.2 Materials and Methods

3.2.1 Sample collection and determination of environmental parameters

During two sampling campaigns in June 2016 and June 2017 hydrothermal fluids (HF), porewater (PW) and seawater (SW) samples were collected by SCUBA divers. Diffusively venting hydrothermal fluids were collected using a funnel system connected to a polyester heat resistant bag with a valve for gas release [153]. The system was placed over a venting spot in order to avoid mixing of hot hydrothermal fluids with seawater. Collection of PW samples was from a sediment depth of 10 cm using 60 mL syringes connected with a polypropylene tube to a perforated 5000 μL pipette tip [92, 134]. Seawater samples were taken manually by opening cleaned 1 L borosilicate glass bottles (SCHOTT) approximately 50 cm below the sea surface to ensure collection of a representative sample, avoiding major-element accumulating biofilms or other surface phenomena [153-155]. Hydrothermal fluids, PW and SW samples presented in this work correspond to two specific venting sites designated in the literature as Spathi Bay (SB) and Rocky Point (RP) (Figure 3.1) [92, 156]. One HF sample (HF1), two PW samples labeled as yellow1 (Y1) and brown1 (B1), and one SW sample (SW1) were collected from the RP area during the campaign in 2016. The names of PW samples were assigned based on the typical color of the sediment surface precipitates, where yellow precipitates are related to the arsenic sulfide minerals previously described in Godelitsas et al. (2015) and brown to precipitates rich in Fe and Mn oxyhydroxides [134]. Y1 was the nearest sample to the venting center (~ 50 cm) and B1 the farthest away (~ 2 m). An extra SW control sample (SW2-Pollonia) was collected on the north shore of Milos from an area without hydrothermal activity (Figure 3.1) [123]. Additional samples of HF and PW were collected during the campaign in 2017 in the areas of RP (HF2) and SB (yellow2, Y2). All plastic and glass material used in the field was cleaned 3 times with 10 % HCl and de-ionized water (18 Ω, Ohm).

Temperature was measured in situ at 10 cm depth using a handheld temperature-probe in a custom-built underwater housing described previously [117]. The pH was determined using a portable pH-meter (Myron L) immediately after the samples were brought on-shore.

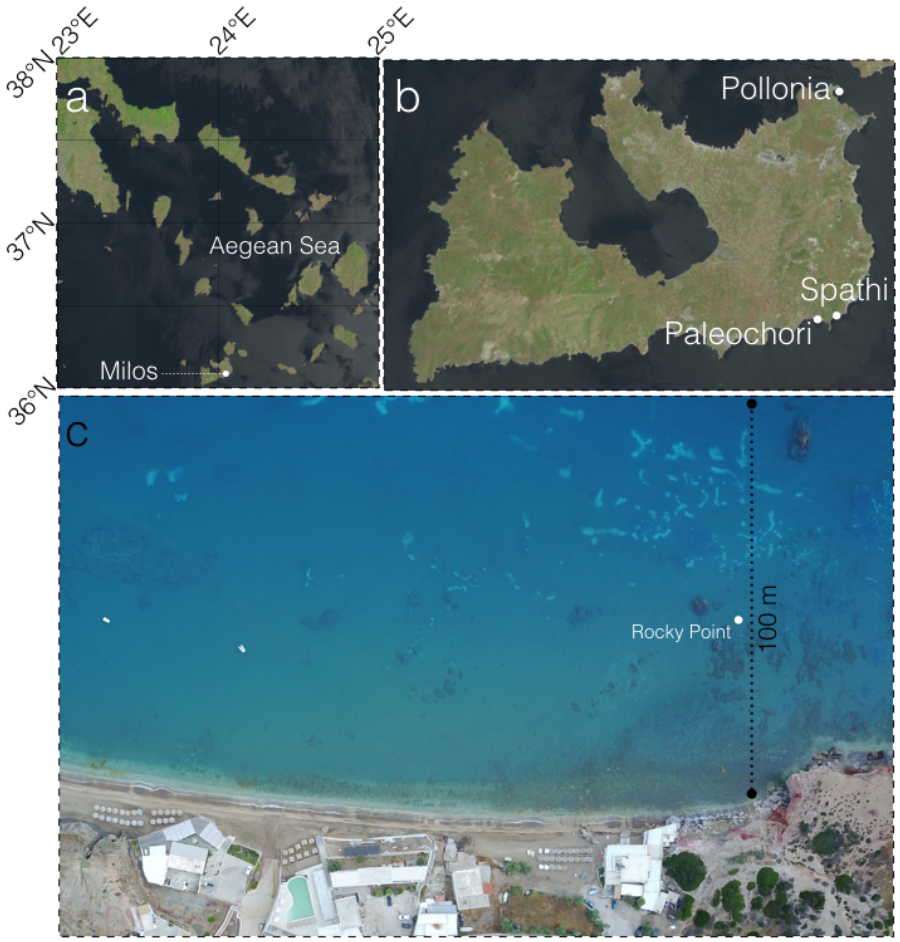

Figure 3.1. Location map and areas sampled during Milos campaign 2016 and 2017. a, Regional map showing the location of Milos Island, situated in the Aegean sea in front of the cost of Athens. b, shows the studied areas off the island. In the north, seawater samples (Pollonia, 36°45'N 24°31'E) were collected and in the south, the bays of Paleochori (36°40´N;24°30´E) and Spathi (36°40´N; 24°31´E) for hydrothermal fluids and porewater samples collection. Images were provided by USGS GloVis, using the data set of Landsat-8. c, drone image of the Paleochori Bay with a dashed line indicating the first 100 m of the total transect sampled, starting at 36°40´29´´N and 24°30´58´´E. Rocky Point area where HF1, HF2, Y1, B1 and SW1 were collected its located 50 m off shore as indicated in the figure.

3.2.2 Sample treatment and storage

After sampling, HF, PW and SW were divided into subsamples for chemical analyses. Samples for anion analysis were filtered using 0.22 µm pore size polyethersulfone (PES) filters and stored in plastic vials at 4 °C until analyses. The sample splits for cations and trace metal determination were filtered using the same type of filter, acidified with ultrapure concentrated HNO_3 to 1 % acid by volume and then stored at 4 °C [134].

For NP identification and As quantification it was collected at least 450 mL of sample, which was sub-divided into 3 groups of minimum 150 mL; 150 mL or more were kept unfiltered (e.g., $HF1_{uf}$, $Y1_{uf}$, $SW1_{uf}$, etc.), the remaining volume, 300 mL or more of the samples were filtered through 200 nm pore size polycarbonate filters and 150 mL were kept for analysis (e.g., $HF1_{200}$,

$Y1_{200}$, $SW1_{200}$, etc.). Finally, the remaining sample, already filtered through a 200 nm polycarbonate pore size filter membrane was filtered through the 20 nm pore size membranes (e.g., $HF1_{20}$, $Y1_{20}$, $SW1_{20}$, etc.). Filtrations were performed using a tower system connected to a vacuum pump. Each sub-group (1. unfiltered, 2. filtered through 200 nm and 3. filtered through 200 and 20 nm), was divided into 50 mL serum bottles previously flushed with N_2 and stored at 4 °C to avoid oxidation or growth of metallic sulfide particles [21]. Filters were kept at 4 °C in petri-dishes after filtration to further analyze NPs. In parallel, from each filtration process, 4 mL were collected in triplicate and acidified (1 % HCl) for As quantification in the fraction between 200 and 20 nm (As_{200-20}). A full list of samples can be found in the Supplementary Material section (ST 3.1)

For physical and chemical characterization, a NP extract was obtained by centrifugation of the sample in ethanol. The samples were first dialyzed overnight with a 12 KDa (< 10 nm) membrane and then diluted 1:2 with ethanol as described for the flocculation of metallic chalcogenide particles and other colloidal metal oxide NPs (i.e., AuO_2, ZnO, CeO_2, CdS, CdSe or CdTe) [157-161]. Finally, centrifugation was performed at 13000 g for 1 h at room temperature. The centrifugate was rinsed 3 times with Milli-Q water and suspended in ethanol for storage at -20 °C.

3.2.3 Geochemical analysis

Anion determination was performed by ion chromatography using a Metrohm IC system. A Perkin Elmer Optima 7300 DV inductively coupled plasma-optical emission spectroscopy (ICP-OES) was used for cation quantification [162]. Samples for ICP-OES analysis were brought to a 3 % HNO_3 (weight/volume; w/v) dilution to reduce problems of salinity and organic matter present in the sample.

3.2.4 Quantification of As

Hydride generation atomic fluorescence spectrometry (HG-AFS) was used to quantify trace concentrations of arsenic in fluid samples. The samples were prepared by adding 5 mL analytical grade 37 % HCl and 0.6 mL potassium iodide/ascorbic acid solution (40 % (w/v) potassium iodide, ≥ 99.5 % purity) and 10 % (w/v) ascorbic acid (≥ 99 % purity in water) to ≤ 20 mL sample. The solution was filled up to 30 mL with de-ionized water and left standing for a reaction time of at least 30 min before quantification with the Millennium Excalibur system (PS Analytical, UK) [162]. An aqueous solution of 0.7 % (w/v) sodium borohydride in 0.4 % (w/v) sodium hydroxide (Analytical grade) was mixed with the sample for the generation of arsenic hydrides from the samples and the development of hydrogen, the fuel gas for the flame. The limit of detection for the set-up was 20 ng L^{-1} As [162-164]. The fraction of As_{200-20} was calculated as the difference between the As concentration in As_{200} and As_{20}.

Arsenic concentrations were furthermore determined by HG-AFS for 17 samples collected along a surface and bottom transect in Paleochori Bay for the fraction As_{200} (< 200 nm). The distance between the individual samples was 20 m and thus the transect extended for approximately 320 m perpendicular to the beach (Figure 3.1). Samples were collected manually by divers (1 meter below the surface and 1 meter above the seafloor) using 20 mL syringes. Each sample was analyzed in triplicate to evaluate precision. The accuracy of the measurements was verified by adding a blank and drift monitor solution after every 5 samples while using the NIST Trace 1643e and IAPSO K15 solutions as external certified references. Analytical uncertainty was determined to be better than 3 %.

3.2.5 Electron microscopy

Unfiltered samples were analyzed by low voltage scanning electron microscopy (SEM) with energy-dispersive X-ray analysis (EDX) for NP detection and elemental analysis. After vigorous mixing, 50 µL of sample were gently poured over carbon-stickers on top of an aluminum holder and once dried were coated with C to increase electrical conductivity required for EDX analysis. A field emission microscope (Zeiss, model iSUPRA 40) with an EDX detector (Bruker, XFlash 6 | 30) was operated at 4-8 kV for higher resolution imaging, while an acceleration voltage of 20 kV was used for elemental analysis [165].

The filters used for HG-AFS quantification of $As_{200\text{-}20}$ fraction where As-NPs were detected were also analyzed by SEM-EDX. The filters were cut with scalpels, rinsed by pouring Milli-Q water on the edges of the filter to avoid detachment of NP and then dried at room temperature. Afterwards, using a plastic tweezer, the filter pieces were placed on carbon stickers for SEM-EDX analysis.

An extract of NP suspended in ethanol was obtained as described above and used to study particle morphology, crystal phase, chemical composition and size distribution by Transmission Electron Microcopy (TEM), Selected Area Electron Diffraction (SAED) and EDX coupled to TEM. The suspensions were diluted (1:10 and 1:100) and sonicated (probe sonicator) for 10 min at 40 % (intensity) on ice and immediately thereafter 4 µL were dispensed on copper grids and dried overnight at room temperature. Samples were analyzed using a TEM Philips CM 20 operated at an acceleration voltage of 80 kV. Non-aggregated samples were chosen for SAED and EDX in a FEI Titan 80-300 kV microscope.

3.2.6 Dynamic light scattering

Poly-dispersity index (PDI) and size distribution were studied by dynamic light scattering (DLS) using a Malvern-Zetasizer DLS system. For size distribution analyses, ethanol (HPLC grade) was used as dispersing agent and the diffraction index of the material was assumed as As_2S_3 with a value of 2.63 [166, 167].

3.3 Results

3.3.1 Environmental parameters

Several parameters (temperature, pH, salinity, etc.) were evaluated to better understand NPs in the context of hydrothermal activity [92, 117]. Table 3.1 summarizes the pH and temperature values of hydrothermal fluids, porewater and seawater collected during the expeditions in 2016 and 2017 in Paleochori and Spathi Bay. The seawater sample collected in Paleochori Bay as a control (SW1), showed a low pH (~6.8), compared to average seawater, which indicates hydrothermal influence. For this reason, a second seawater control was taken at a location far removed from any hydrothermal activity (SW2-Pollonia) [123]. The hydrothermal fluids (HF1 and HF2) had high temperatures and low pH values (Table 3.1). Porewater samples (Y1, Y2 and B1), denoted a significant increase in temperature, whereas the pH remained rather constant, being close to 5.4, reflecting the values of the temperature and pH of the hydrothermal fluids (HF1 and HF2, Table 3.1). The data indicates that the pH remains between 4 and 6 across a broad range of temperatures, from ~40 to 100°C.

Table 3.1 Environmental parameters for fluid samples collected during this research; Milos expedition 2016 and 2017.

Sample	Temperature (°C)	pH
HF1	83.9	5.37
HF2	96.4	5.91
Y1	99.0	4.72
Y2	65.0	5.24
B1	38.1	5.56
SW1	23.4	6.76
SW2-Pollonia	21.4	8.09

3.3.2 Geochemistry of hydrothermal fluids and seawater

Previous research In Milos, showed two distinct types of fluids discharge from the submarine vents, often within a few meters from each other: (1) a high-Cl fluid (enriched in Cl by up to 47 % relative to seawater), which is depleted in Mg and SO_4 and enriched in major (Na) and trace elements (As, Br, Fe, Mn and Si), and (2) a low-Cl fluid, depleted in Cl by up to 66 % relative to seawater, with additional depletions in Br, Na, Mg and SO_4 [134]. As previously mentioned the RP site fluids have chemical characteristics similar to the high-Cl fluids described above [134]. Thus, for samples taken from that site, we anticipated chemical compositions somewhere between the high-Cl endmember and unaltered Eastern Mediterranean seawater i.e., the control sample SW2-Pollonia. Hydrothermal fluids (HF1 and HF2) showed an increase in concentrations of Na, Cl, Si, and Mn and a decrease in SO_4 and Mg compared to SW2-Pollonia (Table 3.2). Porewater samples (Y1, Y2 and B1; Table 3.2) also

showed an influence of hydrothermal activity in their geochemical compositions, with values correlating to those found in the hydrothermal fluids (HF1 and HF2; Table 3.2).

There was a significant difference in the Fe content among the fluids. For example, in porewater sample B1 (Table 3.2) Fe reached concentrations close to 300 μM, while in the hydrothermal fluids the element was not detected. These results correlate with data from Yücel et al., 2013b where the soluble Fe concentrations were analyzed along a transect of a venting spot and was only present in porewater samples collected further away (>0.5 m) from the center of the vent [112]. This is likely caused by subsurface precipitation of Fe-S and quantitative removal of Fe from the fluids [117, 168]. Finally, other elements were variably enriched or depleted compared to SW2-Pollonia (Table 3.2). An alternative way to evaluate the influence of hydrothermal activity is the amount of seawater entrainment in the samples. This common evaluation assumes that Mg is quantitatively removed at higher temperatures in the hydrothermal system, and thus any Mg in the sample is derived from seawater (prior collection). By this calculation, the sample with the least seawater entrainment is porewater Y2, with only 12 % seawater, and the one with the highest entrainment was porewater B1, with approximately 80 % (Table 3.2).

Table 3.2. Chemical composition of hydrothermal fluids (HF), porewater (PW) and seawater (SW) samples from Milos campaign 2016 and 2017.

	HF1	HF2	Y1	Y2	B1	SW2-Pollonia
Major Elements (mM)						
Cl	710.3	878.6	711.6	919.7	944.8	645.6
SO_4	20.1	8.5	26.1	6.71	13.3	32.6
Mg	39.8	25.8	24.2	6.5	41.8	52.5
Na	577.6	615.3	673.4	609.4	513.4	486.9
Trace Elements (μM)						
Br	901.1	1175.1	994.9	1138.8	1197.7	964.9
Fe	b.d.	b.d.	9.5	b.d.	300.4	1.8
Mn	3.1	0.5	84.4	1.8	46.2	b.d
Si	106.3	3594.9	3484.8	2516.6	1261.7	40.9
%SW	76	49	46	12	79	100

b.d. below detection limit. %SW: Percentage of seawater present in the sample.

3.3.3 Arsenic quantification

In order to understand the relevance of As present as a NP, total As was quantified by HG-AFS in the fraction filtered with 200 nm (As_{200}) pore-size membrane and the fraction obtained through filtration using 200 and 20 nm (As_{20}) pore-size membranes as described before. The analysis revealed the presence of arsenic in the size range between 200 and 20 nm ($\%As_{200-20}$, Table 3.3), starting from 5 % in hydrothermally influenced seawater (SW1) to 38 % in the porewater (Y1, Table 3.3). The diffusively discharging hydrothermal fluids (HF1 and HF2) also contained elevated As in the same fraction, with 12 and 20 %, respectively (Table 3.3). Furthermore, when the hydrothermal fluid endmember concentration is considered, the distribution of arsenic in the fraction between 200 and 20 nm seems to be related to seawater mixing, exhibiting a high $\%As_{200-20}$ with a high As_{200-20} endmember concentration when lower seawater mixing occurs, which suggests a dissolution effect. However, arsenic displays non-conservative behavior in the water column, being influenced by phenomena like coprecipitation with Fe oxide particles which should be considered [139].

In order to comprehend the influence of overall As fluxes and transport in the bay the distribution of As in the seawater along the venting area was evaluated. Figure 3.2, shows two transects of soluble arsenic transport within Paleochori Bay (at the surface and close to the bottom). Both transects show clear maxima near to the venting area, with values around 7 and 3 $\mu g\ L^{-1}$ in the bottom and in the surface, respectively. Those values decrease with distance from the area of hydrothermal activity, until reaching a value around 1.5 $\mu g\ L^{-1}$, which is considered the average concentration for seawater [148].

Table 3.3. Trace arsenic quantification in the nanoparticle fraction of fluids (i.e., the filtrate) from the hydrothermal system of Milos.

Sample	As_{200}	A_{20}	As_{200-20}	$\%As_{200-20}$	As_{200-20} (EM)
HF1	0.426	0.373	0.053	12.44	0.220
HF2	6.234	4.934	1.3	20.85	2.549
Y1	4.924	3.051	1.873	38.04	3.469
Y2	2.691	1.996	0.695	25.83	0.790
B1	1.312	1.151	0.161	12.27	0.767
SW1	0.094	0.089	0.005	5.32	0.005
SW2-Pollonia	b.d.	-	-	-	-

b.d. below detection limit. - : not analyzed. All the sample were analyzed in triplicates by HG-AFS. Standard deviation values ranged between ±0.001 to 0.12. All the concentrations are given in μM scale. EM: endmember concentration.

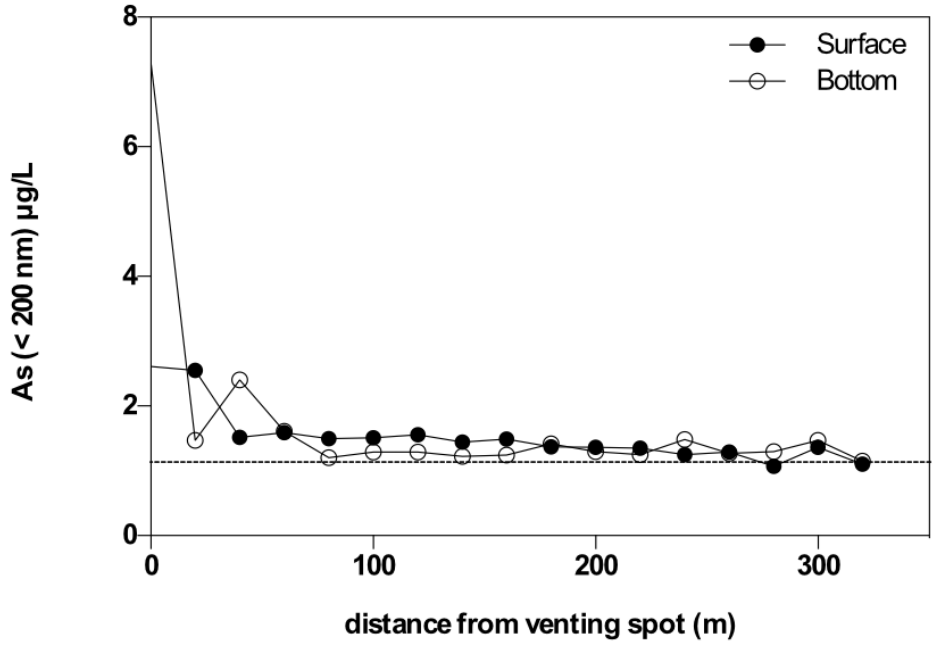

Figure 3.2 Arsenic quantification in a transect along the bay of Paleochori during expedition Milos 2016. Samples of seawater were obtained in two parallel transect, in the surface (black circles) and close to the bottom (white circles). Samples were collected every 20 m approximately starting on top of a the venting spot close to the shore extending from 36°40′29′′N, 24°30′58′′E to 36°40′7′′N, 24°30′58′′E. The dashed line marks the average concentration of the last sample collected in the transect an is used as a background value of the area.

3.3.4 Nanoparticle identification

As a first approach, SEM-EDX analysis of unfiltered samples allows a general overview of the particle diversity. Unfiltered samples of hydrothermal fluid ($HF2_{un}$) and porewater ($Y1_{un}$ and $Y2_{un}$) showed a uniform presence of aggregated spherical particles with diameters ranging from 50 to 200 nm (Figure 3.3). Despite the difference in location and sampling time, all particles had a similar morphology (Figure 3.3a-c). In all areas of the samples, EDX spectra showed similar elemental compositions, indicating NPs rich in As and S with minor presence of Cl and K (Figure 3.3d). To the best of our knowledge, this is the first description of naturally occurring As-rich NP associated with marine hydrothermal activity.

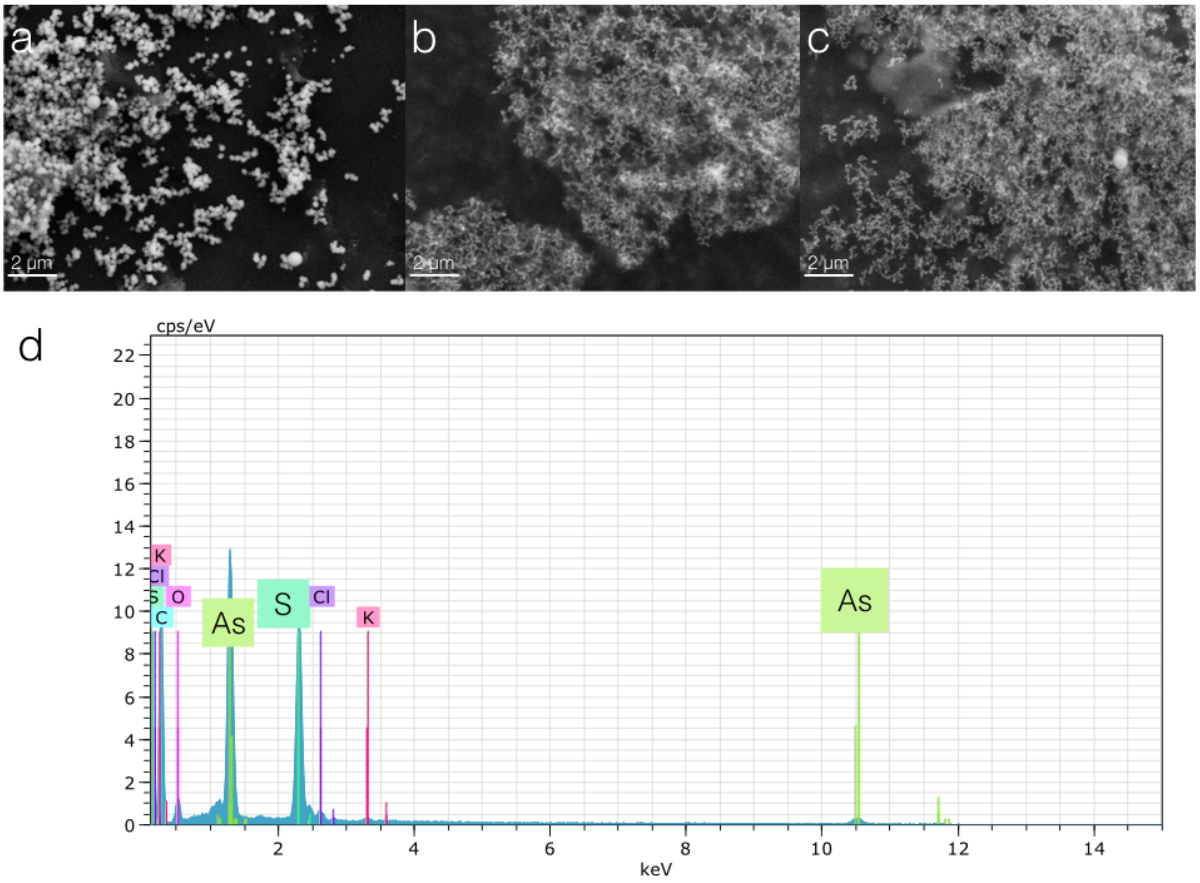

Figure 3.3. SEM-EDX analysis of As-S NP from unfiltered samples of hydrothermal fluids and porewater samples. Spherical nanoparticles with a size between 50-200 nm were found in hydrothermal fluids HF2, a; porewater samples Y1, b; and Y2, c. d, EDX spectrum of particles from hydrothermal fluid HF2, enriched mainly in As, and S, with minor contributions of other elements like Cl and K. EDX analysis was repeated in different zones of the sample and in all the areas sampled, showing similar results (data not shown).

In the hydrothermal sample $HF1_{un}$ micro- to macro-particles with highly irregular structures were found (Supplementary Figure 3.1, SF 3.1). The EDX spectra showed peaks for Fe, S and Si (F3.4c) indicating the presence of FeS or FeS_2 with some enrichment in silica as suggested in the literature [21, 29]. Nevertheless, no nano-structures associated with As were observed. Sample HF1 was collected in a spot with abundant streams of gas bubbles where FeS or FeS_2 precipitation took place. Indeed, precipitation of Fe sulfides from hydrothermal gas was observed in other, similar shallow-water hydrothermal systems [169]. This may explain the absence of NPs in this sample, as it is not a true fluid sample like $HF2_{un}$, but a mixture of hydrothermal gas and seawater.

Porewater $B1_{un}$ had a uniform particle population with a grain-aggregated morphology and particle sizes above 200 nm (Supplementary Figure 3.2, SF 3.2). These aggregates were enriched in Fe, Si and O, which correlated well with the elemental composition of the fluids (SF3.2 and Table 3.2, respectively) and with the precipitation of silica-rich Fe oxyhydroxides described for other shallow Fe rich hydrothermal systems [170]. However, no As was present in the EDX spectra and no other NP structures were identified. The rest of the unfiltered samples showed no representative abundances of defined particles or structures. Although seawater (SW1) could have been influenced due to mixing with hydrothermal fluids, no As, S, Fe, or Si NPs were found (data not shown).

Even though the analysis of unfiltered samples allows an overview of NP presence, the precipitation by simple evaporation (see material and methods section) of the different compounds present in the sample could alter the amount, morphology, size or elemental composition of the particles. In order to distinguish natural NP from possible artifacts, filters used for $As_{200\text{-}20}$ quantification in sample HF2 were also analyzed by SEM-EDX. Figure 3.4 shows the presence of different sized nano-spheres trapped on the 200 and 20 nm pore size membrane filters (Figure 3.4a-b). The presence of the particles on both filters confirms the existence of an As-rich NP fraction in the hydrothermal fluids. Figure 3.4c summarizes the elements atomic weight percentage [Atm.%] obtained from the EDX analysis where the spectrum showed only As, S and O peaks. When compared to an orpiment powder standard the sample had a slightly different As:S ratio (0.66; Figure 3.4c), which was most likely due to a higher oxygen and a lower arsenic and sulfur content in the sample. This suggests the presence of oxidized forms of As or S (arsenic trioxide, arsenic pentoxide, sulfate etc.) as part of an arsenic-sulfur material different from orpiment.

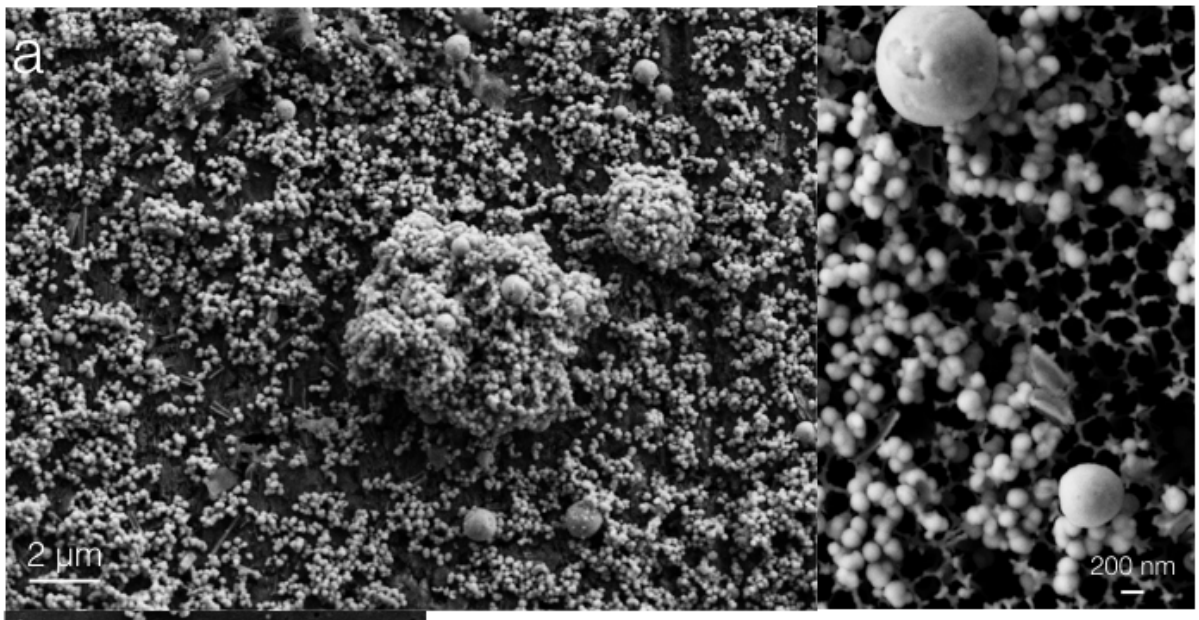

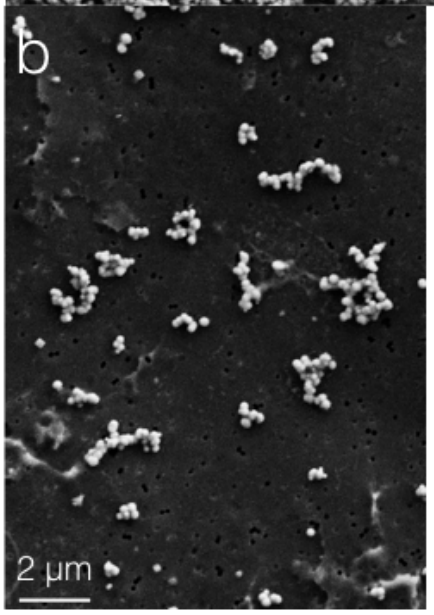

c

	As-S NP	Orpiment
	[At.%]	[At.%]
C	0	0
O	24.56	3.49
S	50.99	58.14
As	24.45	38.37
As/S	0.48	0.66

Figure 3.4. SEM-EDX analysis of As-S NP collected by filtration of hydrothermal fluids from the shallow hydrothermal system off Milos. Images of the nanoparticles present in HF2 trapped on a filter of , a, 200 nm pore size are shown in two different magnifications (left and right), and of , b, 20 nm pore size. c, Table with the atomic weight percentage (At.%) from EDX spectra of sample HF2 showing an As/S ratio between values of each element. Orpiment values were obtained from a fresh orpiment powder used as standard. At.% were normalized according to C content.

3.3.5 Nanoparticle characterization

Based on the results of the NP identification, a concentrated fraction of NPs from the sample $HF2_{un}$ was obtained by ethanol precipitation as described in materials and methods. TEM analyses showed a detailed image of the spherical structures described previously with diameters ranging between 100 and 150 nm (Figure 3.5a). Typically, amorphous materials present a ring pattern during electron diffraction, which was observed (Figure 3.5b) indicating the absence of a crystalline structure. The same area was analyzed by EDX confirming that the amorphous NP consists of mainly As and S, while at the same time discarding the presence of the crystalline mineral orpiment (Figure 3.5c). Finally, DLS experiments determined a PDI value of 0.37, which implies a polydisperse size distribution of the particles with a peak size close to 100 nm and an average diameter size of 245 nm (Figure 3.5d), which was in accordance with the microscopic analyses (Figure 3.4 and 3.7a).

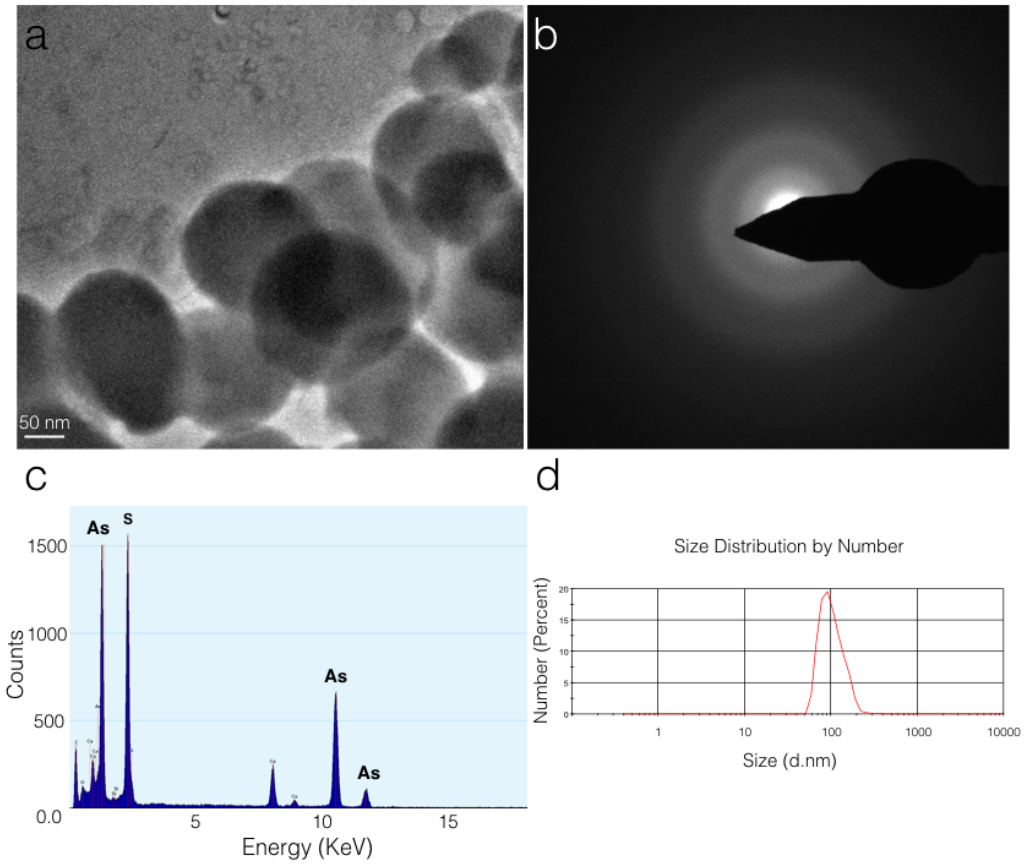

Figure 3.5. Characterization of As-S NP present in hydrothermal fluids from the shallow hydrothermal system of Milos. a, HR-TEM image of the nanoparticles precipitated by centrifugation from sample HF2 in ethanol (1:2). b, Selected area electron diffraction of NPs from sample HF2. The patron shows no crystal phase associated to the selected area of analysis. c, EDX spectrum of the selected area showing peaks only for As and S. The Cu signal represents artifacts from the grid used during the analysis. d, DLS analysis of nanoparticle suspension in ethanol showing a peak size of 91 d.nm, an average size of 245 d.nm. and a PDI of 0.37.

3.4 Discussions

3.4.1 Formation of As-S NP under hydrothermal conditions

The shallow-water hydrothermal system in Paleochori Bay presents remarkable environmental characteristics that lead to the formation of As-S NPs. Fluids enriched in As^{+3} and sulfide (HS^- ,S^{2-}) are probably the significant drivers of this phenomenon [134]. It was suggested that arsenic sulfide species [49], can precipitate on the seafloor as poorly-crystalline arsenic sulfide when the hydrothermal fluids mix with oxygenated seawater [49, 134]. Among those several arsenic sulfide species, di- and tri-thioarsenite monomers, dimeric or trimeric arsenic sulfur and orpiment can result from a fundamental ratio between As and S present in solution at pH values around 4 - 6 [79]. Furthermore, a study of solubility of amorphous As_2S_3 in the temperature range from 25 to 90°C found that the decrease in temperature and pH are the dominant mechanisms for the precipitation of amorphous As_2S_3 in hot spring systems [125]. Hence, in Paleochori Bay the increase in pH as a result of seawater mixing with hydrothermal fluid is not considered as the main driving mechanism of formation, rather the reduction in temperature could be the key parameter inducing the precipitation of As-S NPs. It is important to note that hydrothermal fluids HF2 and pore water samples (Y1 and Y2), in which the NPs were detected, presented a yellow coloration at the moment of filtration, which indicates the presence of As-S rich material. The filtration took place immediately after samples were brought to on-shore facilities. A sampling or storage effect, by reducing the temperature of the sample cannot be completely excluded. Yet, since results were reproducible with unfiltered samples, even after a week of fieldwork, without showing aggregation or bigger particle size due to storage at low temperature (4°C), we assume an insignificant influence from sampling and storage. Therefore, the NPs characterized from the HF2, Y1 or Y2, are very likely to be occurring at the sediment-water interface as diffusively venting fluids mix with seawater (%SW, Table 3.2).

There is a significant body of literature about temperature relevance in NPs synthesis. Kinetic studies in NP generation highlight the importance of temperature in controlling the size during events of nucleation and growth [171, 172]. In the case of chalcogenide materials, which consist of a metal or metalloid (e.g., As) and an element from group 16 of the periodic table (e.g., S, Se, Te, etc.), the synthesis of NPs can be achieved by solvothermal methods that constitute hydrothermal conditions similar to those present in Paleochori Bay (aqueous solvent, 30-90°C, pH 4-6 etc.) [171, 172]. Solvothermal synthesis corresponds to solution-based reactions carried out near the boiling point of the solvent, to prepare thermodynamically stable and metastable species that will take part in the formation of a new solid phase (nanoparticles) through nucleation events [172]. The nucleation mechanisms of NPs have been discussed in depth in literature since they represent a key step in controlling size, morphology, and other properties of particles [173-175]. The nucleation rate of a nanoparticle, strictly depends on the temperature control over supersaturation of the species in solution [174]. Since most of the arsenic sulfide species have a low solubility at 25 °C [125], a continuous temperature decrease of the initial As and S rich end-member fluid (> 90°C) by diffusive discharge along the sediments will favor supersaturation of arsenic sulfide species and increase nucleation rate, enhancing the generation of a new phase that precipitates as amorphous nanoparticles. This also explains the lack of As-S NPs in samples with low As concentrations (HF1 and B1, Table 3.3), probably not reaching

supersaturation conditions or nucleation rates high enough to sustain the formation of the particles. A simple way to determine saturation indices of arsenic sulfide species in the different samples is the use of "geochemical reaction models". Yet, arsenic sulfur species (e.g., As_2S_3, mono-, di-, thioarsenate or thioarsenite) present in the NPs remain unclear. The SAED analysis of the particles (Figure 3.5b) indicates an amorphous material and the EDX spectrum (Figure 3.4c) shows a ratio of As:S ratio differing from As_2S_3. This suggests that a pure precipitation of orpiment or amorphous As_2S_3 during NPs formation is unlikely, but rather a participation of more than one arsenic sulfide species might occur. On the other hand, nucleation mechanisms are not considered under equilibrium condition of simple geochemical models, and even more, the nucleation of amorphous nanoparticles is poorly understood and normally crystalline nucleation models are assumed [174, 175]. The work of Jun et al., (2016) represent a tremendous effort to understand in situ and real-time effects on water chemistry and substrate identity on nanoscale precipitates. They used simultaneous small-angle and grazing incidence small-angle X-ray scattering (SAXS/GISAXS) to study interfacial energies between nuclei and surfaces during Fe and $CaCO_3$ nanoparticles formation [176], which if coupled to X-ray absorption near edge structure (XANES) can also be used to determine arsenic sulfur species present in the NP and the thermodynamic parameters of nucleation. This could be examined in future studies to generate geochemical models of nanoparticle precipitation under hydrothermal conditions.

3.4.2 Importance of nanoparticles for As cycling in the coastal ocean

Our study reveals the presence of an significant percentage of As in the nanoparticulate fraction (200-20 nm, Table 3.3) in hydrothermal fluids and porewater samples, which raises the question of how surrounding biota interact with this phenomenon. For As-S NP, to the best of our knowledge, no studies on their biological effect in a natural marine environment have been performed, but investigations on cancer cells showed their enhanced bioavailability causing programmed cellular death (apoptosis) and anti-migration (metastasis) effects [66-73]. Changes in bioavailability due to particle size can have direct toxic implications for the inhabiting organisms of a marine ecosystem. As mentioned before, metallic and metalloid sulfide materials have low solubility in aqueous solutions (pH 4-6, 25°C) and aggregation of colloidal material can occur. Therefore, a vast majority of the arsenic sulfide particles, including the amorphous As-S NPs may (1) destabilized and dissolve, and/or (2) sink to the seafloor surrounding the venting area. The first scenario implies a direct relation between stability of particles and pH, which has been described for amorphous As_2S_3 with increased solubility at pH 6-8 [125]. In the dissolution experiments of amorphous As_2S_3 by Eary (1992), arsenous acid (H_3AsO_3) was the dominating species in acidic (pH ~ 4) sulfide-deficient solutions, and when an excess of sulfide was present, $H_2As_3S_6^-$ was the main soluble specie [125]. The dissolution and oxidation of amorphous arsenic sulfide were also studied by others [177, 178]. During dissolution experiments at pH 5 to 8 with or without O_2, S species can vary from $H_2S(g)$ (pH 5, no O_2), to elemental sulfur and polysulfides (S_n^{2-}),being the most common formation pathway of polythionates (S_nO_6; pH 6-8) [177, 178]. On the other hand, As^{+3} can account from the 96 % of arsenic species dissolved (pH < 6) to 76 % (pH 8) when no O_2 was present, while in O_2 rich solutions at pH 8 the percentage can decrease to a value below 50 % [177, 178]. Hence, NPs either in the water column or in the porewater are being destabilized by an increase in pH and

along a decreasing gradient of soluble sulfide concentrations as it occurs in Paleochori Bay [45, 88, 134, 168]. This correlates with the distribution of arsenic resistance genes in microbial communities in porewater around venting areas of Paleochori bay as described by Fru et al. (2018). The study of As^{+3} oxidase (*aox*B) and As^{+3} membrane extrusion (*acr*3-1, *acr* 3-2 and *ars*B) genes along a gradient of soluble sulfide, showed a decrease in abundance of arsenic resistance genes when a higher concentration of sulfide was present in the pore-water, suggesting a sequestration of As^{+3} in sulfide minerals and therefore a lower interaction with the microbial community due to reduced mobility [88]. A similar phenomenon could explain the stability of the amorphous As-S NPs, the closer they remain to the venting spot, the more stable the conditions are (pH < 6, high [HS^-,S^{2-}]), avoiding dissolution and oxidation and therefore decreasing their toxicity.

On the other hand, various microorganisms exists that are able to gain energy for growth from arsenic (e.g., arsenotrophy) [89, 164, 179]. The three main types of arsenotrophs far known to occur are heterotrophic arsenite oxidizers, chemotrophic arsenite oxidizers, and dissimilatory arsenate-reducing prokaryotes [180]. Prokaryotic diversity at Milos was evaluated by comparative analysis of 16S rRNA clone sequences and *aio*A-like (arsenic oxidation) functional genes (AFGs). The results indicated AFGs affiliated with either *Alphaproteobacteria* or *Betaproteobacteria* distantly related to described representatives. Most clones (89%) were originated from a deeper layer of low salinity and high soluble arsenic concentrations, which overlap with the 16S rRNA data, suggesting arsenotrophy as a metabolism present in Milos that operates best at low salinity, and under anoxic, dark, sulfide and arsenic-rich conditions. However, the metagenomic analysis of the microbial community associated to an As^{+3} and As^{+5} gradient in Milos [88], indicated the predominance of genes regulating up-take and extrusion of $As^{+3/+5}$ over genes related with the use of As as an electron donor/acceptor, suggesting a low probability for the amorphous As-S NP to be used as a source of energy.

Another possibility is the use of the As-S NP to sustain sulfur-oxidizing metabolisms. In Milos, the white mats are dominated by sulfur-oxidizing *Campylobacteria* (formerly *Epsilonproteobacteria*) [87, 92, 181], which use soluble sulfide present in the fluids to generate energy for their autotrophic life style. These dissolved sulfide oxidizing microorganisms might get competition by mineral-sulfide oxidizing chemolithoautotrophs using the As-S NP in the upper (sulfide deficient) sediment layers of the hydrothermal sediments of Milos, where soluble sulfide content is low due to reactions with oxidized seawater. A comparable phenomenon has been shown for sulfide deposits of ceased hydrothermal deep-sea systems, were levels of soluble sulfide are decreased, and where metaproteomic data identified autotrophic sulfide-oxidizing *Gammaproteobacteria* potentially facilitating metal-sulfide dissolution from sulfide deposits via extracellular electron transfer [182].

Minerals may also play a role in the stability, and thus distribution, of the As NP fraction. Iron sulfides and oxy-hydroxides are both minerals known to occur in hydrothermal plumes and play an important role for As adsorption and transport, controlling the arsenic concentration in solution [139, 169, 183]. In the case of hydrothermal fluid HF1 (SF 3.1) and porewater B1 (SF 3.2), no As NPs were found, but instead Fe- and S-rich or Fe- and O-rich structures were observed. Precipitates of iron sulfides were described for Lihir Island, Papua New Guinea, due

to the interaction of hydrothermal gas and liquid, seawater, and Fe-rich sediments [169]. When hydrothermal H_2S is in contact with oxygenated seawater, H_2SO_4 is formed, leading to the simultaneous dissolution of primary Fe-rich sediment grains and to the formation of marcasite (FeS_2) and pyrite (FeS_2) [169]. It is possible that a similar mechanism takes place in the formation of Fe and S rich particles found in the sample HF1. In the case of Fe-O rich particles found in the hydrothermal system of Papua New Guinea, the interaction of Fe-rich hydrothermal fluids with seawater appears to be the factor controlling the crystalline formation of Fe(III) oxy-hydroxides during its precipitation at a temperature range between 60 and 93 °C. Additionally, the role of other parameters, such as interactions with dissolved organic matter (DOM), the presence of adsorbing agents (e.g., Fe particles) or ultra violet radiation in the speciation of metals and metalloids in aqueous systems are complex and proven to play a role in a shallow-water hydrothermal system like Paleochori Bay [84, 117, 153, 184, 185]. Dissolved organic matter has showed to be relevant for the mobilization of metals like Cu and Fe in shallow hydrothermal systems [128, 153]. Furthermore, DOM has been established as a key factor during HgS nanoparticle generation and dissolution in natural seawater [186-188]. Therefore, its influence upon the nanoparticulate (200-20 nm) fraction of As might be significant, since it can provide thiol groups (-SH) during nucleation of metal-sulfide complexes, probably facilitating the formation of the As-S NPs and potentially even stabilizing the amorphous phase [186-189].

Finally, in terms of legal regulations, the WHO, established arsenic concentrations in drinking water as harmful if above 10 $\mu g\ L^{-1}$, while the EPA gives maximum concentrations in saltwater systems of 63 and 36 $\mu g\ L^{-1}$ for acute and chronic exposition, respectively. However, all these considerations have been developed without a size range specification of the arsenic fraction including As NP. In Milos, the As-NP fraction can easily exceed these concentration (HF2; $As_{200\text{-}20}$, 1.3 μM or 97.4 $\mu g\ L^{-1}$) and without knowledge of its chemical behavior in different biological and environmental contexts, the bioaccumulation of arsenic cannot be assumed as a simple model of arsenic ionic species released from the NP.

3.5 Conclusions

Amorphous As-S NPs with sphere morphology and diameters around 100 nm are described for the first time in an environmental context, specifically in hydrothermal fluids being released into the coastal Mediterranean Sea. The nanoparticulate fraction (between 200 and 20 nm) represent a significant portion of the total soluble arsenic (below 200 nm) concentration, indicating a possible role in the cycling of As in Paleochori Bay, Milos (Greece). A deeper understanding of As NPs and further analyses about their toxicity is required to improve the knowledge about As geochemistry in aqueous environments influenced by hydrothermal venting.

Acknowledgements

This study was supported by Conicyt through a fellowship to VDT (Programa de Capital Humano Avanzado, BECAS-Chile, CONICYT, 2015) and by the Deutsche Forschungsgemeinschaft (DFG, Germany) through the Emmy Noether-Program (grant BU 2606/1-1 to SIB), as wells as DFG grant HE 7594/1-1 (TP). We would like to thank Reshma Kadam and Daniel Carmona Rioja for their support in the Advanced Ceramics laboratories, Petra Witte for performing SEM analyses, and Rebecca Aepfler and Christopher Vogel for their helpful hands during fieldwork. Special thanks go to Athanasios Godelitsas for providing the orpiment standard and for logistical support in Athens, and to Antonios Vichos and the Artemis Deluxe rooms for their generous hospitality on Milos. Grateful thanks furthermore go to Wolfgang Bach for his insightful comments on the manuscript.

Supplementary Material

Figures

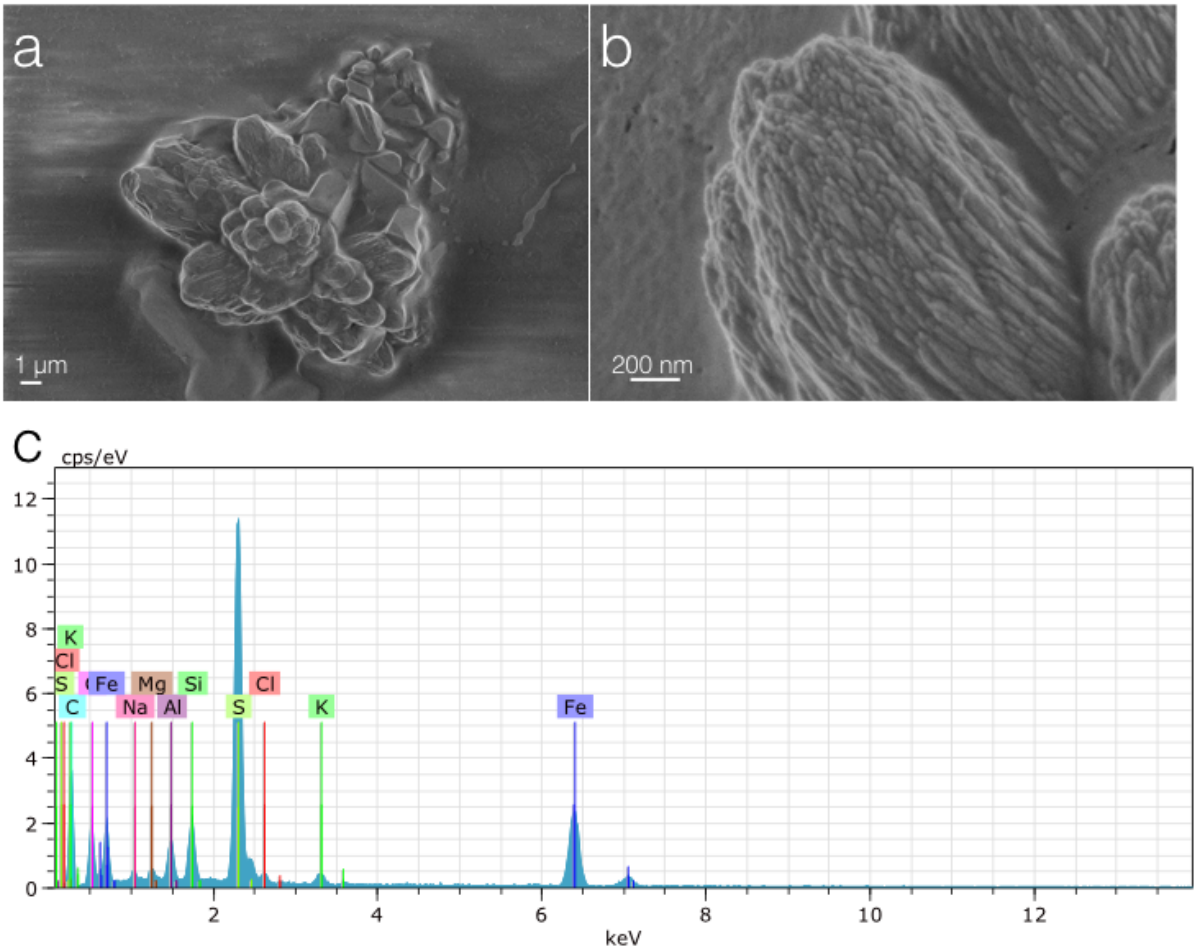

Supplementary Figure 3.1 (SF 3.1) SEM-EDX analysis of Fe-S-Si bulk precipitate present in hydrothermal fluids from the shallow hydrothermal system of Milos. Different magnification of black highly irregular precipitates present in the hydrothermal fluids HF1 (a and b), showed an EDX spectrum (c), enriched mainly in Al, Fe, S and Si, with minor contributions from K, Mg and Na.

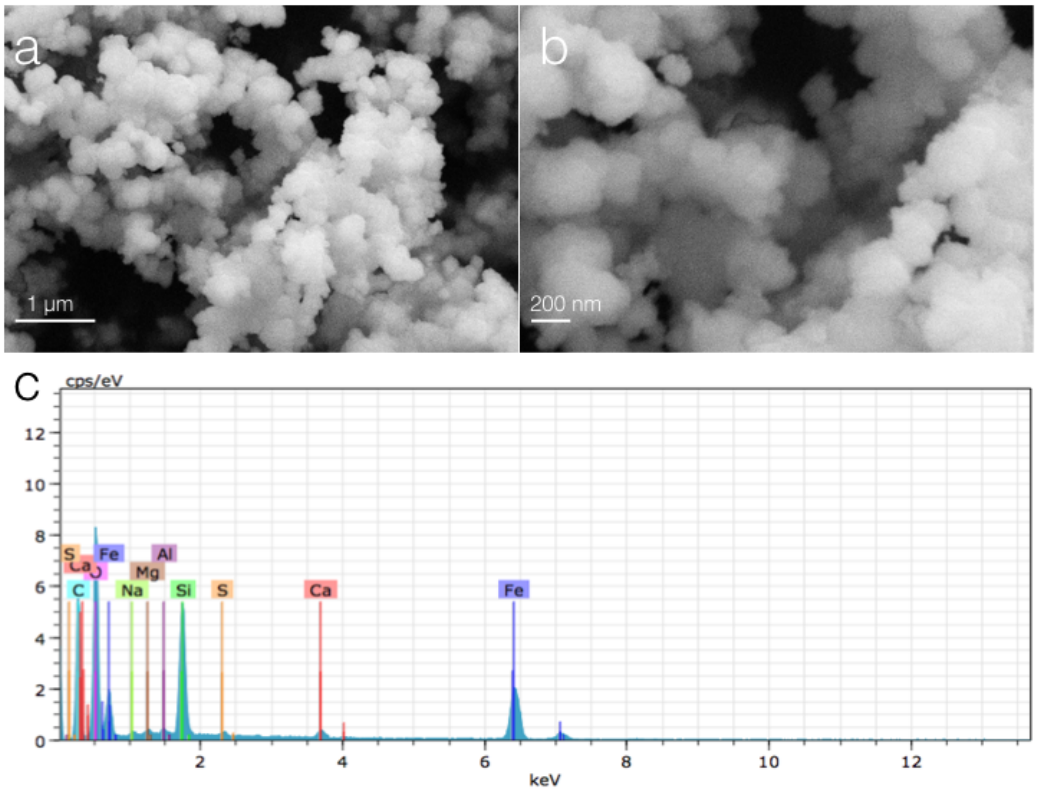

Supplementary Figure. 3.2 (SF 3.2) SEM-EDX analysis of Fe-Si-O suspended particles present in porewater from the shallow hydrothermal system of Milos. Different magnification of orange-brownish material present in the porewater sample B1 (a and b), showed an EDX spectrum (c), enriched mainly in Fe, Si and O, with minor presence of Ca, Mg, Na and S.

Tables

Supplementary Table 3.1 (ST 3.1). List of samples. Milos campaign 2016 and 2017.

Sample	Type	Area	Year	Treatment/Analysis
HF1				
$HF1_{un}$	Hydrothermal Fluid	RP	2016	Unfiltered/SEM
$HF1_{200}$	Hydrothermal Fluid	RP	2016	Filtered (0.2 µm)/Geochemical analysis and As quantification (HG-AFS)
$HF1_{20}$	Hydrothermal Fluid	RP	2016	Filtered (0.2 and 0,02 µm)/As quantification (HG-AFS)
HF2				
$HF2_{un}$	Hydrothermal Fluid	RP	2017	Unfiltered / NP precipitation / SEM
$HF2_{200}$	Hydrothermal Fluid	RP	2017	Filtered (0.2 µm)/Geochemical analysis and As quantification (HG-AFS)
$HF2_{20}$	Hydrothermal Fluid	RP	2017	Filtered (0.2 and 0.02 µm)/As quantification (HG-AFS)
Y1				
$Y1_{un}$	Porewater	RP	2016	Unfiltered / SEM
$Y1_{200}$	Porewater	RP	2016	Filtered (0.2 µm)/Geochemical analysis and As quantification (HG-AFS)
$Y1_{20}$	Porewater	RP	2016	Filtered (0.2 and 0.02 µm)/As quantification (HG-AFS)
Y2				
$Y2_{un}$	Porewater	Spathi	2017	Unfiltered / SEM
$Y2_{200}$	Porewater	Spathi	2017	Filtered (0.2 µm)/Geochemical analysis and As quantification (HG-AFS)
$Y2_{20}$	Porewater	Spathi	2017	Filtered (0.2 and 0.02 µm)/As quantification (HG-AFS)
B1				
$B1_{un}$	Porewater	RP	2016	Unfiltered / SEM
$B1_{200}$	Porewater	RP	2016	Filtered (0.2 µm)/Geochemical analysis and As quantification (HG-AFS)
$B1_{20}$	Porewater	RP	2016	Filtered (0.2 and 0.02 µm)/As quantification (HG-AFS)

SW1				
$SW1_{un}$	Seawater	RP	2016	Unfiltered / SEM
$SW1_{200}$	Seawater	RP	2016	Filtered (0.2 μm)/Geochemical analysis and As quantification (HG-AFS)
$SW1_{20}$	Seawater	RP	2016	Filtered (0.2 and 0.02 μm)/As quantification (HG-AFS)
SW2-Pollonia				
$SW2\text{-}Pollonia_{200}$	Seawater	Pollonia	2016	Filtered (0.2 μm)/Geochemical analysis

RP, Rocky Point; SEM, Scattering electron microscopy; HG-AFS, Hydride generation atomic fluorescence spectrometry.

Chapter 4- Evaluation of environmental parameters in the formation and stability of As bearing nanoparticles

Manuscript title, authors and publication status:

Synthesis of As and S colloidal particles under environmental hydrothermal conditions: role of thiols in arsenic mobilization

V. Duran-Toro[a,*], K. Rezwan[b,c], S.I. Bühring[a] & M. Maas[b,c]

a Hydrothermal Geomicrobiology Group, MARUM Center for Marine Environmental Sciences, University of Bremen, Bremen, Germany
b Advanced Ceramics, University of Bremen, Bremen, Germany
c MAPEX - Center for Materials and Processes, University of Bremen, Bremen, Germany

* Corresponding author: vduran-toro@marum.de

(In preparation, Journal of Environmental Sciences & Technology)

Chapter 4 - Abstract

Arsenic-Sulfur (As-S) mineralization is a natural phenomenon occurring in hydrothermal systems where parameters like temperature and pH can influence the mobilization of the toxic metalloid (As) in a marine environment. However, little is known about the influence of other factors, i.e. organic matter (OM), in As mobility at hydrothermal conditions. In the present study we analyze the influence of temperature and OM (Sulfur containing additives) on As-S precipitation based on the recent findings of As rich nanoparticles described in a hydrothermal system [190]. The detection of a particulate fraction was carried out trough scattering electron microscopy coupled to energy-dispersive X-ray spectroscopy (SEM-EDX). By simple acidification (pH 3-4) the formation of colloidal particles rich in As and S at 25 °C was achieved using aqueous precursors. Scattering spectra (~300 - 550 nm) and dynamic light scattering (DLS) analysis indicated a correlation between particle size and the ratio of the initial precursors (S:As). The results suggest the formation of bigger particles when an excess of soluble sulfide was present (S:As of 2:1, 5:1 or 7:1). Precipitation of As-S colloidal material took place also at different temperatures (25, 45 and 70 °C). Higher temperatures enhanced the formation of monodisperse particles within the first 24 h of incubation, generating colloidal particles with diameter close to 160 nm and reduced As content relative to S present in the material (S:As [Atom. %]). On the other hand, the presence of sulfur containing additives (cysteine and glutathione; GSH) also had an effect on particle size, morphology and elemental composition. A granular film appeared when cysteine was added to the reaction synthesis and particles with diameter size over 1 μm were detected in the presence of GSH. Furthermore, in both cases (cysteine and GSH), a decrease in the S:As [Atom. %] ratio of the material was detected. When the additives were used during synthesis at higher temperatures (75 °C) no films nor microparticles were found. Instead, an ovoidal morphology was observed, with S:As [Atom. %] almost identical to the control (without additives) at high temperature. Crystal phase analysis by selected area electron diffraction (SAED), revealed amorphous phases being stabilized at any given condition (different temperatures or additives) and transmission electron microscopy confirmed the size and morphology of the colloids previously observed. When incubations were carried out for longer periods of time (> 24 h) the dissolution of the material occurred, and a total loss of the colloidal fraction and its scattering signal was observed after 3 days of incubation at 75 °C. Our results indicate that organic sulfur containing compounds, as cysteine or GSH are a key factor in the process of nucleation and growth of amorphous As-S colloidal particles and together with temperature gradients in systems like shallow hydrothermal vents, dictate the stabilization of As bearing nanomaterial in the environment. This findings provide novel insights in As colloidal stability, which denotes the need of a deeper understanding on As chemistry, specifically in hydrothermal and marine ecosystems affected by the pollutant.

4.1 Introduction

Arsenic is classified as a metalloid and present in nature in different oxidation states (-3, +3 or +5). The origin of As in the environment is linked to volcanic or hydrothermal activity and associated with the formation of sulfide minerals [191]. Among the different S bearing mineral phases described, realgar (As_4S_4), orpiment (As_2S_3) and amorphous arsenic sulfide (As_2S_3) are the most abundant [192]. In marine environments, arsenic can appear as the trivalent oxyanion arsenite (AsO_2^-, As^{+3}) and the pentavalent form arsenate (AsO_3^-, As^{+5}) [191-193]. In many hydrothermal systems where realgar, orpiment or amorphous arsenic sulfide precipitation occur, fluids containing high concentrations of soluble arsenic (< 400 nm) have been described [45, 193]. The different arsenic compounds found in hydrothermal fluids correspond to As^{+3} species like arsenite, but depending on the reducing conditions of the system, significant concentration of arsenate and thioarsenate can be detected as well [45]. The occurrence of arsenic sulfide species in hydrothermal fluids derives from the presence of soluble sulfide (HS^-, S^{2-}) [45]. The precipitation of arsenic sulfide species, as any of the minerals mentioned above, strongly depends on the pH and temperature of the system [45, 125, 193]. If the pH or temperature decreases, the solubility of the sulfide species drops, allowing the stabilization of a new phase (solid) [79, 125]. When compared to other elements derived from hydrothermal fluids, arsenic can account only for a particulate (> 400 nm) and a dissolved fraction (< 400 nm), assuming the presence of As in a colloidal fraction (400 - 20 nm) purely by sorption of soluble species on other minerals (FeOOH or FeS_2) or organic matter [46]. However, our group revealed for the first time the occurrence of amorphous As-S rich nanoparticles in the shallow hydrothermal system of Milos (Greece), with a size range between 250 to 50 nm [190]. Changes in physical and chemical properties are well documented to occur at the nanometer scale in different minerals [194], therefore, the existence of As colloidal particles in a marine ecosystem represent a significant and unexplored field in the arsenic geochemical cycle and in the toxicity of the element to different marine organisms. Since As is an aquatic pollutant at low concentrations [195], a better understanding in formation and stability of As nanoparticles in marine environments, especially in hydrothermal systems, is required. In recent years, the interaction of arsenic and OM has gained attention due to its role in arsenic sulfide mineralization processes as an explanation of suppressed arsenic mobility in wet ecosystems [127]. It has been determined that OM from peat samples (rich in sulfur atoms), can establish a covalent bond between S^{-2} and As^{+3} under reducing conditions, playing an active role in arsenic immobilization and furthermore modifying the crystal phase of the analyzed precipitate [127]. When a higher percentage of As^{+3}-OM complex was present in the samples, the absence of realgar or other crystal phases of arsenic was evidenced [127]. Interestingly, the role of OM rich in sulfur is poorly understood in hydrothermal systems, especially its role in formation or stability of As colloidal particles has not yet been studied. On the other hand, the use of thiols or sulfur rich organic compounds as additives in the nucleation, stabilization or capping of different nanoparticles is a relevant field in nanotechnology [196]. However, the most common reason for using thiols in synthesis of colloidal particles is the diverse functionalization of materials surfaces [197]. Glutathione capped CdTe nanoparticles can be used to detect trace concentrations of dissolved Cu in microbial cultures by direct interaction of S and Cu [198]. Glutathione capped Cu nanoparticles have a higher renal clearance (disposal through urine) compared to unmodified Cu nanoparticles [199]. Cysteine modified Ag nanoparticles have a

significant inhibition of growth on *Escherichia coli* and *Pseudomonas aeruginosa* cultures at low concentration of the metal [200]. Cysteine functionalized magnetic Fe_3O_4 nanoparticles can efficiently remove mercury (Hg^{+2}) from aqueous solutions [201]. Therefore, the presence of thiols during arsenic sulfide colloidal particles formation may play a relevant role in an environmental context. The presence of OM rich in thiol groups could change the interaction of As colloidal phases with gases, minerals or even organisms. Variations of the As content, size, structure or crystal phase of the particles can lead to an alteration of As chemistry in the water column or in the sediments of a marine system. Interdisciplinary cross-overs between nanoscience and mineralogy is not new and has already provided insights into mineral crystallization concepts [173]. Environmental and laboratory based research have proven crystals formation can occur through addition or attachment of particles that vary from multi-ion complexes to fully formed nanoparticles [173]. This idea, differ from classical models, which only consider addition of monomeric chemical species [173]. Therefore, raises the question of what is the role of factors like pH, temperature or OM, and more specifically thiols, in the formation of As and S rich colloidal particles and in the mobilization of As in a hydrothermal system.

We report the synthesis of colloidal particles (400 – 20 nm) during arsenic sulfide precipitation under environmental hydrothermal conditions, and how temperature and different thiols, with a biological origin, play a role in the arsenic content, particle size, abundance and stability of the colloids formed. The discovery is in agreement with previous reports by our group under similar hydrothermal conditions and suggests the formation of arsenic sulfide minerals through precipitation of arsenic sulfide colloidal particles as a common step occurring in hydrothermal systems.

4.2 Materials and Methods

4.2.1 Arsenic sulfide precipitation experiments

Precipitation of arsenic and sulfur at environmental hydrothermal conditions was developed as described before with some modifications [79]. A 1 M sodium arsenite ($NaAsO_2$) solution was prepared with ultra-pure Milli-Q water, aliquots of 1 ml were poured into Eppendorf tubes of 1.5 ml and stored at - 20 °C. Sulfur containing additives (Cysteine and Glutathione, GSH) and Glycine were prepared and stored as described before but with a stock concentration of 100 mM. A 1 M Na_2S solution was prepared in an anaerobic chamber (N_2) by dilution of Na_2S*9H_2O crystals in autoclaved Milli-Q water previously cooled under N_2 flux to remove O_2 from solution. Na_2S*9H_2O stock solution was stored in sealed serum bottles at 4 °C. For the precipitation experiments, the reaction was carried out at different precursors ratios (S:As), pH and temperatures, however, the order of addition of the reagents remained the same in every experiment. Firstly, Na_2S*9H_2O was added in 35 mL of Milli-Q water, with final concentrations of 0, 0.6, 1.5, 2.1 or 3 mM; secondly, additives were diluted from stock solutions to 1 mM; thirdly, pH 3 - 4 was adjusted with 1 M HCl; and finally after vigorous agitation, arsenite was added to a final concentration of 300 μM. As soon as arsenic was added to the solution, the reaction mixtures were incubated at different temperatures (25, 45 and 75 °C) to simulate a temperature gradient present in natural systems. pH monitoring of the experiments was performed using a FiveEasy pHmeter Mettler-Toledo and measurements were done every 20 min in the first hour, then the pH was measured once per day during the three days of incubation. The reactions were performed in propylene centrifugation tubes to avoid trace element contamination from glassware material.

4.2.2. UV-VIS spectrophotometry

Samples from different arsenic sulfide precipitation experiments were collected for analyzing UV-VIS spectra between wavelength 300 – 550 nm at several time intervals. Spectra were obtained using a Spectrophotometer UV-1280 Shimadzu with a quartz cuvette for UV range wavelengths. Samples were analyzed unfiltered to obtain the optical density as a result of both light scattering and absorption of the particles suspended in solution.

4.2.3 Dynamic light scattering

Samples from different arsenic sulfide precipitation experiments were collected for analyzing particle size distribution by poly dispersity index (PDI). Size distribution plots were obtained using a Malvern Zeta-sizer, with the refractive index of As_2S_3 (2.65) as reference material [167]. Samples were analyzed unfiltered to obtain a representative scattering effect of all particles suspended in solution.

4.2.4 Scattering electron microscopy coupled to energy-dispersive X-ray spectroscopy (SEM-EDX)

Morphology, size and elemental composition of particulate material (> 200 nm) was studied by SEM-EDX analysis of 200 nm pore-size polycarbonate membranes used during filtration of arsenic sulfide precipitation experiments at different time and temperature of reaction as described before [190]. For SEM sample preparation, filters were dried in a desiccator using silica glass beads as desiccating agent for a period of 5 days. Afterwards, pieces of the filter were cut and glued to carbon stickers in aluminum holders. Each filtration consisted of 5 mL of sample to assure proper particle abundance on the filter. A Zeiss, model iSUPRA 40 SEM with an EDX detector (Bruker, XFlash 6|30) was operated at low voltage (3-5 kV) for high definition images and at 15 kV for EDX spectrum determination. EDX spectra were performed on each sample, accounting for at least 5 spots of a 5 μm^2 area of analysis.

4.2.5 Particle abundance

The software Image J (version 1.52k) was used for particle counting. The image scale was set using the burned-in scale in the micrograph, afterwards the image was set on gray scale (8 bit) and particle edges were established. The threshold was tuned for better contrast between particle edge and empty space. To link the disconnected grain boundaries and obtain an accurate correlation between number of particles and counts, the Watershed algorithm was ran and an iteration step of media filter value was included in order to erase artificial connecting lines inside of particles. If necessary, lines inside of particles were removed manually. Finally, the Particle Analysis function was used to determine the number of particles, the analyzed area and the Feret´s diameter.

4.2.6 Transmission electron microscopy coupled to selected area electron diffraction (TEM-SAED)

Morphology and crystal phase identification of suspended material was studied by TEM-SAED analysis of particles formed during arsenic sulfide precipitation experiments at different temperatures of reaction or in the presence of additives [190]. For TEM samples preparation, cupper grids were cover with 5 µL of a Milli-Q dilution (1:100) of the reactions solutions and dried in a desiccator using silica glass beads overnight. A FEI Titan microscope in SAED modality was operated at an interval of 80 to 300 kV according to electron beam sensitivity of the particles.

4.3 Results

4.3.1 Influence of synthesis parameters on the formation of colloidal particles during As and S precipitation at environmental hydrothermal conditions

Arsenic and sulfur precipitation experiments were performed according to Rochette et al. (2000) with some modifications in order to study the formation of a particulate fraction (> 200 nm) at temperature close to environmental hydrothermal conditions [190]. The initial pH was adjusted between 3 - 4 prior addition of arsenite without presence of a buffer solution to avoid interaction of an arsenic sulfide phase with buffer molecules. The pH was checked during the experiments and showed no variations along the reaction time (Supplementary Figure 4.1, SF 4.1).

The presence of colloidal particles, rich in As and S, with a spherical shape and a diameter around 200 nm is shown in Figure 4.1. A peak of oxygen (O) in the EDX spectrum suggests the presence of oxidized forms of either As or S also being part of the particles. The high peak of carbon (C) corresponds to an artifact due to the sample preparation on a polycarbonate filter. The normalized atomic weight percentage (S:As [Atom. %]) of the particles indicate a ratio close to 6, which differs from arsenic sulfide minerals like orpiment or amorphous arsenic sulfide (As_2S_3) with theoretical number of 1.5 or even realgar with a value of 1.

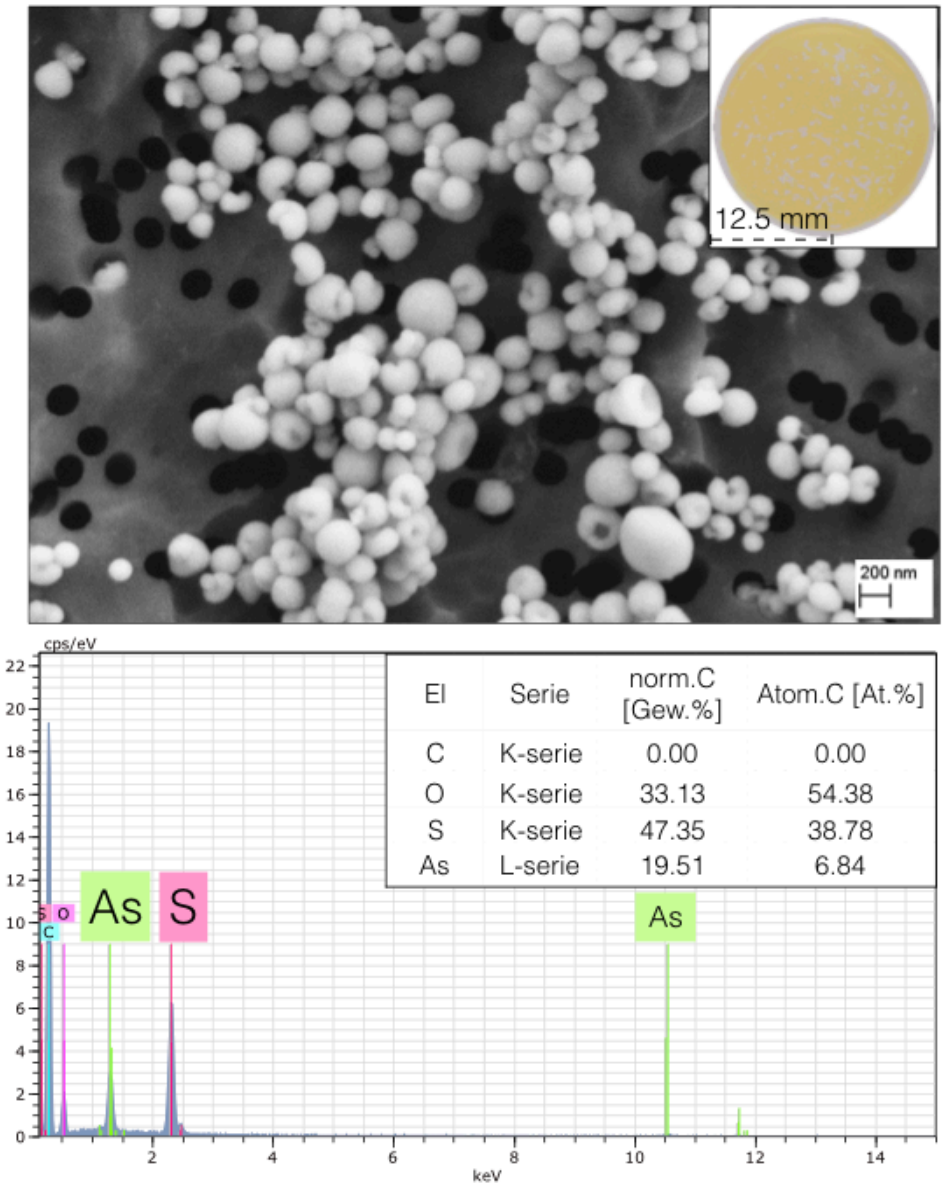

Figure 4.1. SEM-EDX analysis of the particulate fraction formed during As and S precipitation. The SEM image shows the presence of spherical particles with a diameter near 200 nm. The upper right inset shows a picture of the yellow precipitate obtained after filtration. The EDX spectrum of colloidal particles shows main peaks for As and S.

The presence of colloidal particles can be tracked by changes in optical properties like absorbance or light scattering (Tyndall effect) in the UV-VIS wavelength range. Consequently, absorbance/scattering spectra of reaction solutions were obtained in the wavelength range of 300 – 550 nm. Figure 4.2 shows the scattering spectra of different reaction solutions with As and S precursors at initial ratios (S:As) from 2:1 to 7:1. The spectra shows a colloidal light scattering pattern with an increase of light scattering in an exponential manner at small wavelength values (300 – 400 nm, Figure 4.2).

Size distribution of synthesized particles in suspension was evaluated by DLS (Figure 4.2), showing a bi-modal system with major particle size at 13 and 140 nm and a moderately high polydispersity index (PDI > 0.2) when low precursors ratios were applied (2:1 and 5:1). However, when a higher ratio (7:1) was established, the smaller particle sizes disappeared, presenting mostly particles with a size close to 140-160 nm and a more narrow size distribution with PDI < 0.2.

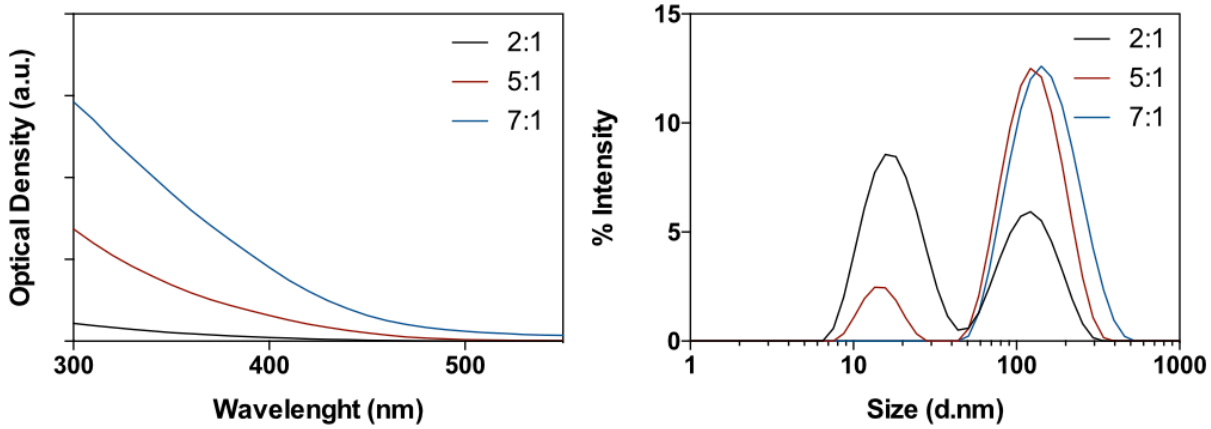

Figure 4.2. Scattering spectra and DLS analysis of reaction solutions for As and S precipitation. Optical density spectra (Left) and DLS analysis (right) of reaction synthesis with different S and As precursors ratio (2:1, 5:1, 7:1) were analyzed in the wavelength range between 300 and 550 nm and for hydrodynamic radius and size distribution of particles. Aliquots for both analyses were collected after 24 h of incubation at 25 °C and pH 3 - 4.

No variations of the scattering signal over time (0 to 24 h) suggest that the reaction finished at the beginning of the time frame and the particles remained stable under 25 °C and pH near 4 during the 24 h of incubation (Supplementary Figure 4.2, SF 4.2).

The evaluation of temperature influence on the formation of particles was done by SEM-EDX analysis and by light scattering spectra of the reaction solutions. The temperatures (25 – 75 °C) and S:As ratio (5:1) used, mimic values present at hydrothermal systems [45, 190]. Figures 4.5a, 4.5b and 4.5c, show the particulate fraction collected after 24 h at 25, 45 and 75 °C, respectively. Spherical particles with a size ranging between 20 to 300 nm can be observed in the analyzed filtrates (Figure 4.3 a-c).

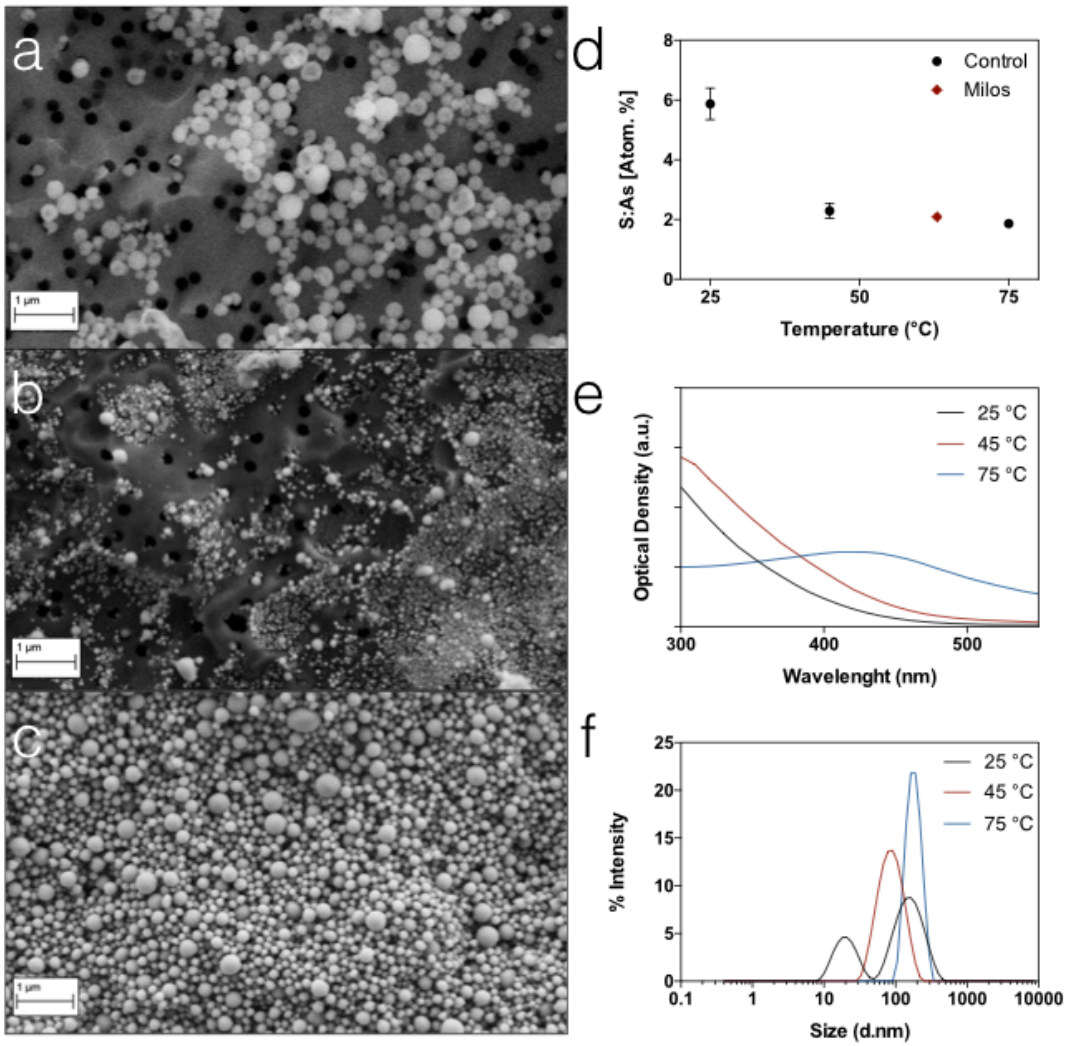

Figure 4.3. Influence of temperature on colloidal particle formation during As and S precipitation. a, b, and c, SEM images of colloidal particles collected by filtration of reaction synthesis at temperatures 25, 45 or 75 °C (respectively). d, shows the S:As ratio in the samples obtained from EDX analysis of atomic weight percentage or [Atom. %]. The standard deviation of each sample was calculated from at least five independent measurements. The red rhombus symbol represents the Atom. % of As-S-rich nanoparticles described in Durán-Toro et al., 2019. e, Optical density spectra (300 - 550 nm) of unfiltered samples (containing the colloidal particles) from reaction synthesis at different temperatures. f, DLS analysis of unfiltered samples from reaction synthesis at different temperatures. Size distribution analysis indicated polydispersity index (PDI) values of 0.62, 0.12 and 0.045 for reaction temperatures of 25, 45 and 75 °C, respectively.

The particle count protocol (refer to Materials and Methods section) suggested a correlation between reaction temperature and number of particles by area unit (Supplementary Table 4.1, SF 4.1 and Supplementary Figure 4.3, SF 4.3). An increase in the reaction temperature enhanced particle formation during As and S precipitation (Figure 4.3a and 4.3c).

When the atomic weight percentage ratio of S and As was determined from the EDX spectra of each sample, the decrease in S:As [Atom. %] correlated with an increase in temperature and exhibited similar values to the amorphous arsenic sulfide nanoparticles detected in the hydrothermal system off Milos (Figure 4.3d) [190]. Figure 4.3e, shows the changes in the scattering spectra of the reaction synthesis at different incubation temperatures. When the reaction was carried at 45 °C, an increase in the optical density (scattering) signal was observed (Figure 4.3e), while when the reaction temperature raised to 75 °C, the spectra presented a shoulder peak at 450 nm (Figure 4.3e), which indicate a change in the optical properties of the colloidal particles, perhaps due to a change on its chemical composition or crystal phase (Figure 4.3d). The temperature displayed an influence on the size distribution of the formed particles, showing bigger particles due to incubations at higher temperatures (Figure 4.3f) and poly-dispersity indexes closer to monodisperse distribution with values of 0.62, 0.12 and 0.045 for reaction temperature of 25, 45 and 75 °C, respectively. The temperature effect resembles the variations in size distribution observed in changes of precursors proportion (Figure 4.2), where the smaller particles disappeared and only bigger particles with a peak diameter size close to 140-160 nm remained in solution (Figure 4.3f).

4.3.2 Influence of thiols in colloidal particle formation during As and S precipitation at environmental hydrothermal conditions

In order to evaluate the role of thiols in the formation or stabilization of As and S rich particles under environmental hydrothermal conditions, the morphology, elemental composition and particle size distribution of the colloids formed in the presence of additives were studied by SEM-EDX and DLS. Since the chemical structures of some thiols contain other functional groups i.e. OH, CHO or NH_2 (Figure 4.4), glycine was used as control to evaluate its effect excluding possible interactions of non-thiolic groups within the formed As-S phase.

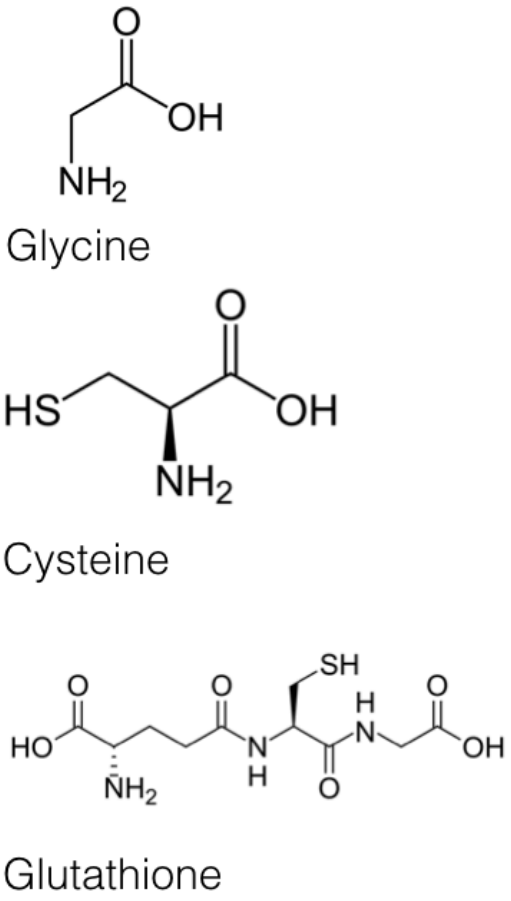

Figure 4.4. Chemical structure of additives used during As and S precipitation experiments.

Figure 4.5a-4.5d shows the morphology and size of the particles collected on polycarbonate filters (0.2 µm) from synthesis reaction at 25 °C after 24 h of incubation with and without additives. Figure 4.5a and 4.5b shows nanospheres with particle diameters close to 200 nm obtained from synthesis without (Figure 4.5a) and with glycine (Figure 4.5b). Remarkably, when cysteine or GSH were added, a film of grain-aggregated material and microscopic structures were formed (Figure 4.5c and 4.5d, respectively). EDX analysis indicated As and S as the main constituents (data not shown), for conditions with or without additives. The ratio between atomic weight % of elements (S:As [Atom.%]) present in the different samples, suggest an alteration on the material chemical composition based on the presence of thiol molecules (Figure 4.5e). The S:As [Atom.%] of the particles formed in the presence of additives (cysteine and GSH) decrease compared to the control, or as for the glycine treatment (Figure 4.5e). Size distribution analysis by DLS (Figure 4.5f) correlates with SEM images, showing two major particles sizes for the control and glycine treatments and an increase in particle size in the presence of a thiol rich additive. When cysteine is used in the reaction, particles exhibited a broad range of sizes, from 20 to 200 nm and when GSH was added, a significant increase to >1 µm was observed (Figure 4.5f).

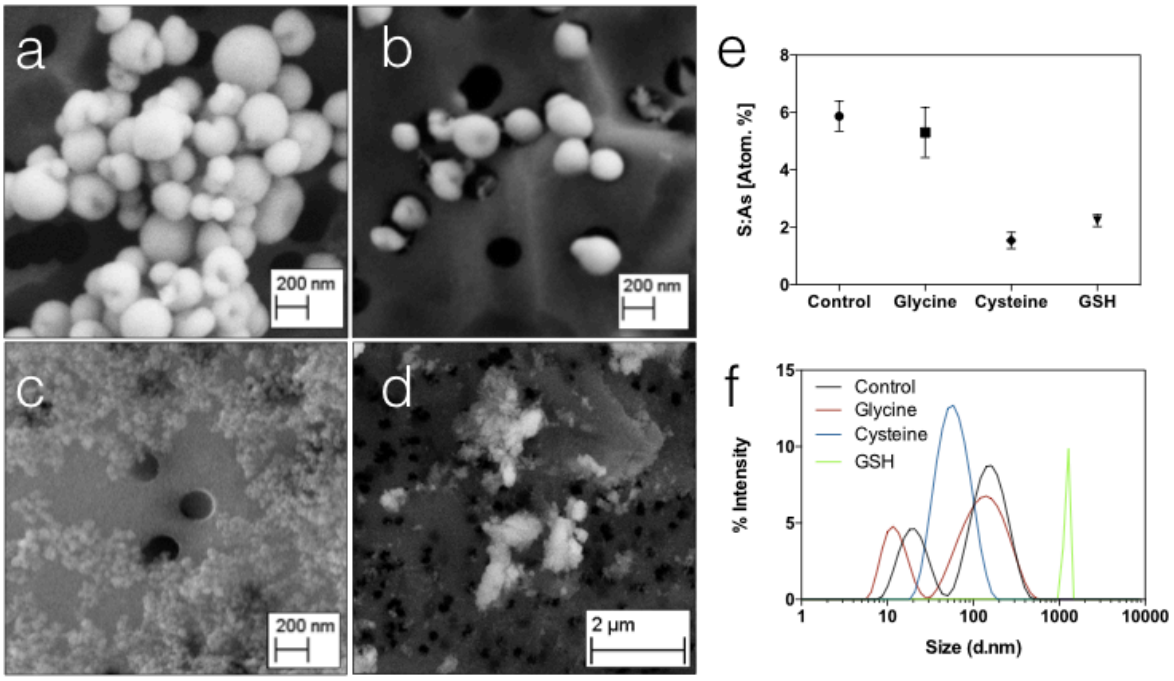

Figure 4.5. SEM-EDX and DLS analysis of colloidal particles synthesized in the presence of thiol additives at 25 °C. SEM images of the colloidal particles collected in polycarbonate filters (0.2 µm pore size) after 24 h incubation at 25 °C without additive, a; with glycine, b; cysteine, c; and GSH, d. e, EDX analysis of the samples showing atomic weight percentage ratio between S and As, S:As [Atom. %]. Standard deviations correspond to at least 3 measurements per sample. f, DLS study of particles size distribution in synthesis reactions. Measurements were performed without filtration. The main diameters indicate a bi-modal system with particles of 160 and 19 nm and PDI values near 0.5 for both control and glycine. In the case of cysteine a broad range between 200 and 20 nm was observed and a PDI value near 0.2. Finally, with GSH, size distribution showed particle sizes over 1000 nm and a PDI value above 0.6.

On the other hand, Figure 4.6a-d shows the morphology and size of particles formed at 75 °C, with and without additives and after 24 h of incubation. Figure 4.6a and b show spheres with very similar particle diameters (100 to 300 nm) obtained from synthesis without (Figure 4.6a) and with glycine (Figure 4.6b). When thiols were added to the synthesis, no film or grain-aggregated material appeared as for cysteine (Figure 4.6c) or GSH treatments at lower temperatures (Figure 4.6d). Instead, oval shape particles were detected, with a size ranging from 20 to over 300 nm (Figure 4.6c and 4.6d). Interestingly, the S:As [Atom.%] present in the samples, suggest a chemical composition alteration controlled by temperature increase rather than an influence of thiols (Figure 4.6e). The S:As [Atom.%] ratio of the material remained similar when compared to the control or in the presence of glycine, reaching values between 1.9 and 2.3 with or without thiols incorporated into the reaction (Figure 4.6e). Size distribution analysis (Figure 4.6f) correlates with SEM images, showing in the control and glycine treatment a major particle size at 180-200 nm and a similar range of particle diameter distribution when thiols were present (Figure 4.6f).

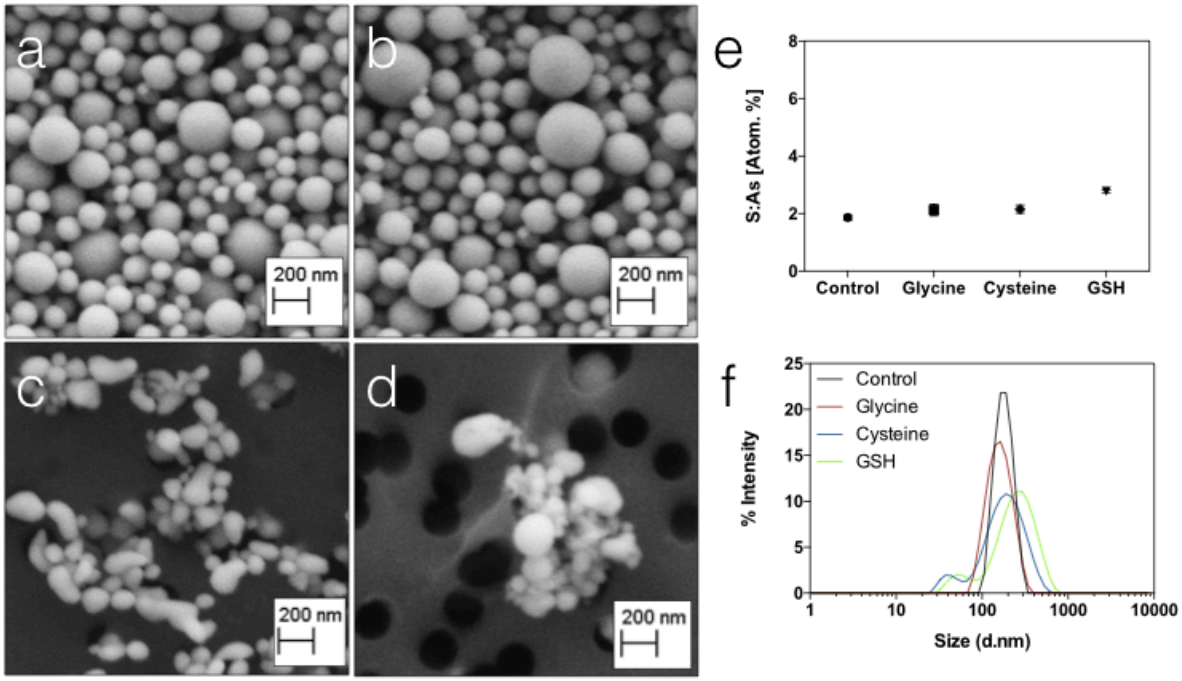

Figure 4.6. SEM-EDX and DLS analysis of colloidal particles synthesized in the presence of thiol additives at 75 °C. SEM images of the colloidal particles collected on polycarbonate filters (0.2 µm pore size) after 24 h incubation at 75 °C without additive, a; with glycine, b; cysteine, c; and GSH, d. e, EDX analysis of the samples showing atomic weight percentage ratio between S and As, S:As [Atom. %]. Standard deviations correspond to at least 3 measurements per sample. F, DLS study of particles size distribution in synthesis reactions. Measurements were performed without filtration. The main diameters indicate particles of 180 nm and PDI values of 0.045 and 0.1 for control and glycine, respectively. In the case of cysteine and GSH a peak size of 160 nm in a broad range was observed with PDI values of 0.3.

Crystal phase identification was carried by TEM-SAED experiments of particles formed in reactions solutions at different temperatures (25 and 75 °C) and in the absence (Control) and presence of thiol based additives. TEM images (Figure 4.7) confirmed size and morphology of previous experimental conditions, showing spherical morphology and size close to 100 nm for control conditions at 25 and 75 °C after 24 h of incubation (Figure 4.7a and 4.7b). When cysteine was added to the reaction at 25 °C, the granular aggregation described earlier can be observed (Figure 4.7c). If the temperature is elevated to 75 °C the granular formation disappear and instead ovoidal particles are found in extended agglomerations (Figure 4.7d). When GSH was used as additive, the formation of bigger particles was detected at 25 °C (Figure 4.7e), while at higher temperatures a similar ovoidal morphology was identified (Figure 4.7f). SAED analysis of the particles indicates an amorphous phase present in all the materials, denoting an absence of a crystal phase in all the colloids formed, independent of temperature control or the presence of additives during As-S precipitation (Figure 4.7).

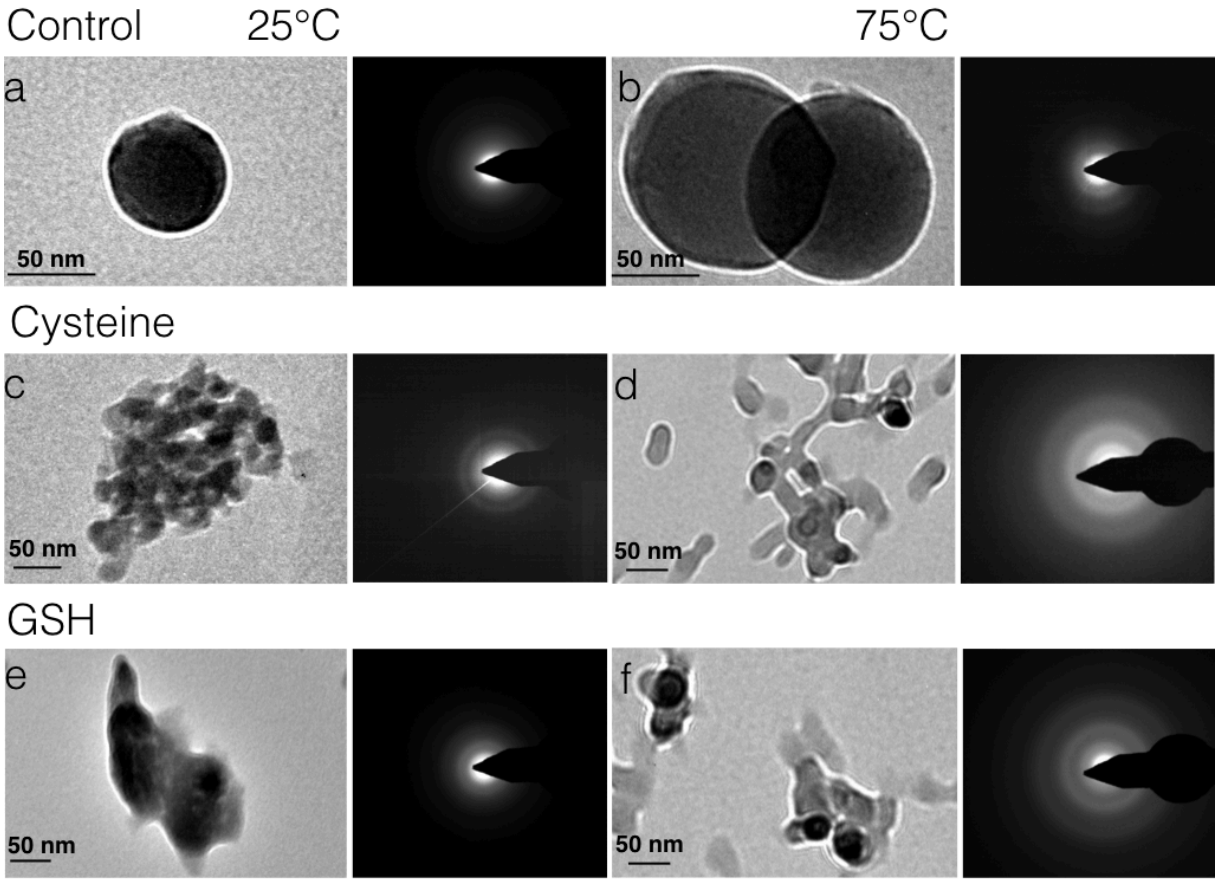

Figure 4.7. TEM-SAED analysis of colloidal particles synthesized in the presence of thiol additives at different temperatures. TEM images of the colloidal particles after 24 h incubation without additives (Control) at 25 °C, a; at 75 °C, b; or incubated with cysteine at 25 °C, c; at 75 °C, d; or in the presence of GSH at 25 °C, e; and at 75 °C, f. SAED analysis of the samples is showed at the right of each TEM image, indicating amorphous phases (absence of crystal phase) or ring patterns in every condition. Samples in the presence of thiol additive where specially sensitive to the electron beam, thus, the microscope was operated at a lower voltage (80 kV).

4.3.3 Stability of As and S rich colloidal particles at environmental hydrothermal conditions

Optical density spectra of the reaction synthesis at 25 or 75 °C with different additives registerd over time (24 and 72 h) (Figure 4.8). No major differences were observed when glycine was used as an additive to the reaction at any given condition (Figure 4.8). In the presence of cysteine or GSH an increase in the scattering was observed after the first 24 h of incubation when compared to the control or to the presence of glycine (Figure 4.8a, left). Once the temperature of incubation was increased to 75 °C, the scattering spectra of the control, glycine and GSH showed a scattering shoulder between 400 and 500 nm (Figure 4.8a, right). However, when cysteine was added to the reaction a more pronounced shape was observed, with a maximum signal at 420 nm (Figure 4.8a, right). After 72 h of incubation, no further modification was noticeable in the spectra with or without additives at 25 °C (Figure 4.8b, left). Nonetheless, the OD signal associated with the particles had vanished completely after 72 h at 75 °C with or without additives (Figure 4.8b, right). This result indicates the dissolution of the arsenic sulfide phase after 72 h, which was corroborated by absence of As- and S-rich colloidal particles in the SEM-EDX analysis of the samples on polycarbonate filters (data not shown).

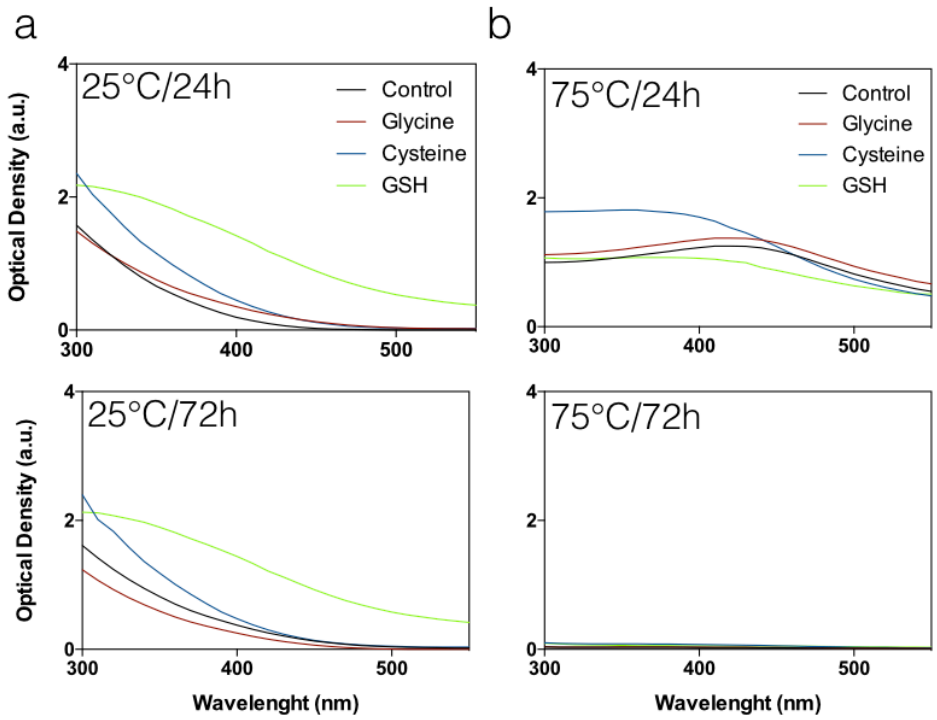

Figure 4.8. Optical density spectra of As and S precipitation reaction solutions at different temperature and incubation times. Absorbance/scattering spectra of As and S precipitation solutions with S and As precursors ratio 5:1, at 25 and 75 °C and in the presence of control (without additive), glycine, cysteine or glutathione (GSH) (1 mM). Aliquots of reaction synthesis were collected at 24 and 72 h and analyzed without filtration.

4.4 Discussions

4.4.1 Formation of colloidal particles during As and S precipitation at environmental hydrothermal conditions

Precipitation of arsenic sulfide minerals represents a key step in As mobilization in different ecosystems [49, 127]. Normally, studies of As distribution in the environment reports the existence of a particulate (> 400 nm) and a soluble (< 400 nm) fraction [46], and the presence of As in the colloidal size range (400 – 20 nm) as a simple sorption process of the soluble species in colloidal OM or iron particles [46]. So far, the existence of As colloidal particles have been identify only in the shallow hydrothermal system of Paleochori Bay (Milos, Greece), where temperature values exceed those of many other environments where arsenic sulfide minerals can be found [190]. Rochette et al. (2000) studied the precipitation of As and S from water soluble precursors at a broad ratio of concentrations in the micromolar range, pH below 5 and N_2 atmosphere at 25 °C. Under these conditions, different soluble arsenic sulfide species, from thioarsenate to orpiment were formed. However, even though Rochette et al. (2000) established the formation of a solid phase over 200 nm, they did not further characterize the material and a colloidal particle formation cannot be discarded or assumed. Other studies have performed similar experiments on As and S precipitation although focusing on the formation of thin As_2S_3 films through chemical bath deposition [58, 59, 202, 203]. The thickness of the films can be controlled by the presence of additives like ethylene diamine tetra acetic acid (EDTA) rich in carboxylic (-COOH) groups or other molecules with phenolic (-OH) or amine ($-NH_2$) groups [58, 59, 202, 203]. Figure 4.1, shows colloidal As and S rich spherical particles, as a result of As and S precipitation by pH decrease (between 3 and 4) under 25 °C and at O_2 rich atmosphere. The lack of additives, buffer solutions or surfaces containing molecules with functional groups that control the nucleation or growth of an As-S phase could explain the occurrence of colloidal spheres instead of a thin As_2S_3 film. Our results (Figure 4.1) support the idea of As colloidal particles formation as a natural phenomenon occurring during As and S precipitation in the environment at low pH and temperature when an excess of soluble sulfide relative to As occurs (S:As of 2:1, Figure 4.1). Perhaps, in early stages of arsenic sulfide minerals formation, a particle attachment mechanism represents a crystallization pathway as has been described for other mineral models (i.e. TiO_2, $Ca_3(PO_4)_2$ or Zeolite) [173]. Yet, further experiments on As and S precipitation at higher temperatures have not been performed. Most of the reaction conditions for As and S precipitation in the present work resemble shallow water hydrothermal systems (pH 4 – 6; 30 – 90 °C; [As]: 78 μM; [HS^-,S^{2-}]: 3 mM) [49, 134] and constitute a first approach to understand the influence of temperature over As colloidal particle generation in the environment. Only dissolution assays of arsenic sulfide minerals have been performed so far, indicating a decrease in their phase stability and amorphous phases of arsenic sulfide minerals as the main precipitate at temperatures near 90 °C [125]. Based on the influence of temperature, the discovery of amorphous As and S rich nanoparticles in the shallow hydrothermal system off Milos was explained as a consequence of a temperature drop due to mixing of seawater and hot (> 60°C) hydrothermal fluids. A mix between As and S rich fluids and seawater could causes an oversaturation of the arsenic sulfide species due to their low solubility at temperatures range of 20 to 25 °C [190]. Nonetheless, the data presented here

indicate a more complex explanation (Figure 4.3). If the synthesis of the particles takes place at higher temperatures, the As-S phases formed would encounter a dissolution due to increased solubility [125]. However, in an initial step, during the first 24 h of reaction, the temperature exhibited an enhancing effect, boosting the yield of nanoparticle formation (Figure 4.3a - c). Also, at elevated reaction temperatures in the first 24 h, a different S and As content within the particles formed at 45 or 75 °C was observed (Figure 4.3d). These S:As [Atom. %] values are remarkably similar to those found in the natural nanoparticles discovered in the Milos hydrothermal system (Figure 4.3d). Altogether, our results support the hypothesis of particle formation occurring and being favored at higher temperatures (> 25 °C). However, the variation of the S:As [Atom. %] ratio with temperature increase represents a change in the chemical composition of the particles that should be further discussed. This S:As [Atom. %] variation can be explained either due to a dissolution process, by a crystal phase alteration or by particle growth, where one or more arsenic sulfide species are incorporated or lost, changing the content of S and As in the particles or its mineral phase. The change in size distribution at 75 °C (Figure 4.3f) does not correlate with a significant increase in the particle size (Figure 4.3f), and since no alteration in the crystal phase was observed (Figure 4.7), a more plausible explanation comes from an increasing abundance of particles (ST 4.1 and SF 4.3), followed by a dissolution process of the particles changing their S:As [Atom. %] ratio. The stability of the particles was further assessed by OD variations over time at different temperatures (Figure 4.8). A total dissolution of the particles after 72 h of incubation at 75 °C (Figure 4.7b, right) was detected, and, when the temperature decreased to 25 °C, the integrity of the signal associated to the presence of the colloidal material remained unaltered (Figure 4.7b, left). These results confirm dissolution as a process occurring at high temperatures, capable of varying the chemical composition of the particles over time. The temperatures here analyzed (75 °C) are similar to values recorded in shallow hydrothermal systems and suggests dissolution of initially formed particles may also occur within 24 h in a natural hydrothermal system. Nevertheless, it is likely that particles formed under high temperature hydrothermal conditions remain stabilized once the fluids are mixed with cold seawater. Suggesting that As-S rich particles with similar S:As [Atom. %] ratio to the colloidal particle described are stabilized in porewater and hydrothermal fluids samples from Paleochori bay, avoiding dissolution by high temperatures once mixed with seawater (Figure 4.3) [190].

4.4.2 Influence of thiols on the formation of colloidal particles during As and S precipitation under environmental hydrothermal conditions

The interaction between OM and metals in hydrothermal systems, specifically in shallow vents, has been proven to be a selective process in which co-precipitation or interaction of OM and relevant elements like Fe or Cu dictates geochemical cycles in marine environments [128, 153]. However, little is known about the interaction of As and OM in hydrothermal systems. Langner et al., (2012) described the interaction of OM and As in wet peats, establishing sulfur-rich OM as an immobilizing agent of the metalloid in the environment. The chemical interaction was explained through a covalent bond between the S and As atoms under acidic and low temperature (~ 25 °C) conditions. In a similar way, sulfur-containing additives like cysteine and GSH are commonly used in the synthesis or functionalization of metallic colloidal particles

[201, 204]. This suggests a role for sulfur-rich OM, specifically thiols, in the formation of an As-rich colloidal fraction in the environment. Figure 4.5 shows how the presence of thiols during the precipitation of As and S altered the morphology, chemical composition and size distribution of the formed particles. In the case of cysteine, granular structures with a S:As [Atom. %] ratio lower than the control and a broader particle size distribution were observed (Figure 4.5c, 4.5e and 4.5f). In a similar way, with GSH, particles with a low S:As [Atom. %] ratio and size exceeding 1 µm were detected (Figure 4.5d, 4.5e and 4.5f). These findings drastically differ from colloidal particles formed without additives or compounds without a thiol group (glycine) (Figure 4.5). The high affinity of AsO_2^- ions in solution for sulfhydryl (-SH) groups, suggest the stabilization of different As-S phases based on the presence of thiol additives. These novel As-S phases could be formed through a direct bond between As and the S atom present in the amino acid as suggested by Langner et al. (2012). The appearance of granular aggregates correlate with As_2S_3 films formed due to interaction with additives, where film thickness reaches 300 nm and a grain size vary from 15 to 30 nm [58, 59]. These results suggest an analogous phenomenon occurring in the hydrothermal system off Milos, where similar morphologies, size, S:As [Atom. %] ratio and crystal phase were described [190]. Thus, we suggest thiols have a great impact upon nucleation and growth of As-rich colloidal material and in consequence, on the mobility of the metalloid in marine environments, where OM rich in S represent a key component. Furthermore, in the context of a hydrothermal system, where temperature represent an important parameter controlling the generation of particles in the colloidal fraction (Figure 4.3), Figure 4.6 showed the impact of temperature on morphology, elemental composition and size distribution when thiols were present in the reaction. Figure 4.6 and 4.8 suggest temperature as a predominant factor in the formation and stability of As colloidal particles over the presence of additives or S rich OM, altering the morphologies and S:As [Atom. %] in the colloidal materials. Most amino acids and short peptides do not undergo decomposition at temperature near 75 °C, and in the case of cysteine an oxidation to cystine and only a posterior degradation or inactivation can be observed in minor quantities at temperatures close to autoclaving (100 °C) [205-207]. However, decomposition of additives or in the case of a hydrothermal system, S rich OM, should not be discarded. The oxidation of cysteine to cystine does not represent a limitation on the interaction between the As and S atoms, since the electrons present in the valance layer should stay available for a covalent bond with the metalloid as described in literature [127]. Thus, the outcomes described can be completely attributed to a temperature effect upon the chemical solubility of the stabilized As-S phase based on cysteine or GSH interaction rather a degradation of the additive itself.

4.5 Conclusions

The precipitation of colloidal As particles by pH decrease was achieved based on water-soluble precursors. The resulting colloidal particles exhibited spherical shape, were rich in As and S atoms, with a size range of 10 to 300 nm. Particle properties like size, polydispersity, yield or S and As atomic weight % ratio can be easily tuned by synthesis parameters, like S and As precursor ratios or temperature. Additives, like thiols, furthermore represent a key parameter over colloidal particle formation at low temperatures, favoring the generation of As- and S-rich aggregates instead of individual and well defined particles. If hydrothermal conditions are mimicked, temperature controls the process even in the presence of additives in the reaction. At first stage, a higher temperature enhances the yield of particle generation, yet is followed by a change in particle solubility, encountering a phase destabilization and a total dissolution. The morphology, size and more importantly the S:As [Atom. %] ratio in the particles correlate with a temperature increase and exhibit values notably similar to As- and S-rich particles found in the shallow hydrothermal system off Milos (Greece). Our results suggest the precipitation of As and S rich colloidal particles as a natural phenomenon in environments with reduced conditions, low pH within a gradient of temperatures and soluble sulfide exceeding As concentrations. A better understanding on colloidal chemistry of As in the environment is demanded, where a detailed comprehension of the real impact of nanomaterials can lead to novel regulations of pollutants in aquatic ecosystems.

Acknowledgements

This study was supported by Conicyt through a fellowship to VDT (Programa de Capital Humano Avanzado, BECAS-Chile, CONICYT, 2015) and by the Deutsche Forschungsgemeinschaft (DFG, Germany) through the Emmy Noether-Program (grant BU 2606/1-1 to SIB). We would like to thank the Advanced Ceramics laboratories and Petra Witte for performing SEM analyses.

Supplementary material

Figures

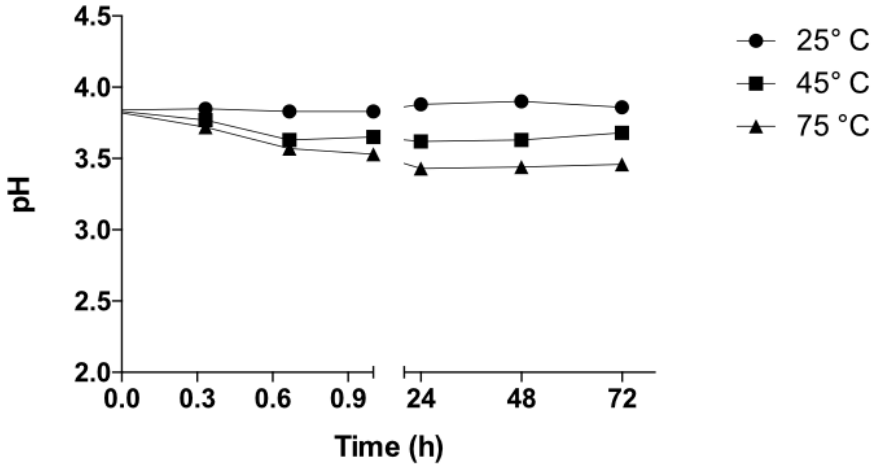

Supplementary Figure 4.1 (SF 4.1). pH variations of As and S precipitation solutions at different temperatures. pH values were determined over time at three different reaction temperatures (25, 45 and 75 °C) of colloidal particles synthesis at S:As precursors ratio 5:1 during 72 h.

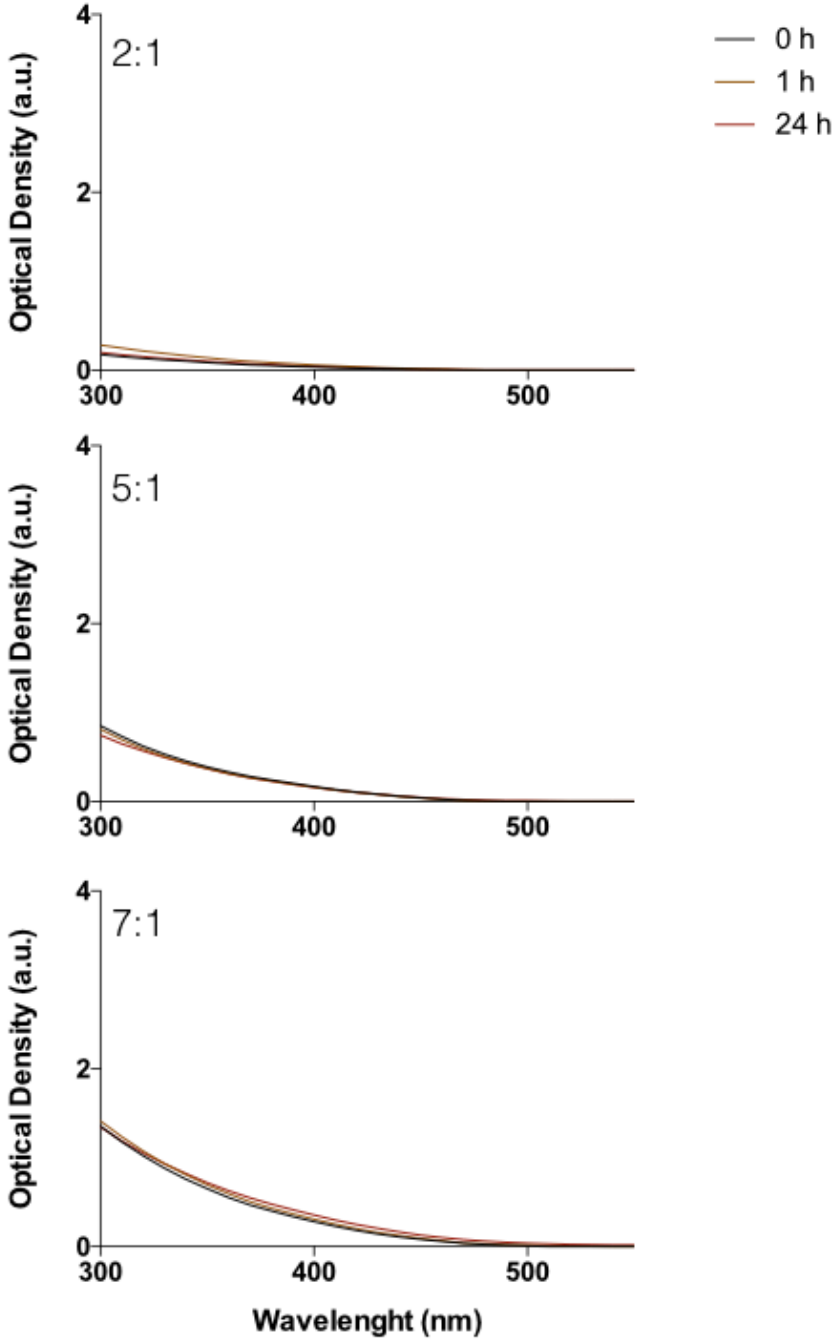

Supplementary Figure 4.2 (SF 4.2). Optical density spectra of As and S precipitation reactions over time. Scattering of reaction solutions with different S and As precursors ratio (2:1, 5:1, 7:1) were analyzed in the wavelength range between 300 and 550 nm. Aliquots were collected at 0, 1 and 24 h of incubation at 25 °C and pH 3 - 4.

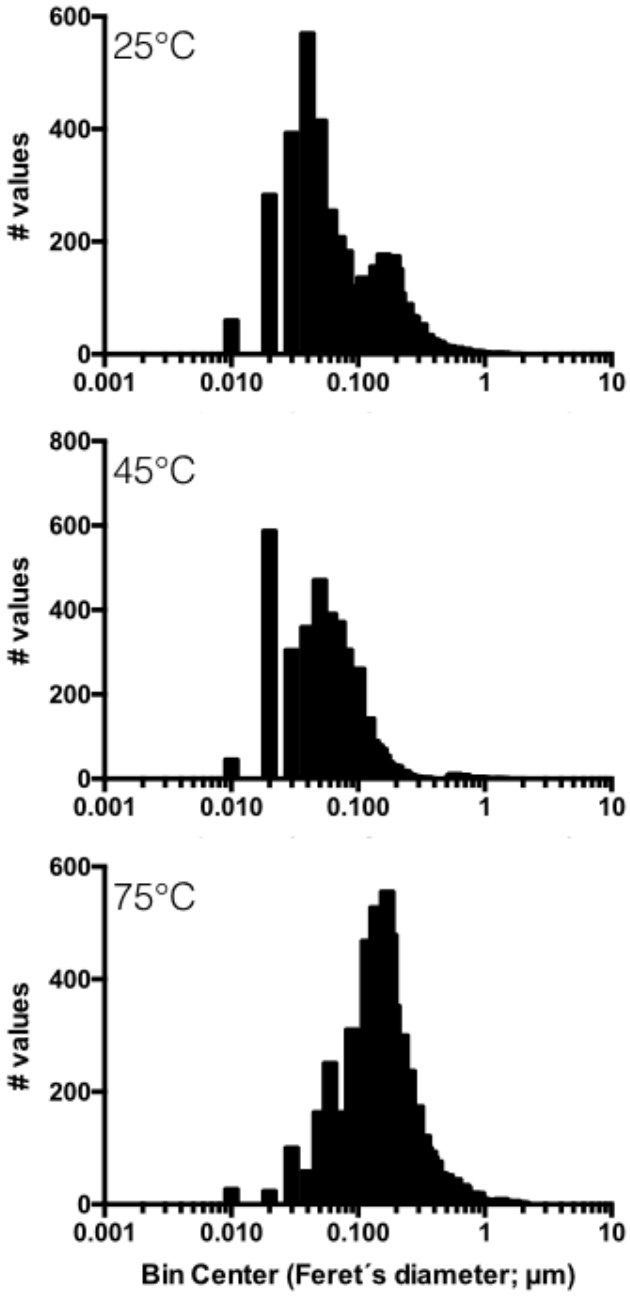

Supplementary Figure 4.3 (SF 4.3). Particle count with ImageJ sofware. Watershed algorithm was run to obtained Feret´s diameter (diameter size) according to the nanometer scale set in the SEM images of colloidal particles synthesized at 25, 45 or 75 °C. At least 1000 particles were counted to stablish statistical analysis by size distribution or size frequency (Bin center).

Tables

Supplementary Table 4.1 (ST 4.1). Particle Counts by Watershed algorithm in reaction synthesis at different temperatures.

Sample	Count	Total Area	Scale	# of particle/area unit
25 °C	2665	144.330	53.34 pixel/µm	18.46
45 °C	4371	33.088	106.67 pixel/µm	132.10
75 °C	4207	16.489	106.67 pixel/µm	255.14

Chapter 5- Toxicity of As colloidal particles in marine microorganisms

Manuscript title, authors and publication status:

Lipid response of *Shewanella oneidensis* MR1 to arsenic colloidal particles.

V. Duran-Toro[a*] and S. I. Bühring[a].

a, Hydrothermal Geomicrobiology Group, MARUM Center for Marine Environmental Sciences, University of Bremen, Bremen, Germany

* Corresponding author: vduran-toro@marum.de

(In preparation, Journal Science of the Total Environment)

Chapter 5-Abstract

The study of arsenic (As) toxicity in marine environments have been centered on the effect of soluble forms of the metalloid in microbial communities, however, little is known about its impact as a colloidal material. The present work, evaluated the effect of arsenic colloidal particles (As_{CP}) upon the marine bacterial model *Shewanella oneidensis* MR1. The toxicity of the particles was compared to soluble species, arsenite (As^{+3}) and arsenate (As^{+5}), by growth inhibition assays, determination of growth rate and analysis of the lipid response to the metalloid. The different forms of arsenic (375 μg mL^{-1} or 5 mM), decreased cell density (cell mL^{-1}) after incubation, presenting a growth inhibition of 49 % in the presence of As^{+3}, of 14 % with As_{CP} and of 4 % with As^{+5}. Optical density (OD_{600}) growth curves of bacterial cultures showed a decrease in growth rates. The most significant drop in growth rate was observed with As^{+3}, from 0.137 h^{-1} to ~ 0.08 h^{-1}. A similar effect (μ, 0.1 h^{-1}) was observed in the presence of As_{CP}. Total lipid extracts (TLE) from cultures in stationary phase were analyzed by high performance liquid chromatography coupled to quadrupole time of flight mass spectrometry (HPLC–qToF-MS) for intact polar lipids (IPLs) identification. Changes in IPLs were detected, specifically in aminolipids and aminophospholipids. The structural lipid phosphatidylethanolamine (PE), increased in relative abundance by 17.7 or 15% with As^{+3} or As_{CP}, respectively. Ornithine lipids (also an amino lipid) were identified and showed an amendment-induced increase of 0.4% (As^{+3}) and 2.6% (As_{CP}). Three compounds (UN1, UN2 and UN4) were tentatively assigned to aminolipids and two of them (UN1 and UN2) showed a decrease after As treatment. On the other hand, UN4, specifically reacted to As^{+3} by a 10% increase. The present work indicates a sensitive lipid response to As^{+3} species by *S. oneidensis* MR1, suggesting a mechanism related with amine sequestration during arsenic stress. A similar response was observed when As_{CP} were added to bacterial cultures, suggesting a toxicity linked to As^{+3}, perhaps via release of dissolved As^{+3} species from the colloidal structure. An arsenic sensitive lipid response represents a great tool for environmental monitoring of ecosystems contaminated by the metalloid and demands a deeper focus upon a correct chemical structure elucidation of candidate molecules as biomarkers and the need for a better understanding of soluble and colloidal arsenic influence upon bacterial cell membranes. Our results provide novel insights in As colloidal fractions toxicity in microorganism as well as in environmental models, suggesting dissolution of As bearing nanomaterials as a relevant process in the metalloid chemistry of marine ecosystems.

5.1 Introduction

Nanoparticles are materials with at least one of their dimensions in the nanometer scale, normally between 1 to 100 nm [50]. When materials are confined to the nanometer scale they can exhibit novel or enhanced properties like solubility, UV-VIS absorption or antimicrobial effects [50]. Nanomaterials can occur in the environment, for instance, hydrothermal systems have been described as a source of metallic and metalloid bearing nanostructures [21, 29, 30, 190]. In the shallow hydrothermal system off Paleochori bay, our group identified for the first time As rich colloidal (400 - 20 nm) particles [190]. The detection of these particles in hydrothermal fluids and porewater samples offshore, suggested an influence of non-described forms of the metalloid over marine organism. During the past decade, the influence of As rich hydrothermal fluids upon the indigenous microbial community in the hydrothermal area off Milos was investigated by means of arsenic resistance gene distribution and bacterial and archaeal diversity, with most of the data focused in the effect of soluble As (below 400 nm) species [87, 88, 92, 143]. To our best knowledge, no study has so far addressed the impact of As nanoparticles or colloidal particles (400 – 20 nm) upon microorganism.

Commonly, nanoparticles toxicity is linked to the release of dissolved species, which may enter the cell and affect the inner redox status, macromolecule configurations, metabolic reactions or gene expression of the organism. [152, 208-211]. In the case of dissolved As, toxicity has been related to an increase in the oxidation rate of thiols (R-SH) inside of the cell, altering the redox status and favoring the generation of reactive oxygen species (ROS) with the concomitant oxidation of macromolecules [212-217]. Lipid oxidation, specifically lipoperoxidation of membranes induced by ROS, generate the accumulation of reactive agents (i.e. aldehydes) inside of cells, and represent a mechanism of toxicity associated to arsenic [39, 218-225]. However, a lipid response to ROS induced during As stress or a direct interaction of lipids and As species have not been considered as an arsenic detoxification mechanism. Different As responses are described in prokaryotes, most of them related to transporter or channel proteins, chelating proteins or peptides and oxidizing or reducing enzymes [95, 226]. The role of these proteins is to regulate arsenate uptake, arsenate reduction, arsenite exportation or arsenite sequestration [95, 226]. Nonetheless, other macromolecules could be part of As detoxification, for instance, membranes, in a direct reaction to As or reactive species induced by arsenic oxidative stress [224].

A bacterial model commonly used in toxicity assays of nanoparticles suspensions (TiO_2, Au, $Li_xNi_yMn_zCo_{1-y-z}O_2$, Cu-$TiO_2$, ZnO or Fe-ZnO, CdSe or ZnSe etc.) is *Shewanella oneidensis* [227-235]. Because of its ubiquity, highly studied genome and relevant metabolism, *S. oneidensis* represent an excellent candidate for evaluation of a microbial response to As-rich colloidal particles in marine environments [236-242]. *Shewanella* spp., as many gram-negative bacteria, has a detoxification system (*ars* operon) and a dissimilatory pathway (*arr* operon) for As^{+5} reduction, which can be induced or inhibited based on environmental conditions [99, 100, 243, 244]. Recently, biotransformation of arsenic (As^{+3} or As^{+5}) was observed through partial methylation of the inorganic forms of the metalloid under anaerobic and aerobic atmospheres coupled to Fe reduction, representing a novel mechanism for As detoxification in *Shewanella* spp. cultures [242]. Finally, mineralization of As^{+3} as a detoxification step was observed by

formation of arsenic sulfide nanotubes when different *Shewanella* spp. strains under anoxic atmospheres were exposed to 5 mM arsenate [77]. However, among all these mechanism of As detoxification, a lipid response to arsenic has not been considered.

Shewanella spp. represent an interesting bacterial model to evaluate the toxicity of As colloidal particles and to develop novel insights in bacterial lipid response to As stress. To achieve this goal, As-rich colloidal particles were synthesized (Duran-Toro et al., 2020. In prep) and their toxicity was evaluated by growth inhibition and evaluation of membrane lipid adaptations by HPLC-qToF-MS.

5.2 Materials and Methods

5.2.1 Synthesis of arsenic rich colloidal particles

Generation of an As colloidal particle stock (100 mg mL^{-1}) was obtained as described in Duran-Toro et al. (2020, in preparation). Reaction synthesis consisted of ultra-pure Milli-Q water (18 Ω), a soluble precursor of S^{-2} (Na_2S*9H_2O, 1M) at 3 mM final concentration and pH near 4. Once pH was adjusted using HCl (1M), the arsenic soluble precursor ($NaAsO_2$, 1 M) was amended to the solution at a final concentration of 300 µM. Reaction temperature was set at 25 °C during the 24 h of incubation. In order to concentrate the particles, reaction solution was filtered on polycarbonate (PC) membrane filters (pore size 0.2 µm). Filters were subsequently dissolved in chloroform (10 mL) and the suspended material was aliquoted in 1.7 mL Eppendorf tubes for centrifugation at 20000 rpc for 5 min. Particles were rinsed three times with 1 mL of 0.1 M acetate buffer (0.0941 M CH_3COONa and 0.0059 M CH_3COOH) at a pH below 5 and centrifuged as described before. Finally, particles were dried at room temperature overnight, resulting in a yellow powder that was stored at 4 °C for further toxicity experiments. Aggregation of particles was studied through dynamic light scattering (DLS), morphology changes were monitored by transmission electron microscopy (TEM) and chemical composition was confirmed by energy dispersive x-ray spectroscopy (EDX) of the particles collected in PC filters. Size distribution and polydispersity index (PDI) were obtained in a Malvern zeta-sizer DLS from a 1 mL aqueous suspension of freshly prepared As colloidal particles at a concentration of 0.1 mg mL^{-1} (of the material). Colloidal particle suspension was sonicated (bath sonication) for 10 mins prior DLS studies. 5 µL of the colloidal particles suspension was placed on top of a Cu-grid and dry overnight at room temperature for TEM characterization. TEM analysis of the samples was carried in a transmission electronic microscope Philips CM 20 operated at an acceleration voltage of 80 kV. The elemental composition of the particles collected during filtration was determined in a field emission microscope (Zeiss, model iSUPRA 40) with an EDX detector (Bruker, XFlash 6|30) operated at an acceleration voltage of 20 kV.

5.2.2 Cell counting

The protocol for cell counts in environmental samples described elsewhere [245] was followed with minor modifications. An aliquot of a cell suspension was diluted (1:4) in HEPES buffer (0.1 M, pH 6.8; sterile by filtration). The suspension was then filtered onto PC filters (0.2 µm) using a vacuum pump. Filters were removed once dried under vacuum pressure and then incubated with the fluorescent probe Syber Green I for DNA staining. For incubations with Syber Green I, a 0.025 % volume/volume (v/v) dilution was made from the original concentration of the probe stock. The dilution was performed under sterile conditions using filtered (0.02 µm) Milli-Q water to avoid external contaminations. 50 µL of the staining solution (SG-I 0.025%) were poured into a petri dish, and on top of the staining solution the filter with the collected cells was placed assuring an even distribution of the staining solution. The Petri dish was closed and covered (to avoid light exposition) and cells were incubated at room temperature for 15 min. Filters were removed and carefully located on top of sorbent tissue. Afterwards, 10 µL of 5 % (w/v) ascorbic acid in 1:1 PBS (Phosphate Buffer Saline 0.1 M, pH

7.1) : Glycerol sterile mixture, were placed on top of a microscopic slide and on it the filter was mounted for cell counts. Total cell numbers were obtained in an optical microscope designed with a square-grid in the lens to record number of particles per square area (156.25 μm^2). A minimum of 500 cells were counted per sample to avoid statistical errors.

5.2.3 Growth Inhibition

A mother culture of *S. oneidensis* MR1 was incubated in luria broth medium (LB, NaCl 1 % w/v; tryptone 1 %; yeast extract 0.5 %; pH 7.1). Once the mother culture entered exponential growth phase (14 h, $OD_{600} \sim 0.7$), the total cell number was determined with the fluorescent probe Syber Green I as described before [245] and a cell pellet was obtained by centrifugation (4000 rpc, 20 min). Using the cell number of the mother culture, an initial cell density for growth inhibition experiments was set at $\sim 10^6$ cell mL^{-1} by suspension of the cell pellet in fresh LB medium. The new suspensions (in triplicate) were incubated at 28 °C and amended with 0 (control), 93.75, 187.5 or 375 µg mL^{-1} arsenic, in the form of colloidal particle (As_{CP}), or the soluble species arsenate (As^{+5}) or arsenite (As^{+3}). Cell density, in the new suspensions, was determined at the beginning of the incubation and after 16 h to stablish a bacteriostatic or bacteriolytic effect of the metalloid. A maximum growth was stablished under control conditions and a decrease in cell density was registered as growth inhibition percentage.

5.2.4 Growth over time and growth rate (µ) calculation

Shewanella oneidensis MR1 cultures (LB, pH 7.1 and 28 °C) were inoculated at a starting OD_{600} between 0.1 and 0.05. Cultures were amended immediately with 375 µg mL^{-1} (5 mM) arsenic as colloidal particle (As_{CP}), arsenate (As^{+5}) or arsenite (As^{+3}). Culture growth was followed as an increase of OD_{600} values over time by measuring optical density of aliquots in a UV-VIS spectrophotometer shimadzu (UV-1280). Linear regression of the natural logarithms of OD_{600} [$Ln(OD_{600})$] over time was used to calculate specific growth rate (µ, h^{-1}).

5.2.5 Total lipid extracts (TLE)

Cell pellets of *S. oneidensis* MR1 cultures at early stationary phase without treatment (Control) and amended with 375 µg mL^{-1} of arsenic as colloidal particle (As_{CP}), arsenate (As^{+5}) or arsenite (As^{+3}) were obtained by centrifugation (4000 rcf, 20 min). Pellets were stored at −20 °C to preserve lipid integrity. At least 200 mg of wet weight from cell pellets were deposited in teflon tubes containing 4 g of combusted sand (600 °C, 6 h). A bacterial lipid standard containing synthetic phosphatidylcholine 21C was added to determine lipids recovery percentage from extraction and further procedures. Cells were lysed and lipids extracted using bath sonication of cell suspensions in phosphate and TCA (trichloroacetic acid) extraction buffers as described elsewhere [120, 246]. Organic phase separation using ultrapure Milli-Q water and DCM (dichloromethane) in a liquid-liquid system was done as described in literature [120, 246]. Organic phase containing lipids extract were evaporated at 40 °C under N_2 flow, afterwards the lipid extract was suspended in 1 mL DCM:Methanol (5:1) and transferred into 2 mL glass vials

(combusted) for its storage at −20 °C prior its analysis. When necessary solvent of lipid extracts was evaporated and the solid extract store at – 80 °C for longer storage periods.

5.2.6 Lipid identification by HPLC-qTOF-MS

Glyco-, amino- and phospholipid present in TLE were analyzed in a Dionex Ultimate 3000RS UHPLC instrument connected via an electrospray ionization source to a Bruker maXis high resolution quadrupole time-of-flight mass spectrometer (HPLC-ESI-qTOF-MS) under conditions described previously [120]. Compounds separation consisted of hydrophilic interaction liquid chromatography (HILIC) [120]. Detection of lipids was done in positive ionization mode, scanning a mass to charge ratio (m/z) range from 100 to 2000. Identification of lipids was based on exact masses of parent ions (present as either H^+ or NH_4^+ adducts) together with characteristic fragmentation patterns. In each MS scan, tandem experiments (MS2) were focused on most abundant ions detected. Additionally, external standard (phosphatidylethanolamine-diacylglycerol, PE-DAG; phosphatidylglycerol-diacylglycerol, PG-DAG; and glucosyl-diacylglycerol, G-DAG) were set to calibrate response factors of the method. Identification of ornithine lipid (OL) and di-phosphatidylglycerol (DPG) was performed according to published mass spectra [247-249]. When no standard was available or no possible structure was designated to a molecule a response factor of 1 was assumed.

5.3 Results

5.3.1 Characterization of arsenic colloidal particles

Transmission electron microscopy analysis of the colloidal particles showed spherical morphology and a diameter size ranging between 50 to 250 nm (Figure 5.1a). Size distribution was observed in DLS experiments, with peak at 11 and 106 nm (Figure 5.1b). The PDI indicated particle aggregation with a value over 0.3, which correlates with agglomeration of particles observed by TEM (Figure 1a) and a minor peak of aggregates with size near 500 nm (Figure 5.1b). Chemical composition obtained by EDX spectra exhibited particles rich in As, S and O (Figure 5.1c). Due to use of polycarbonate filters, the presence of C was assumed as an artifact of sample preparation (Figure 5.1c). Elemental weight percentage (Weight %) generated from EDX analysis revealed that up to 16 % of the material consist of As (Figure 5.1d). Weight % value was used in further experiments to calculate As concentration in particle aqueous suspensions.

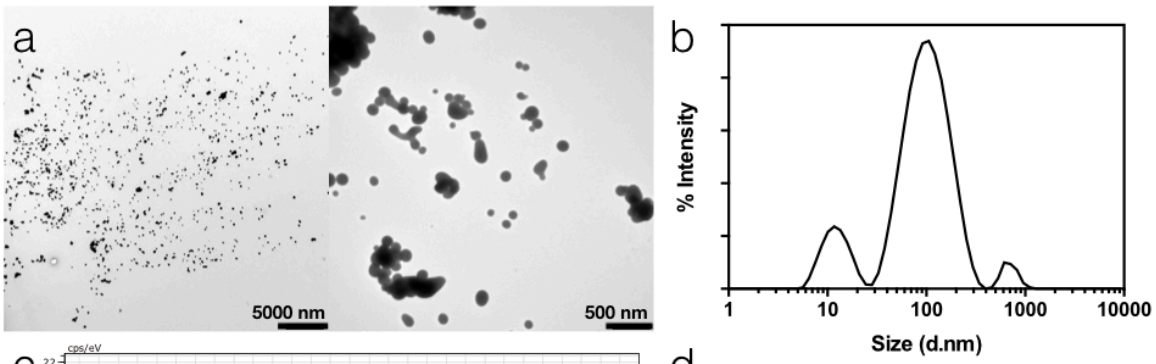

El	Serie	norm. C
		[Weight.%]
C	K-Serie	0,00
O	K-Serie	39.76
S	K-Serie	44.25
As	L-Serie	15.99
---	--------	--------
	Summe:	100,00

Figure 5.1. Characterization of arsenic colloidal particles. a, TEM images at two different magnifications (7000x, left and 14000x, right) of As_{CP} collected by filtration (0.2 µm) and suspended in Milli-Q water (pH near 6). b, DLS study of unfiltered samples showed PDI values of 0.45, indicating aggregation of particles with a size close to 500 nm. c, EDX spectrum of As_{CP} showed main peaks of As, S and O. High abundance of O and C its attributed to the use of polycarbonate filter and oxyanion in the reaction synthesis. d, weight percentage [Weight. %] of elements present in the sample.

5.3.2 Antimicrobial effect of colloidal and soluble arsenic

Arsenic incubation experiments in *Shewanella oneidensis* MR1 cultures did not indicate a bacteriolytic or bacteriostatic effect within the presence of the soluble inorganic form arsenate (As^{+5}), yet a mild toxic effect with arsenite (As^{+3}) at concentrations equal or below 187.5 µg mL^{-1} were detected (Supplementary Figure 5.1, SF 5.1).

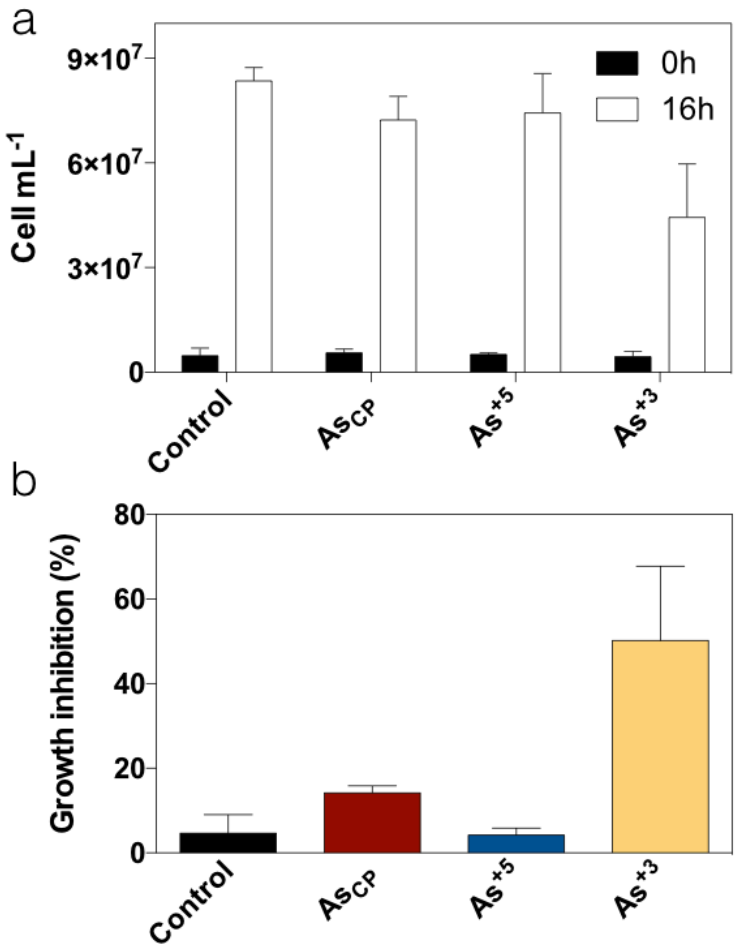

Figure 5.2. Growth inhibition of arsenic soluble species and arsenic colloidal particles on *S. oneidensis* MR1. A mother culture of *S. oneidensis* MR1 was grown during 14 h incubation, at 28°C in LB medium. Once the culture reached exponential phase, cells were harvested and resuspended in fresh LB medium amended with 375 µg mL^{-1} of arsenic as colloidal particles As_{CP}, arsenate (As^{+5}), arsenite (As^{+3}) or without arsenic (Control). a, Cells were counted in the beginning of the incubation and after 16 h. b, The difference in cell density after the incubation time was used to calculate the growth inhibition percentage. The average difference in the control condition was assumed as 100% growth. Each condition was replicated at least 3 times.

When 375 µg mL^{-1} of As^{+3} was present in the incubations the most detrimental effect was observed (Figure 5.2). The growth inhibition was determined as a reduction on the maximum cell density variation between the beginning of the experiment, and after 16 h of incubation (Figure 5.2a). The cell density in the control, 8.7×10^7 cell mL^{-1}, was reduced to 4.3×10^7 cell

mL^{-1} in the presence of As^{+3} (Figure 5.2a), representing a growth inhibition percentage close to 50 % (Figure 5.2b). A minor inhibition of growth (14 %) was observed in the presence of As_{CP}, while no significant variations were observed in the treatments with As^{+5}. Due to the bacteriostatic effects detected with As^{+3}, the highest concentration tested (375 µg mL^{-1}) was used as reference in the rest of the experiments.

Time course optical density changes of *S. oneidensis* MR1 cultures (LB, pH 7.1 and 28 °C) treated with 375 µg mL^{-1} confirmed a bacteriostatic effect and a higher toxicity of As^{+3} upon microbial growth when compared to colloidal particles or As^{+5} (Figure 5.3a). Optical density (OD_{600}) values on stationary phase of cultures correlate with cell density variations (Figure 5.2 and 5.3a), however, during previous growth phases the change in OD_{600} showed an early tolerance to arsenic (Figure 5.3a).

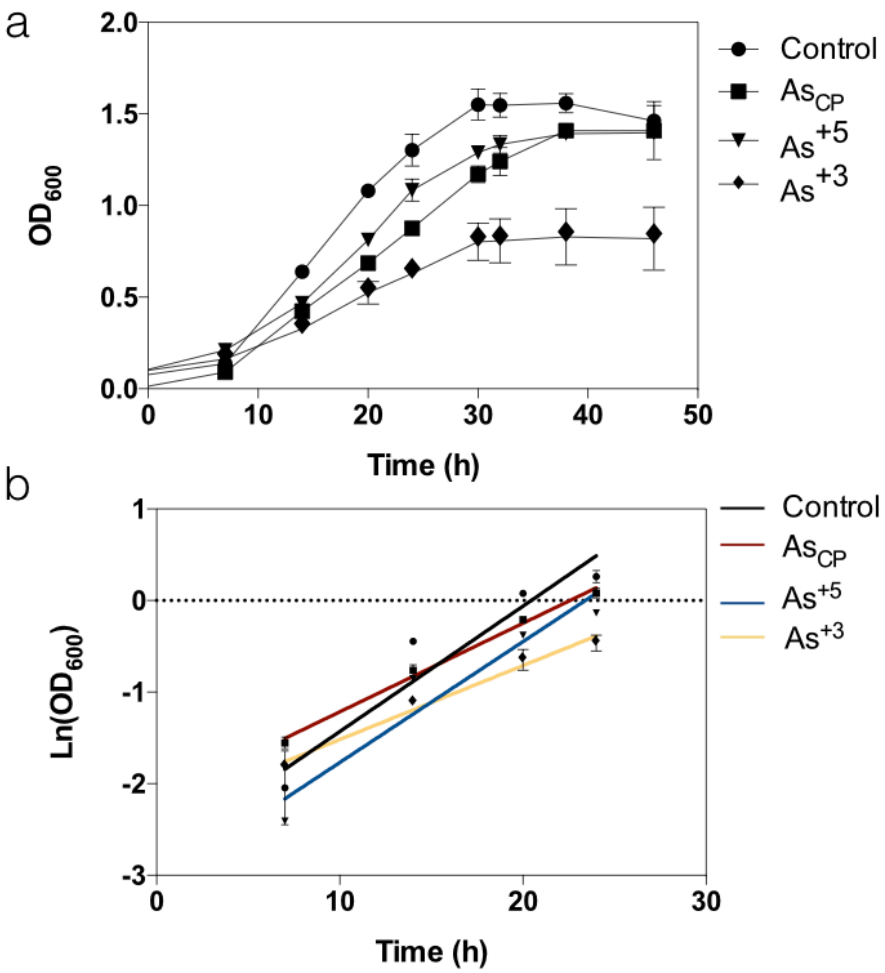

Figure 5.3. Arsenic soluble species and arsenic colloidal particles effect upon *Shewanella oneidensis* MR1 growth. a, Time course of OD_{600} *S. oneidensis* MR1 cultures amended with 0 (control) and 375 µg mL^{-1} of arsenic as colloidal particles (As_{CP}), arsenate (As^{+5}) or arsenite (As^{+3}). b, Regression line of $Ln(OD_{600})$ variations over time at exponential growth phase. Slope values correspond to number of division per time unit or specific growth rate (µ, h^{-1}). R^2 values in every regression were higher than 0.91.

Alteration on the growth slope during exponential growth phase indicate a decrease in specific growth rate (μ, h^{-1}) as a consequence of arsenic toxicity, which was confirmed by linear regression analysis of $Ln(OD_{600})$ over time (Figure 5.3a). Growth rates declined from 0.13 h^{-1} in the control (without arsenic), 0.10 h^{-1} with As_{CP}, to a μ value near 0.08 h^{-1} observed in the As^{+3} treatment (Figure 5.3b, Table 5.1). No significant variation on μ was obtained during *S. oneidensis* MR1 cultures amended with As^{+5} (Table 5.1).

Table 5.1. Arsenic effect upon growth rate of *Shewanella oneidensis* MR1

	Control	As_{CP}	As^{+5}	As^{+3}	Reference value [250]
μ (h^{-1})	0.137	0.10	0.132	0.08	0.1 - 0.2

As_{CP}: arsenic colloidal; arsenate: As^{+5}; arsenite: As^{+3}.

5.3.3 Lipid response to colloidal and soluble arsenic

Total lipid extracts (TLE) were successfully obtained from early stationary phase cultures of *S. oneidensis* MR1 control experiments and for those treated with 375 μg mL^{-1} As_{CP}, As^{+5} or As^{+3}. The extracts were analyzed by HPLC-qTOF-MS for compounds identification based on exact mass detection and fragmentation patron of parental ions (MS2). Diacylglycerol and acyl/etherglycerol (AEG) core structures, were identified by co-elution of compounds with similar m/z. Unidentified lipids were assigned as aminolipids or aminophospholipids based on MS2 similarities to amino acid fragmentation patrons [251]. Figure 5.4 shows the changes in relative abundance of intact polar lipids (IPLs) present in the TLE of *S. oneidensis* MR1 cultures without arsenic (Control) or with As_{CP}, As^{+5} or As^{+3}. Aminolipids and aminophospholipids marked the major responses to arsenic in all three different metalloid forms (Figure 5.4). Unknown compounds lipids, UN1 and UN2, exhibited a substantial decrease with As_{CP} and As^{+3} treatment, from 5.3 to 2.2 or 0.5 % and from 12.7 to 5.1 or 1.4 %, respectively (Figure 5.4). UN4 shows the most specific response to an arsenic form, increasing from 0.72 to 11.6 % only in the presence of As^{+3} (Figure 5.4). On the other hand ornithine lipids increased from 6.8 % (control) to 7.2 (As^{+3}) or 9.4 % (As_{CP}). Finally, the major intact polar lipid detected, the aminophospholipid PE-DAG/AEG was found to increase in relative abundance from 44.8 % (control) to 62.2 (As^{+3}) or 59.7 % (As_{CP}). Other intact polar lipids also varied its relative abundance, PG-DAG/AEG decreases from 8.7 to ~4% in all arsenic treatments (Figure 5.4). While di-phosphatidylglycerol (DPG) remained stable with a low abundance (0.5 %), and glycolipid G-DAG disappears only when As^{+3} was present (Figure 5.4). A specific lipid response to As^{+5} was not evidenced, except for a decrease in PE and UN3, from 12.7 (control) to 8.7 %, rather a similar behavior was observed compared to the control (Figure 5.4).

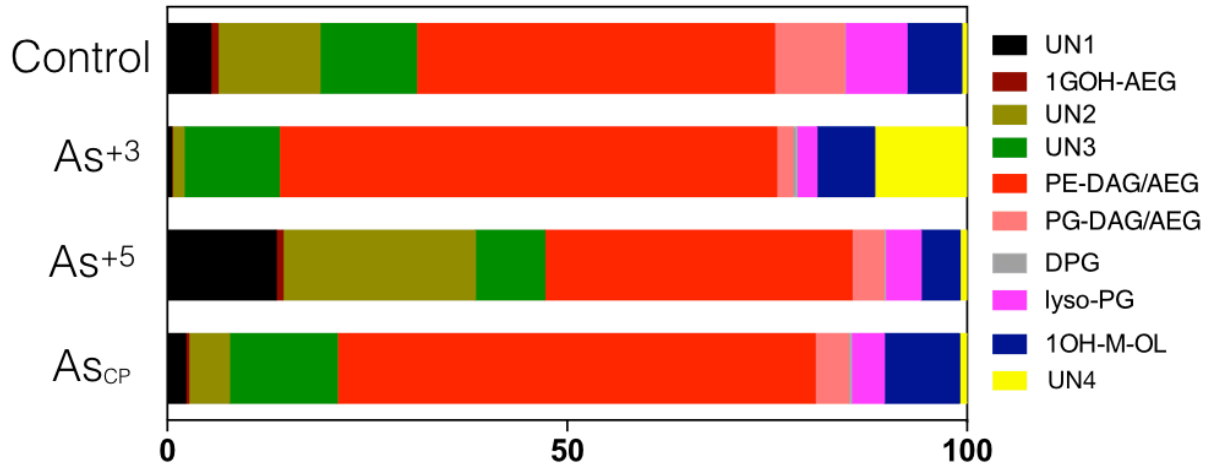

Figure 5.4. Effect of arsenic soluble species and arsenic colloidal particles upon intact polar lipids abundance in *Shewanella oneidensis* MR1 cultures. 1GOH-AEG: monoglucosyl-monohydroxy-acyletherglycerol; PE-DAG/AEG: phosphatidylethanolamine-diacylglycerol/ acyletherglycerol; PG-DAG/AEG: phosphatidylglycerol-diacylglycerol/acyletherglycerol; DPG: di-phosphatidylglycerol; 1OH-M-OL: monohydroxy-methyl-ornithine lipid. As_{CP}: arsenic colloidal; arsenate: As^{+5}; arsenite: As^{+3}.

5.4 Discussions

5.4.1 Arsenic tolerance of *Shewanella oneidensis* to soluble and colloidal forms

Shewanella oneidensis is a highly studied gram negative bacterium, a marine microorganism with multiple mechanisms of arsenic resistance [237, 242-244]. Among these mechanisms can be found detoxification pathways of arsenate reduction, exportation systems of the trivalent form of the metalloid, and enzymatic methylation steps which results in the generation of volatile organoarsenic compounds like monomethylarsonic (MMA) or di-methylarsinic (DMA) acids [237, 242-244]. *Shewanella* spp. have been reported to tolerate concentrations over 10 mM (749 mg L^{-1}) arsenate and 20 μM (1.5 mg L^{-1}) arsenite in anoxic atmospheres and rich culture media [77, 242, 244]. Compared to other gram negative bacteria, *Shewanella* spp. , do not represent a highly arsenic resistant organism [95, 252]. For instance, *Escherichia coli* can tolerate ~2.7 mM (200 mg L^{-1}) as either arsenite or arsenate [95], or *Corynebacterium glutamicum*, capable to tolerate 12 mM arsenite and > 400 mM arsenate [252]. Rather, *Shewanella* spp. produces specific responds to the metalloid at quite low concentrations [237, 242-244]. Changes in growth curves of *S. oneidensis* MR1 can be observed at low concentration of arsenite (~6.7 μM or 0.5 mg L^{-1}) which correlates with methylation activity and the generation of MMA and DMA [237, 242].

The results presented in Figure 5.2 and 5.3, are in agreement with bacterial resistance to arsenic, where *S. oneidensis* MR1 showed a higher tolerance to the oxidized form of the metalloid (arsenate). The experiments (Figure 5.2 and 5.3) were carried under oxygen rich atmosphere, thus, only detoxification pathways like *ars* operon activity can be expected, discarding the use of arsenic as an electron acepto coupled to the metabolism of *S. oneidensis* MR1. The experimental set-up (aerobic conditions) could explains the arsenic concentrations tolerated by *S. oneidensis* MR1 (Figure 5.2 and 5.3), which exceed values described in literature [77, 242, 244]. Table 5.1 specified the range of growth rate for aerobic cultures of *S. oneidensis* MR1. Higher growth rates and OD observed in aerobic cultures (Figure 5.3 and Table 5.1) [250], suggest additional mechanism of cellular response employed during arsenic stress. Perhaps, cellular responses like arsenic methylation or novel mechanisms (interaction with lipids, Figure 5.4) could explain better the bacterial response to arsenic in marine oxygen rich environments. This deserve further attention since several ecosystems affected by arsenic, including the sediments off Paleochori bay, where colloidal arsenic rich particles were described to occur [190], share as a mechanism of adaptation to arsenic the use of specific transportation systems instead of metabolic cycling of the element (*arr* or *aoi* genes) [88]. Our results raise the question about the importance in the environment of non-enzymatic mechanisms of response to arsenic in microbial communities. Furthermore, in the case of As_{CP}, a similar but milder effect was observed (Figure 5.2 and 5.3), extending the hypothesis to colloidal materials, and suggesting a common mechanism of toxicity between As_{CP} and As^{+3} soluble species.

5.4.2 Variation of aminolipids and aminophopholipids as response during colloidal arsenic and soluble arsenic stress

Shewanella spp. membrane lipids described so far correlate with gram-negative models [253, 254]. Di-phosphatidylglycerol, DPG, acyl-phosphatidylglycerol (acyl-PG), and PE being the most abundant detected [253]. In some novel species (*Shewanella* sp. nov.), unknown aminolipids or aminophospholipids have been identified as components of the lipid membrane [255, 256]. Interestingly, the main effect of As_{CP} upon relative abundance of IPL from *S. oneidensis* MR1 cultures was a distinctive variation of aminolipids and aminophospholipids (Figure 5.4). Little is known about arsenic stress and changes in membrane composition in bacteria, perhaps one of the few works described until date correspond to an adaptive fatty acid membrane profile stablished in *Bacillus* sp. ORAs2 and *Pseudomonas* sp. ORAs5 when exposed simultaneously to arsenic and toluene [121]. The changes in fatty acid content were linked to growth rate variation, where an increase in fatty acid saturation was observed at lower growth rate values [121]. Nonetheless, no studies on IPL composition were performed during arsenic incubations. On the other hand, in eukaryotic cells, a direct interaction or variation in aminolipid content can occur as a response to rising levels of aldehydes produced by oxidative stress, which as mentioned earlier, can be triggered by arsenic toxicity [257]. 4-hydroxy-2-alkenals or 4,5-epoxy-2-alkenals, common products (aldehydes) of lipid membrane oxidation, react through covalent bonding with PE as a result of oxidized fatty acid chains in the presence of oxidative stress inducers [257]. p-hydroxyphenylacetaldehyde, and other aldehydes generated by myeloperoxidase enzymatic activity, can modify phospholipid amino groups of low density lipoprotein in human atherosclerotic intima and represent a similar mechanism of aldehydes removal [258]. Yet, no evidence of aminolipids or aminophospholipids, like PE, have been associated to aldehydes sequestration during oxidative stress or arsenic toxicity in bacteria [248, 259]. So far, only environmental stressors (low pH, high temperature, P deficiency, high salinity etc.) has been attributed to variation of bacterial aminolipids and aminophopholipids abundance [113-118]. Even though arsenic has been stablished as an oxidative agent in bacterial cells, generating lipoperoxidation of cell membrane [122], no further analysis of IPLs have been performed in gram-negative (*Eschericia coli*) or gram-positive (*Bacillus subtilis*) bacteria, in *Shewanella* spp. or any other bacterial model. The changes described here (Figure 5.4), represent a first study in membrane adaptation to arsenic stress in *Shewanella* spp. and should be contrasted with other microbial models in order to fully address a change in relative abundance of aminolipids or aminophospholipids as a common mechanism of adaptation to high arsenic stress in bacteria. In the case of temperature and pH stress, which represent the most documented environmental factors to induce IPL changes upon microbial cells, the soil bacterium *Pseudopedobacte*r *saltans*, presented an increased fractional abundance of lysine-containing IPLs (aminolipids) at lower temperature and higher pH values [114]. This correlates with gradient temperature response of IPLs isolated from marine sediments in the shallow hydrothermal system off Paleochori bay (Milos, Greece), where the heat increase dictated a decrease in betaine and ornithine lipid content [117]. On the other hand, phosphorus (P) deficiency triggers substitution of membrane phospholipids for a variety of non-phosphorus lipids, among them the aminolipids, representing a conserved response in phylogenetically diverse marine heterotrophic bacteria, like *Alphaproteobacteria* and *Flavobacteria* [115]. Finally, salinity can also play a role in aminophospholipid abundance in

bacterial cell membrane, the moderate halophile *Vibrio costicola* exhibited a decrease in PE content when incubated under increasing concentrations of NaCl [113]. In the case of temperature and pH, the cell stress derives, as with arsenic, in the generation of ROS [122, 260, 261]. Perhaps, the changes in aminolipids or aminophospholipids represent a wide-spread mechanism in microbial cells to deal with ROS or other reactive agents (i.e. aldehydes) produced during membrane lipoperoxidation. Nonetheless, some of the environmental stressors like P deficiency or high salinity, exhibited changes in aminolipid or aminophospholipid abundance due to structural responses to maintain cell integrity more than a specific response to reactive agents formed [115, 116, 262]. Based on our observations, it seems necessary to discriminate between these two mechanism (reactive species sequestration or cell integrity maintenance) in order to fully understand the effect of As colloidal particles upon bacterial cell membranes. Detection of ROS in biological systems with membrane specific fluorescent probes can distinguish events of oxidative stress allocated in the membrane, helping to distinguish not only the generation of ROS but also the specific location of the stress [263]. On the other hand, if changes in aminolipids or aminophospholipids abundance derives from a maintenance of cell structure, rather than a ROS sequestration, studies of lipid ratios between aminolipid and glycolipids or phospholipids should be performed together with analysis of cell size or morphology changes in order to distinguish a structural or biomechanical adaptation as described to occur in archaea, which have shown variation in their cell morphologies due to saline stress [119]. The elucidation of As colloidal particle effect upon cell membrane of a marine organism like *S. oneidensis* MR1 will contribute in the understanding of microbial responses to As colloidal fraction in the environment and to fully comprehend the cell and lipid adaptation of other microorganism to environmental stressors.

5.4.3 Mechanism of toxicity of As rich colloidal particles

Synthesized arsenic colloidal particles (As_{CP}) exhibited a size over 50 nm and the tendency to agglomerate (PDI > 0.3) when suspended in an aqueous solutions, forming aggregates with a size close to 500 nm (Figure 5.1). Size, morphology (spheres) and As weight percentage (∼16 %) correlate with the synthesis method described previously (Duran-Toro et al., 2020. In prep). Incorporation of particles into the cells is very unlikely based on size ranges, therefore, a direct interaction with the cell membrane or release of soluble species of As should be assumed as the mechanism of toxicity (Figure 5.1). The arsenic precursor used in colloidal particle synthesis was $NaAsO_2$, which contains arsenic in oxidation state +3, suggesting the release of dissolved species of As^{+3} from the particles. In growth inhibition experiments (Figure 5.2 and 5.3), a similar but less significant response to As colloidal particles can be observed when comparing the effect of As^{+3}. Perhaps, a minor release of As^{+3} species can account for the moderate toxicity in cell density variations and changes in growth rate when As colloidal particles were added (Figure 5.2 and 5.3). Also, the lipid response (Figure 5.4), studied through variation of IPL, reflected a similar profile for As^{+3} and As_{CP} (Figure 5.4), supporting the idea of As^{+3} release from the colloidal particles as a possible mechanism. Moreover, a pH increase over 6, can alter phase stability of arsenic-sulfide precipitates and represent a mechanism of dissolution of arsenic sulfide minerals like orpiment (As_2S_3) or realgar (As-S) as described before [125, 264]. Thus, LB medium set at pH 7.1 could explain a destabilization of the particles

and a concomitant release of As^{+3} from its structure. *Shewanella* spp. can grow in the presence of arsenate (As^{+5}) as an electron acceptor under anaerobic conditions at the same concentration (375 µg mL^{-1} or 5 mM) used in the growth inhibition experiments reported (Figure 5.2 and 5.3) [77], and as it can be observed neither the cell density nor the growth rate was altered under As^{+5} influence (Figure 5.2 and 5.3; Table 5.1). Thus, the oxidation of arsenic (As^{+3}) and release of As^{+5} from the colloidal particles does not provide a satisfactory explanation for As_{CP} toxicity. Finally, a direct interaction of the colloidal particles with the membrane or extracellular structures as has been described in literature for metallic nanoparticles should not be discarded as part of the toxic effect and most be evaluated in the future [152, 208-211]. In order to truly understand the mechanism of toxicity related to As colloidal particles, TEM studies of *S. oneidensis* cells exposed to the particles could provide insights about changes in particles size, variation in cell size or morphology associated to particle-cell interaction, or generation of membrane vessels as a mechanism of response to the stressor. Also, quantification and speciation of arsenic by sensitive methods like inductively coupled plasma mass spectrometry, could help in the detection of arsenic release from colloidal particles, quantification of arsenic uptake by bacterial cells or determination of oxidation state of the species released. A clear understanding on As colloidal particle toxicity will contribute in the analysis or models of As colloidal fractions distribution, stability and toxicity in environments where generation of As colloidal material can occur.

5.5 Conclusions

Toxicity of As colloidal particles in *Shewanella oneidensis* MR1 cultures was studied. A bacteriostatic effect of colloidal particles was observed by decrease in the number of cell and a reduction of growth rates in cultures incubated with the metalloid as a colloidal particle. The toxicity correlated with variations of intact polar lipid abundance, suggesting a lipid adaptation as a potential mechanism of response to arsenic stress. The colloidal particles showed a similar toxicity and lipid response compared to soluble As^{+3}, suggesting the release of dissolved As^{+3} species from the colloidal particles as a mechanism of action. No effect of soluble As^{+5} was observed at the given concentration (375 µg mL^{-1}), discarding arsenic oxidation and release of As^{+5} as a mechanism of toxicity. The main intact polar lipid variation was exhibited in treatments of As^{+3} and As colloidal particles, consisting in a change of aminolipid and aminophospholipid abundance. Further experiments to elucidate a mechanism of toxicity and a lipid response associated to it, i.e. release of arsenic soluble species, generation of reactive oxygen species, adaptation of cellular morphology etc., will significantly contribute in the understanding of lipid adaptation as a mechanism of response to arsenic stress or to other toxic colloidal materials being released into the ocean in marine bacterial communities.

Acknowledgements

This study was supported by Conicyt through a fellowship to VDT (Programa de Capital Humano Avanzado, BECAS-Chile, CONICYT, 2015) and by the Deutsche Forschungsgemeinschaft (DFG, Germany) through the Emmy Noether-Program (grant BU 2606/1-1 to SIB).

Supplementary Material

Figures

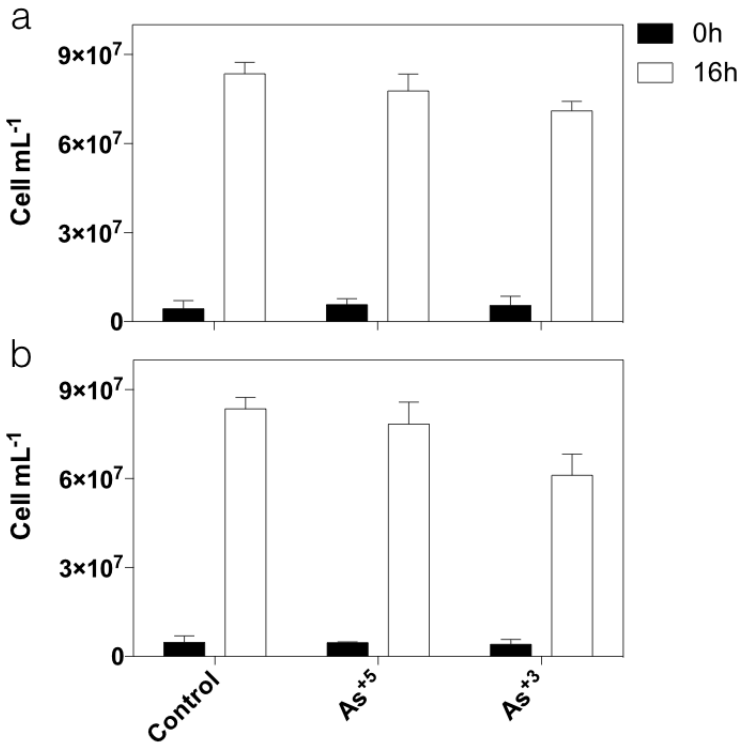

Supplementary Figure 5.1 (SF 5.1). Growth inhibition of arsenic soluble species on *S. oneidensis* MR1. A mother culture of *S. oneidensis* MR1 was grown during 14 h at 28°C in LB medium. Once the culture reached exponential phase, cells were harvested and resuspended in fresh LB medium amended with 93.75 (a) and 187.5 (b) µg mL^{-1} of arsenate (As^{+5}) or arsenite (As^{+3}) or without arsenic (Control). Cells were counted in the beginning of the incubation and after 16 h. Each condition was replicated at least 3 times.

Chapter 6 - Conclusions and Future Perspectives

6.1 Conclusions

This doctoral dissertation focused in the study of arsenic nanoparticles in hydrothermal environments and their implications for marine chemistry and biological toxicity. Using interdisciplinary approaches, from geochemical characterization of hydrothermal fluids, to high resolution microscopic techniques, the parameters ruling the generation and stability of colloidal arsenic particles in hydrothermal systems were evaluated. Furthermore, toxicity associated to the colloidal material was examined in the marine bacteria *Shewanella oneidensis* MR1.

From a general overview, the results indicate marine hydrothermal systems with fluids rich in arsenic as a:

- Source of amorphous arsenic nanoparticles, contributing to the dispersion of arsenic into the ocean.

Regarding the experiments conducted to understand key parameters of As nanoparticles formation and stability:

- Generation of amorphous arsenic sulfide colloidal particles can naturally occur in the environment during the precipitation of As and S at low pH values.

- The reaction temperature and the presence of additives rich in thiol groups, can modify the abundance, morphology, size and chemical composition of arsenic colloidal particles.

- The stability of amorphous arsenic sulfide colloidal particles decreases at high temperatures, favoring total dissolution of the suspended material over time.

The toxicity assays indicated:

- Arsenic rich nanoparticles have a bacteriostatic effect upon *Shewanella oneidensis* MR1.

- The toxicity of the nanoparticles was characterized by a decrease in growth rates and a significant variation of intact polar lipids containing amino groups in their structures.

Altogether, this thesis highlights the relevance of high resolution techniques like electron microscopy coupled to EDX or SAED modalities and the quantification of elements at trace concentrations (ICP-OES or HG-AFS), in the emerging cross-over of geology and material science. A better characterization of natural or engineered nanomaterials present in ecosystems will provide a deeper understanding of the unexplored colloidal chemistry of elements like As, their impact in marine environments, in a local and, at a global scale.

6.2 Future perspectives

To estimate an emission flux of As nanoparticles in the hydrothermal systems off Milos.

In Paleochori Bay, venting fluxes (fluids) influencing the water column can vary from 50 to 80 L h^{-1} [265]. If we assume that all these fluxes were as high in amorphous arsenic sulfide NP content as values measured for hydrothermal fluid HF2 (As_{200-20}, 1.3 μM; Table 3.3), we can calculate an As NP flux emission of 5 - 8 mg h^{-1} (0.043 - 0.068 Kg yr^{-1}). This general assumption suggest that an As NP flux can influence the coastal ecosystem off Milos, establishing the need for further evaluations of arsenic dispersion in the bay. Therefore, considering the colloidal (400-20 nm) fraction described so far (Figure 3.4 and 4.2), the quantification of As in multiple transects along the Paleochori and Spathi bay or other areas of the Island, will greatly contribute in stablishing hydrothermal activity in Milos as a source of arsenic bearing colloidal material and will provide spatial and quantitative evidence of As impact.

To determine As rich hydrothermal fluids as a source of As bearing colloidal particles to the ocean.

On a global scale, As discharge into the ocean by submarine volcanism activity corresponds to 4.87×10^9 Kg yr^{-1} [266], which compared to soluble arsenic present in river water fluxes (3.6 - 61×10^9 Kg yr^{-1}) [266], or atmospheric input in the north hemisphere (2.2 - 73×10^9 Kg yr^{-1}) [266], represents a significant input of As to seawater. Considering that a percentage of the fluxes is generated from dissolution of colloidal particles (400 and 20 nm), or directly correspond to nanomaterial suspended in the "soluble" fraction (below 200 nm), it becomes of a greater significance stablishing if fluids from different hydrothermal systems i.e. MOR or Tutum bay (Papua New Guinea) also contain fractions of As colloidal particles. An extensive field work along several locations should allow to address this question, stablishing fluxes of dissolved (< 20 nm) and colloidal As fractions and contributing in the development of geochemical models of As distribution in the ocean, incorporating the unexplored fraction of colloidal arsenic.

To quantify dissolution of As bearing nanoparticles in marine environments.

Based on the discussions of Chapter 3 and 4, it results critical to evaluate and quantify physicochemical parameters of nanomaterials stability in the ocean. Perhaps the most relevant linked to the toxic effect described in Chapter 5 (Bacteriostatic effect in *Shewanella oneidensis* MR1 cultures) is the release of dissolved arsenic species from As colloidal particles. Quantification of nanomaterials dissolution (Coefficient of dissolution) is a current challenge in environmental sciences and can be encompass by novel fluid filtration systems [267] coupled to sensitive quantification methods of elements in solution (ICP-OES). Figure 4.8 showed how temperature dictated the dissolution of As colloidal particles over time, in this case, the dissolution rate can be established conducting different experimental set-ups. Static (batch reactor) and dynamic approaches (flow reactors similar to non-compendial dissolution models) of As based colloidal material dissolution should be considered [268]. Other environmental

parameters (pH, ionic strength, OM etc.) can be evaluated in a similar way. The data collected will provide accurate information about chemical dissolution of As in a marine context, which can be later used in legal frame works discussions of toxic colloidal materials presence in aquatic resources.

To evaluate aminolipids and aminophospholipids variations as a common response in bacteria to As colloidal and dissolved fractions.

Several bacteria are used to evaluate pollutants toxicity, among them *Escherichia coli*, *Bacillius subtillis*, *Agrobacterium tumefaciens* etc., each related to different aspects of the role of bacteria in the environment. Therefore, a broader number of microorganism, perhaps, considering representatives of each phylum (i.e. *Bacteroides, Cyanobacteria, Nitrospirae* etc.) or classes (i.e. *Alphaproteobacteria*, *Deltaproteobacteria*, *Gammaproteobacteria* etc.) can be used to replicate the results presented in Chapter 5 (Figure 5.4). Similarities in variations of aminolipids or aminophospholipids abundance in the different Phyla or Classes, will suggest the use of lipids containing amino groups as a common response of bacteria to soluble and colloidal As forms. Furthermore, if a known molecule (IPL), highly sensitive to arsenic, stable through time and present in the majority of the organisms; is identified, it should be considered as a biomarker of arsenic stress in bacteria. To test this hypothesis, a first step will be to obtain a total lipid extract of an As rich location in order to identify via UHPLC-ESI-ToF-MS the presence of the potential biomarker and its correlation with the concentration of As in the samples. This will contribute in the development of novel tools in environmental monitoring and a greater understanding of As toxicity in aquatic ecosystems.

To evaluate the generation of reactive oxygen species as part of the mechanism of toxicity associated to As colloidal particles in bacteria.

Along Chapter 5 remains unclear the molecular mechanism associated to the toxicity showed by the As colloidal particles in cultures of *Shewanella oneidensis*. However, it was suggested the generation of ROS due to the described mechanism of toxicity of As inside of cells (Figure 1.6) [80]. Thus, ROS sensitive probes can be used to correlate the exposition of bacterial cells to As rich colloidal particles. Current developments in fluorescent ROS probes, allows to identify near membrane ROS generation [263]. Using liposoluble probes, events of oxidative damage generated in the membrane can be accurately determined [263]. In order to evaluate the role of ROS in the variations of IPL in bacterial models, similar experiments (Chapter 5) should be consider using known oxidative stress inducers, i.e. H_2O_2. The evaluation of IPL changes in cultures of *Shewanella oneidensis* treated with H_2O_2 can lead to novel insight about aminolipids or aminophospholipds specific response to oxidative stress and in consequence in the effect of metallic colloidal particles upon microbial communities in the environment.

Acknowledgments

I would like to acknowledge all those who supervised, contributed, helped, or simply were present in the development of this doctoral dissertation. Thank you Dr. Solveig Bühring, for giving me the opportunity to do my thesis in the Hydrothermal Geomicrobiology group and all the scientific and personal support during these 4 years. Thank you Dr. Michael Maas and Prof. Dr. Kurosch Rezwan for the chance of collaborating with the Advanced Ceramics group, for the scientific discussions and the great influence of the materials science in my professional career. Thank you Prof. Dr. Kai-Uwe Hinrichs and Dr. Marcus Elvert for allowing me to work in the facilities of the MARUM institute and to get to know all the people in the department of Organic Geochemistry. Thank you to Dr. Matthias Kellermann and Dr. Lars Wörmer for your help during the lipid analysis and the moments shared outside of the laboratories. Thanks to all the people in the Organic Geochemistry and Advanced Ceramics group for the nice memories and help in the day to day work. Acknowledgments to Prof. Dr. Thomas Pichler, his group in Geochemistry and Hydrogeology and Dr. Roy Price for the scientific support during the laboratory work and the field expedition in Milos (Greece).

Many thanks to Xavi Prieto and his family, for being such remarkable friends. Thank you to Emilia Sogin and Patrick Curry, for the tremendous experience of getting to know each other. To Niek Stortenbeker for our great friendship. To Wibke Hübenthal and Kim Rosenboom for the great climbing trips. To Mareike Tödter for all the conversations and the significant amounts of hours spent watching movies and series. To Gonzalo Gómez Saez and Nur García, for welcoming me in the early days of this trip. To Diego Filún and Felipe VM for keeping Chile closer to Bremen. To Florian Wiecke for the challenging routes in the DAV.

Thank you to my friends in Chile, for the support, the advices, the help and the laugh. Thank you to Luis Saona and Alejandro Gran who shared with me the experience of living abroad. Thank you to Melany Rios for caring about me. To Mabel Araneda and Carolina Maragaño, dear and reliable friends, who provided additional energy when it was needed. To Felipe Quinteros, María Jesús Ovalle, Gonzalo Pavez, Pablo Aranda, Hernán Manríquez and Juan Pablo Méndez, thank you for everything.

Finally, all my heart to my family. Mother and Father, Jeannette and Aldo, because you always encouraged me. To my sister Catalina, for always keeping an eye on me. To my brother Simon and his family, for being the joy in many videos, pictures and calls. To Nadine, for being part of this family, a strong woman, who I truthfully admire.

References

1. Pinet, P.R., *Invitation to oceanography*. 2019: Jones & Bartlett Publishers.

2. Karleskint, G., R. Turner, and J. Small, *Introduction to marine biology*. 2012: Cengage Learning.

3. Millero, F.J., *The physical chemistry of seawater.* Annual Review of Earth and Planetary Sciences, 1974. **2**(1): p. 101-150.

4. Liss, P.S., *The chemistry of near-surface seawater*, in *Dynamic processes in the chemistry of the upper ocean*. 1986, Springer. p. 41-51.

5. Holland, H.D., *Sea level, sediments and the composition of seawater.* American Journal of Science, 2005. **305**(3): p. 220-239.

6. Demicco, R.V., et al., *Model of seawater composition for the Phanerozoic.* Geology, 2005. **33**(11): p. 877-880.

7. Morel, F.M.M. and N. Price, *The Biogeochemical Cycles of Trace Metals in the Oceans.* Science (New York, N.Y.), 2003. **300**: p. 944-7.

8. Field, C.B., et al., *Primary production of the biosphere: integrating terrestrial and oceanic components.* science, 1998. **281**(5374): p. 237-240.

9. Wright, J. and A. Colling, *CHAPTER 6 - THE SEAWATER SOLUTION*, in *Seawater: its Composition, Properties and Behaviour (Second Edition)*, J. Wright and A. Colling, Editors. 1995, Pergamon. p. 85-127.

10. Bundschuh, J. and T. Pichler, *Arsenic in marine hydrothermal systems: Source, fate and environmental implications.* Chemical Geology, 2013. **348**: p. 1.

11. Varekamp, J.C. and P.R. Buseck, *The speciation of mercury in hydrothermal systems, with applications to ore deposition.* Geochimica et Cosmochimica Acta, 1984. **48**(1): p. 177-185.

12. Toner, B.M., et al., *Preservation of iron (II) by carbon-rich matrices in a hydrothermal plume.* Nature Geoscience, 2009. **2**(3): p. 197.

13. Halpern, B.S., et al., *Spatial and temporal changes in cumulative human impacts on the world's ocean.* Nature Communications, 2015. **6**(1): p. 7615.

14. Clarke, F.W. and H.S. Washington, *The composition of the earth's crust*. Vol. 127. 1924: US Government Printing Office.

15. Boyd, P.W. and M.J. Ellwood, *The biogeochemical cycle of iron in the ocean.* Nature Geoscience, 2010. **3**(10): p. 675-682.

16. Cullen, J.T., B.A. Bergquist, and J.W. Moffett, *Thermodynamic characterization of the partitioning of iron between soluble and colloidal species in the Atlantic Ocean.* Marine Chemistry, 2006. **98**(2): p. 295-303.

17. Barbeau, K., et al., *Photochemical cycling of iron in the surface ocean mediated by microbial iron (III)-binding ligands.* Nature, 2001. **413**(6854): p. 409.

18. Boyd, P., et al., *Remineralization of upper ocean particles: Implications for iron biogeochemistry.* Limnology and Oceanography, 2010. **55**(3): p. 1271-1288.

19. Mawji, E., et al., *Hydroxamate siderophores: occurrence and importance in the Atlantic Ocean.* Environmental science & technology, 2008. **42**(23): p. 8675-8680.

20. Gordon, R.M., K.H. Coale, and K.S. Johnson, *Iron distributions in the equatorial Pacific: Implications for new production.* Limnology and Oceanography, 1997. **42**(3): p. 419-431.

21. Yücel, M., et al., *Hydrothermal vents as a kinetically stable source of iron-sulphide-bearing nanoparticles to the ocean.* Nature Geoscience, 2011. **4**(6): p. 367.

22. Hawkes, J.A., et al., *The stabilisation and transportation of dissolved iron from high temperature hydrothermal vent systems.* Earth and Planetary Science Letters, 2013. **375**: p. 280-290.

23. Fitzsimmons, J.N., et al., *Iron persistence in a distal hydrothermal plume supported by dissolved–particulate exchange.* Nature Geoscience, 2017. **10**: p. 195.

24. Findlay, A.J., et al., *Iron and sulfide nanoparticle formation and transport in nascent hydrothermal vent plumes.* Nature Communications, 2019. **10**(1): p. 1597.

25. Sander, S.G. and A. Koschinsky, *Metal flux from hydrothermal vents increased by organic complexation.* Nature Geoscience, 2011. **4**(3): p. 145.

26. Lu, P.J. and D.A. Weitz, *Colloidal Particles: Crystals, Glasses, and Gels.* Annual Review of Condensed Matter Physics, 2013. **4**(1): p. 217-233.

27. Hochella, M.F., et al., *Nanominerals, mineral nanoparticles, and earth systems.* science, 2008. **319**(5870): p. 1631-1635.

28. Bosch, J., et al., *Anaerobic, Nitrate-Dependent Oxidation of Pyrite Nanoparticles by Thiobacillus denitrificans.* Environmental Science & Technology, 2012. **46**(4): p. 2095-2101.

29. Gartman, A., A.J. Findlay, and G.W. Luther III, *Nanoparticulate pyrite and other nanoparticles are a widespread component of hydrothermal vent black smoker emissions.* Chemical Geology, 2014. **366**: p. 32-41.

30. Kadar, E., et al., *Metallic nanoparticle enrichment at low temperature, shallow CO2 seeps in Southern Italy.* Marine Chemistry, 2012. **140-141**: p. 24-32.

31. Council, N.R., *Arsenic: medical and biologic effects of environmental pollutants.* 1977.

32. Neff, J., *Arsenic in the Ocean*. 2002. p. 57-78.

33. Sugawara, K. and S. Kanamori, *The spectrophotometric determination of trace amounts of arsenate and arsenite in natural waters with special reference to phosphate determination.* Bulletin of the Chemical Society of Japan, 1964. **37**(9): p. 1358-1363.

34. Water, S. and W.H. Organization, *Guidelines for drinking-water quality [electronic resource]: incorporating first addendum. Vol. 1, Recommendations.* 2006.

35. Masuda, H., *Arsenic cycling in the Earth's crust and hydrosphere: interaction between naturally occurring arsenic and human activities.* Progress in Earth and Planetary Science, 2018. **5**(1): p. 68.

36. Hughes, M.F., *Arsenic toxicity and potential mechanisms of action.* Toxicology Letters, 2002. **133**(1): p. 1-16.

37. Flora, S., et al., *Arsenic induced oxidative stress and the role of antioxidant supplementation during chelation: a review.* Journal of Environmental Biology, 2007. **28**(2): p. 333.

38. Ding, W., L.G. Hudson, and K.J. Liu, *Inorganic arsenic compounds cause oxidative damage to DNA and protein by inducing ROS and RNS generation in human keratinocytes.* Molecular and cellular biochemistry, 2005. **279**(1-2): p. 105-112.

39. García-Chávez, E., et al., *Lipid oxidative damage and distribution of inorganic arsenic and its metabolites in the rat nervous system after arsenite exposure: Influence of alpha tocopherol supplementation.* NeuroToxicology, 2006. **27**(6): p. 1024-1031.

40. Scott, N., et al., *Reactions of arsenic (III) and arsenic (V) species with glutathione.* Chemical research in toxicology, 1993. **6**(1): p. 102-106.

41. Delnomdedieu, M., et al., *Transfer of arsenite from glutathione to dithiols: a model of interaction.* Chemical research in toxicology, 1993. **6**(5): p. 598-602.

42. Martin, J.H. and R. Michael Gordon, *Northeast Pacific iron distributions in relation to phytoplankton productivity.* Deep Sea Research Part A. Oceanographic Research Papers, 1988. **35**(2): p. 177-196.

43. Balzer, W., et al., *Arsenic in solution, colloidal and particulate phases of East-Hainan estuaries.* Continental Shelf Research, 2013. **57**: p. 73-81.

44. Wu, J., et al., *Soluble and colloidal iron in the oligotrophic North Atlantic and North Pacific.* Science, 2001. **293**(5531): p. 847-849.

45. Price, R., et al., *Arsenic cycling, thioarsenates and orpiment precipitation at a shallow sea hydrothermal system, Milos Island, Greece.* Arsenic in Geosphere and Human Diseases: As 2010, 2010: p. 66-68.

46. Bauer, M. and C. Blodau, *Arsenic distribution in the dissolved, colloidal and particulate size fraction of experimental solutions rich in dissolved organic matter and ferric iron.* Geochimica et Cosmochimica Acta, 2009. **73**(3): p. 529-542.

47. Serrano, S., et al., *Arsenic speciation in the dispersible colloidal fraction of soils from a mine-impacted creek.* Journal of hazardous materials, 2015. **286**: p. 30-40.

48. Mills, G., Z. Li, and D. Meisel, *Photochemistry and spectroscopy of colloidal arsenic sesquisulfide.* The Journal of Physical Chemistry, 1988. **92**(3): p. 822-828.

49. Godelitsas, A., et al., *Amorphous As-sulfide precipitates from the shallow-water hydrothermal vents off Milos Island (Greece).* Marine Chemistry, 2015. **177**: p. 687-696.

50. Jeevanandam, J., et al., *Review on nanoparticles and nanostructured materials: history, sources, toxicity and regulations.* Beilstein journal of nanotechnology, 2018. **9**(1): p. 1050-1074.

51. Bao, X.-Y., et al., *Heteroepitaxial growth of vertical GaAs nanowires on Si (111) substrates by metal− organic chemical vapor deposition.* Nano letters, 2008. **8**(11): p. 3755-3760.

52. Choi, D.Y., et al., *Nano-phase separation of arsenic tri-sulphide (As2S3) film and its effect on plasma etching.* Journal of Non-Crystalline Solids, 2007. **353**(8-10): p. 953-955.

53. Malik, M.A., P. O'Brien, and M. Helliwell, *A new synthesis of InAs quantum dots from [t Bu 2 AsInEt 2] 2.* Journal of Materials Chemistry, 2005. **15**(14): p. 1463-1467.

54. Soci, C., et al., *A systematic study on the growth of GaAs nanowires by metal− organic chemical vapor deposition.* Nano letters, 2008. **8**(12): p. 4275-4282.

55. Tichá, H., et al., *Temperature dependence of the optical gap in thin amorphous films of As2S3, As2Se3 and other basic non-crystalline chalcogenides.* Journal of Physics and Chemistry of Solids, 2000. **61**(4): p. 545-550.

56. Mane, R.S., B.R. Sankapal, and C.D. Lokhande, *Thickness dependent properties of chemically deposited As2S3 thin films from thioacetamide bath.* Materials chemistry and physics, 2000. **64**(3): p. 215-221.

57. Mane, R.S., V.V. Todkar, and C.D. Lokhande, *Low temperature synthesis of nanocrystalline As2S3 thin films using novel chemical bath deposition route.* Applied surface science, 2004. **227**(1-4): p. 48-55.

58. Sartale, S.D. and C.D. Lokhande, *Preparation and characterization of As2S3 thin films deposited using successive ionic layer adsorption and reaction (SILAR) method.* Materials research bulletin, 2000. **35**(8): p. 1345-1353.

59. Ubale, A.U., et al., *Characterization of nanostructured As2S3 thin films synthesized at room temperature by chemical bath deposition method using various complexing agents.* Thin Solid Films, 2013. **542**: p. 160-166.

60. Yesugade, N.S., C.D. Lokhande, and C.H. Bhosale, *Structural and optical properties of electrodeposited Bi2S3, Sb2S3 and As2S3 thin films.* Thin Solid Films, 1995. **263**(2): p. 145-149.

61. Perrière, J., et al., *Formation of GaAs nanocrystals by laser ablation.* Applied physics letters, 2001. **78**(19): p. 2949-2951.

62. Velea, A., et al., *Photoexpansion and nano-lenslet formation in amorphous As2S3 thin films by 800 nm femtosecond laser irradiation.* Journal of Applied Physics, 2012. **112**(3): p. 033105.

63. Malik, M.A., et al., *Gallium arsenide nanoparticles: synthesis and characterisation.* Journal of Materials Chemistry, 2003. **13**(10): p. 2591-2595.

64. Li, X.-S., et al., *Zirconium arsenate-modified magnetic nanoparticles: preparation, characterization and application to the enrichment of phosphopeptides.* Analyst, 2012. **137**(4): p. 959-967.

65. Pal, A., et al., *Wet-chemical synthesis of spherical arsenic nanoparticles by a simple reduction method and its characterization.* Advanced Materials Letters, 2012. **3**(3): p. 177-180.

66. Wu, J.-Z. and P.C. Ho, *Evaluation of the in vitro activity and in vivo bioavailability of realgar nanoparticles prepared by cryo-grinding.* European Journal of Pharmaceutical Sciences, 2006. **29**(1): p. 35-44.

67. Baláž, P., et al., *Mechanochemical preparation and anticancer effect of realgar As4S4 nanoparticles.* Materials Letters, 2009. **63**(17): p. 1542-1544.

68. Balaz, P., et al. *Arsenic sulphide As4S4 nanoparticles: Physico-chemical properties and anticancer effects*. Trans Tech Publ.

69. Baláž, P., et al. *In-vitro Testing of Arsenic Sulfide Nanoparticles for the Treatment of Multiple Myeloma Cells*.

70. Bujňáková, Z., et al., *Arsenic sulfide nanoparticles prepared by milling: properties, free-volume characterization, and anti-cancer effects.* Journal of materials science, 2015. **50**(4): p. 1973-1985.

71. Zhao, W., et al., *Effect of size and processing method on the cytotoxicity of realgar nanoparticles in cancer cell lines.* International journal of nanomedicine, 2011. **6**: p. 1569.

72. An, Y.-l., et al., *Preparation and characterization of realgar nanoparticles and their inhibitory effect on rat glioma cells.* International journal of nanomedicine, 2011. **6**: p. 3187.

73. Zhao, Q.-H., et al., *Anticancer effect of realgar nanoparticles on mouse melanoma skin cancer in vivo via transdermal drug delivery.* Medical Oncology, 2010. **27**(2): p. 203-212.

74. Wang, J., et al., *Arsenic (II) sulfide quantum dots prepared by a wet process from its bulk.* Journal of the American Chemical Society, 2008. **130**(35): p. 11596-11597.

75. Wu, J., et al., *Studies on orpiment (As2S3) quantum dots and their self-assemblies.* Australian Journal of Chemistry, 2017. **70**(10): p. 1093-1098.

76. Jiang, S., et al., *Biogenic formation of As-S nanotubes by diverse Shewanella strains.* Appl. Environ. Microbiol., 2009. **75**(21): p. 6896-6899.

77. Lee, J.-H., et al., *Biogenic formation of photoactive arsenic-sulfide nanotubes by Shewanella sp. strain HN-41.* Proceedings of the National Academy of Sciences, 2007. **104**(51): p. 20410-20415.

78. Newman, D.K., T.J. Beveridge, and F. Morel, *Precipitation of arsenic trisulfide by Desulfotomaculum auripigmentum.* Appl. Environ. Microbiol., 1997. **63**(5): p. 2022-2028.

79. Rochette, E.A., et al., *Kinetics of arsenate reduction by dissolved sulfide.* Environmental Science & Technology, 2000. **34**(22): p. 4714-4720.

80. Fowler, B.A., *Biological and environmental effects of arsenic*. Vol. 6. 2013: Elsevier.

81. Cheng, H., et al., *Geochemical processes controlling fate and transport of arsenic in acid mine drainage (AMD) and natural systems.* Journal of hazardous materials, 2009. **165**(1-3): p. 13-26.

82. Price, R.E. and T. Pichler, *Distribution, speciation and bioavailability of arsenic in a shallow-water submarine hydrothermal system, Tutum Bay, Ambitle Island, PNG.* Chemical geology, 2005. **224**(1-3): p. 122-135.

83. Ahmann, D., et al., *Microbial mobilization of arsenic from sediments of the Aberjona watershed.* Environmental Science & Technology, 1997. **31**(10): p. 2923-2930.

84. Callac, N., et al., *Modes of carbon fixation in an arsenic and CO 2-rich shallow hydrothermal ecosystem.* Scientific reports, 2017. **7**(1): p. 14708.

85. Das, S., et al., *Dissimilatory arsenate reduction and in situ microbial activities and diversity in arsenic-rich groundwater of Chianan Plain, Southwestern Taiwan.* Microbial ecology, 2016. **71**(2): p. 365-374.

86. Akerman, N., *Microbial diversity and geochemical energy sources of Tutum Bay, Ambitle Island, Papua New Guinea, an arsenic-rich, shallow-sea hydrothermal system.* 2009.

87. Giovannelli, D., et al., *Diversity and phylogenetic analyses of bacteria from a shallow-water hydrothermal vent in Milos island (Greece).* Frontiers in microbiology, 2013. **4**: p. 184.

88. Fru, E.C., et al., *Arsenic and high affinity phosphate uptake gene distribution in shallow submarine hydrothermal sediments.* Biogeochemistry, 2018. **141**(1): p. 41-62.

89. Meyer-Dombard, D., et al., *Prokaryotic populations in arsenic-rich shallow-sea hydrothermal sediments of Ambitle Island, Papua New Guinea.* Geomicrobiology Journal, 2012. **29**(1): p. 1-17.

90. Zobrist, J., et al., *Mobilization of arsenite by dissimilatory reduction of adsorbed arsenate.* Environmental Science & Technology, 2000. **34**(22): p. 4747-4753.

91. Jeanthon, C. and D. Prieur, *Resistance to heavy metals of heterotrophic bacteria isolated from the deep-sea hydrothermal vent polychaete, Alvinella pompejana.* Progress in oceanography, 1990. **24**(1-4): p. 81-88.

92. Price, R.E., et al., *Archaeal and bacterial diversity in an arsenic-rich shallow-sea hydrothermal system undergoing phase separation.* Frontiers in microbiology, 2013. **4**: p. 158.

93. Wu, J. and B. Rosen, *Metalloregulated expression of the ars operon.* Journal of Biological Chemistry, 1993. **268**(1): p. 52-58.

94. Carlin, A., et al., *The ars operon of Escherichia coli confers arsenical and antimonial resistance.* Journal of bacteriology, 1995. **177**(4): p. 981-986.

95. Diorio, C., et al., *An Escherichia coli chromosomal ars operon homolog is functional in arsenic detoxification and is conserved in gram-negative bacteria.* Journal of bacteriology, 1995. **177**(8): p. 2050-2056.

96. Wu, J. and B.P. Rosen, *The arsD gene encodes a second trans-acting regulatory protein of the plasmid-encoded arsenical resistance operon.* Molecular microbiology, 1993. **8**(3): p. 615-623.

97. Wu, J. and B. Rosen, *The ArsR protein is a trans-acting regulatory protein.* Molecular microbiology, 1991. **5**(6): p. 1331-1336.

98. Ahmann, D., et al., *Microbe grows by reducing arsenic.* Nature, 1994. **371**(6500): p. 750-750.

99. Saltikov, C.W. and D.K. Newman, *Genetic identification of a respiratory arsenate reductase.* Proceedings of the National Academy of Sciences, 2003. **100**(19): p. 10983-10988.

100. Murphy, J.N. and C.W. Saltikov, *The cymA gene, encoding a tetraheme c-type cytochrome, is required for arsenate respiration in Shewanella species.* Journal of bacteriology, 2007. **189**(6): p. 2283-2290.

101. Malasarn, D., J.R. Keeffe, and D.K. Newman, *Characterization of the arsenate respiratory reductase from Shewanella sp. strain ANA-3.* Journal of bacteriology, 2008. **190**(1): p. 135-142.

102. Slyemi, D. and V. Bonnefoy, *How prokaryotes deal with arsenic.* Environmental microbiology reports, 2012. **4**(6): p. 571-586.

103. Anderson, G., J. Williams, and R. Hille, *The purification and characterization of arsenite oxidase from Alcaligenes faecalis, a molybdenum-containing hydroxylase.* Journal of Biological Chemistry, 1992. **267**(33): p. 23674-23682.

104. Ellis, P.J., et al., *Crystal structure of the 100 kDa arsenite oxidase from Alcaligenes faecalis in two crystal forms at 1.64 Å and 2.03 Å.* Structure, 2001. **9**(2): p. 125-132.

105. Kulp, T., et al., *Arsenic (III) fuels anoxygenic photosynthesis in hot spring biofilms from Mono Lake, California.* Science, 2008. **321**(5891): p. 967-970.

106. Erhlich, H., *Bacterial oxidation of As (III) compounds In: Environmental Chemistry of Arsenic (Frankenberger, WT Jr. Jr., Ed.)*. 2001, Marcel Dekker, New York.

107. Sun, W., et al., *Anaerobic oxidation of arsenite linked to chlorate reduction.* Appl. Environ. Microbiol., 2010. **76**(20): p. 6804-6811.

108. Oremland, R.S., et al., *Arsenic in the evolution of earth and extraterrestrial ecosystems.* Geomicrobiology Journal, 2009. **26**(7): p. 522-536.

109. Rosen, B.P. and Z. Liu, *Transport pathways for arsenic and selenium: a minireview.* Environment international, 2009. **35**(3): p. 512-515.

110. Sanders, O.I., et al., *Antimonite is accumulated by the glycerol facilitator GlpF in Escherichia coli.* Journal of bacteriology, 1997. **179**(10): p. 3365-3367.

111. Bhattacharjee, H., et al., *Aquaglyceroporins: ancient channels for metalloids.* Journal of biology, 2008. **7**(9): p. 33.

112. Yücel, M., et al., *Eco-geochemical dynamics of a shallow-water hydrothermal vent system at Milos Island, Aegean Sea (Eastern Mediterranean).* Chemical Geology, 2013. **356**: p. 11-20.

113. Hanna, K., et al., *The effect of salt concentration on the phospholipid and fatty acid composition of the moderate halophile Vibrio costicola.* Canadian journal of microbiology, 1984. **30**(5): p. 669-675.

114. Moore, E.K., et al., *Lysine and novel hydroxylysine lipids in soil bacteria: amino acid membrane lipid response to temperature and pH in Pseudopedobacter saltans.* Frontiers in microbiology, 2015. **6**: p. 637.

115. Sebastián, M., et al., *Lipid remodelling is a widespread strategy in marine heterotrophic bacteria upon phosphorus deficiency.* The ISME journal, 2016. **10**(4): p. 968.

116. Smith, A.F., et al., *Elucidation of glutamine lipid biosynthesis in marine bacteria reveals its importance under phosphorus deplete growth in Rhodobacteraceae.* The ISME journal, 2019. **13**(1): p. 39.

117. Sollich, M., et al., *Heat stress dictates microbial lipid composition along a thermal gradient in marine sediments.* Frontiers in microbiology, 2017. **8**: p. 1550.

118. Taylor, C.J., A.J. Anderson, and S.G. Wilkinson, *Phenotypic variation of lipid composition in Burkholderia cepacia: a response to increased growth temperature is a greater content of 2-hydroxy acids in phosphatidylethanolamine and ornithine amide lipid.* Microbiology, 1998. **144**(7): p. 1737-1745.

119. Kellermann, M.Y., et al., *Important roles for membrane lipids in haloarchaeal bioenergetics.* Biochimica et Biophysica Acta (BBA) - Biomembranes, 2016. **1858**(11): p. 2940-2956.

120. Wörmer, L., et al., *Application of two new LC–ESI–MS methods for improved detection of intact polar lipids (IPLs) in environmental samples.* Organic Geochemistry, 2013. **59**: p. 10-21.

121. Pepi, M., et al., *Membrane fatty acids adaptive profile in the simultaneous presence of arsenic and toluene in Bacillus sp. ORAs2 and Pseudomonas sp. ORAs5 strains.* Extremophiles, 2008. **12**(3): p. 343-349.

122. Xie, Z., et al., *Influence of Arsenate on Lipid Peroxidation Levels and Antioxidant Enzyme Activities in Bacillus cereus Strain XZM002 Isolated from High Arsenic Aquifer Sediments.* Geomicrobiology Journal, 2013. **30**(7): p. 645-652.

123. Dando, P.R., et al., *Gas venting rates from submarine hydrothermal areas around the island of Milos, Hellenic Volcanic Arc.* Continental Shelf Research, 1995. **15**(8): p. 913-929.

124. Olmsted, J. and G. Williams, *Handbook of Chemistry and Physics*. 2007, New York: CRC Press-Taylor & Francis Group.

125. Eary, L.E., *The solubility of amorphous As2S3 from 25 to 90°C.* Geochimica et Cosmochimica Acta, 1992. **56**(6): p. 2267-2280.

126. Besold, J., et al., *Monothioarsenate Transformation Kinetics Determining Arsenic Sequestration by Sulfhydryl Groups of Peat.* Environmental Science & Technology, 2018. **52**(13): p. 7317-7326.

127. Langner, P., C. Mikutta, and R. Kretzschmar, *Arsenic sequestration by organic sulphur in peat.* Nature Geoscience, 2012. **5**(1): p. 66.

128. Kleint, C., et al., *Organic Cu-complexation at the shallow marine hydrothermal vent fields off the coast of Milos (Greece), Dominica (Lesser Antilles) and the Bay of Plenty (New Zealand).* Marine Chemistry, 2015. **173**: p. 244-252.

129. El-Sayed, M.A., *Some interesting properties of metals confined in time and nanometer space of different shapes.* Accounts of chemical research, 2001. **34**(4): p. 257-264.

130. El-Sayed, M.A., *Small is different: shape-, size-, and composition-dependent properties of some colloidal semiconductor nanocrystals.* Accounts of chemical research, 2004. **37**(5): p. 326-333.

131. Sharma, V.K., et al., *Natural inorganic nanoparticles–formation, fate, and toxicity in the environment.* Chemical Society Reviews, 2015. **44**(23): p. 8410-8423.

132. Jomova, K., et al., *Arsenic: toxicity, oxidative stress and human disease.* Journal of Applied Toxicology, 2011. **31**(2): p. 95-107.

133. Pichler, T., et al., *A natural laboratory to study arsenic geobiocomplexity.* Eos, Transactions American Geophysical Union, 2006. **87**(23): p. 221-225.

134. Price, R.E., et al., *Processes influencing extreme As enrichment in shallow-sea hydrothermal fluids of Milos Island, Greece.* Chemical Geology, 2013. **348**: p. 15-26.

135. Grund, S.C., K. Hanusch, and H.U. Wolf, *Arsenic and arsenic compounds.* Ullmann's encyclopedia of industrial chemistry, 2000.

136. Price, R.E., et al., *Enhanced bioaccumulation and biotransformation of As in coral reef organisms surrounding a marine shallow-water hydrothermal vent system.* Chemical Geology, 2013. **348**: p. 48-55.

137. Filomeni, G., G. Rotilio, and M.R. Ciriolo, *Cell signalling and the glutathione redox system.* Biochemical pharmacology, 2002. **64**(5-6): p. 1057-1064.

138. Aiuppa, A., et al., *Mineral control of arsenic content in thermal waters from volcano-hosted hydrothermal systems: insights from island of Ischia and Phlegrean Fields (Campanian Volcanic Province, Italy).* Chemical Geology, 2006. **229**(4): p. 313-330.

139. Pichler, T., J.A.N. Veizer, and G.E.M. Hall, *Natural input of arsenic into a coral-reef ecosystem by hydrothermal fluids and its removal by Fe (III) oxyhydroxides.* Environmental Science & Technology, 1999. **33**(9): p. 1373-1378.

140. Breuer, C. and T. Pichler, *Arsenic in marine hydrothermal fluids.* Chemical Geology, 2013. **348**: p. 2-14.

141. Douville, É., et al., *Le comportement de l'arsenic (As) et de l'antimoine (Sb) dans les fluides provenant de différents systèmes hydrothermaux océaniques.* Comptes Rendus de l'Académie des Sciences-Series IIA-Earth and Planetary Science, 1999. **328**(2): p. 97-104.

142. Kallmeyer, J., *Life at Vents and Seeps*. Vol. 5. 2017: Walter de Gruyter GmbH & Co KG.

143. Sievert, S.M., et al., *Spatial heterogeneity of bacterial populations along an environmental gradient at a shallow submarine hydrothermal vent near Milos Island (Greece).* Appl. Environ. Microbiol., 1999. **65**(9): p. 3834-3842.

144. Dando, P.R., et al., *Microbiology of shallow hydrothermal sites off Palaeochori Bay, Milos(Hellenic Volcanic Arc).* Cahiers de Biologie Marine, 1998. **39**(3): p. 369-372.

145. Caporale, A.G., et al., *Effect of particle size of drinking-water treatment residuals on the sorption of arsenic in the presence of competing ions.* Journal of hazardous materials, 2013. **260**: p. 644-651.

146. Guo, H., B. Zhang, and Y. Zhang, *Control of organic and iron colloids on arsenic partition and transport in high arsenic groundwaters in the Hetao basin, Inner Mongolia.* Applied Geochemistry, 2011. **26**(3): p. 360-370.

147. Neubauer, E., et al., *Colloid-associated export of arsenic in stream water during stormflow events.* Chemical Geology, 2013. **352**: p. 81-91.

148. Smedley, P.L. and D.G. Kinniburgh, *Source and behaviour of arsenic in natural waters.* United Nations synthesis report on arsenic in drinking water. World Health Organization, Geneva, Switzerland. http://www. who. int/water_sanitation_health/dwq/arsenicun1. pdf, 2001: p. 1-61.

149. AshaRani, P.V., et al., *Cytotoxicity and genotoxicity of silver nanoparticles in human cells.* ACS nano, 2008. **3**(2): p. 279-290.

150. Durán, N., et al., *Potential use of silver nanoparticles on pathogenic bacteria, their toxicity and possible mechanisms of action.* Journal of the Brazilian Chemical Society, 2010. **21**(6): p. 949-959.

151. Prabhu, S. and E.K. Poulose, *Silver nanoparticles: mechanism of antimicrobial action, synthesis, medical applications, and toxicity effects.* International nano letters, 2012. **2**(1): p. 32.

152. Xia, T., et al., *Comparison of the mechanism of toxicity of zinc oxide and cerium oxide nanoparticles based on dissolution and oxidative stress properties.* ACS nano, 2008. **2**(10): p. 2121-2134.

153. Gomez-Saez, G.V., et al., *Interaction between iron and dissolved organic matter in a marine shallow hydrothermal system off Dominica Island (Lesser Antilles).* Marine Chemistry, 2015. **177**: p. 677-686.

154. Ferreira, M.F., et al., *Accumulation of nutrients and heavy metals in surface sediments near Macao.* Marine Pollution Bulletin, 1996. **32**(5): p. 420-425.

155. Goering, J.J. and D.W. Menzel. *The nutrient chemistry of the sea surface*. Elsevier.

156. Bayraktarov, E., et al., *The pH and pCO2 dependence of sulfate reduction in shallow-sea hydrothermal CO2–venting sediments (Milos Island, Greece).* Frontiers in microbiology, 2013. **4**: p. 111.

157. Brust, M., et al., *Synthesis of thiol-derivatised gold nanoparticles in a two-phase liquid–liquid system.* Journal of the Chemical Society, Chemical Communications, 1994(7): p. 801-802.

158. Chen, H.-I. and H.-Y. Chang, *Homogeneous precipitation of cerium dioxide nanoparticles in alcohol/water mixed solvents.* Colloids and Surfaces A: Physicochemical and Engineering Aspects, 2004. **242**(1-3): p. 61-69.

159. Du, Y., et al., *A general method for the large-scale synthesis of uniform ultrathin metal sulphide nanocrystals.* Nature communications, 2012. **3**: p. 1177.

160. Pérez-Donoso, J.M., et al., *Biomimetic, mild chemical synthesis of CdTe-GSH quantum dots with improved biocompatibility.* PloS one, 2012. **7**(1): p. e30741.

161. Rodrıguez-Paéz, J.E., et al., *Controlled precipitation methods: formation mechanism of ZnO nanoparticles.* Journal of the European Ceramic Society, 2001. **21**(7): p. 925-930.

162. Pichler, T. and A. Mozaffari, *Distribution and mobility of geogenic molybdenum and arsenic in a limestone aquifer matrix.* Applied Geochemistry, 2015. **63**: p. 623-633.

163. Pichler, T., et al., *Suitability of the shallow water hydrothermal system at Ambitle Island (Papua New Guinea) to study the effect of high pCO2 on coral reefs.* Marine pollution bulletin, 2019. **138**: p. 148-158.

164. Price, R.E., J.P. Amend, and T. Pichler, *Enhanced geochemical gradients in a marine shallow-water hydrothermal system: Unusual arsenic speciation in horizontal and vertical pore water profiles.* Applied Geochemistry, 2007. **22**(12): p. 2595-2605.

165. Los, C. and W. Bach, *Sulfidation of major rock types of the oceanic lithosphere; An experimental study at 250 °C and 400 bars.* Lithos, 2018. **323**: p. 208-217.

166. Murdock, R.C., et al., *Characterization of Nanomaterial Dispersion in Solution Prior to In Vitro Exposure Using Dynamic Light Scattering Technique.* Toxicological Sciences, 2007. **101**(2): p. 239-253.

167. Rodney, W.S., I.H. Malitson, and T.A. King, *Refractive Index of Arsenic Trisulfide.* Journal of the Optical Society of America, 1958. **48**(9): p. 633-636.

168. Yücel, M., *Down the thermodynamic ladder: A comparative study of marine redox gradients across diverse sedimentary environments.* Estuarine, Coastal and Shelf Science, 2013. **131**: p. 83-92.

169. Pichler, T., et al., *Fe sulfide formation due to seawater-gas-sediment interaction in a shallow-water hydrothermal system at Lihir Island, Papua New Guinea.* Economic Geology, 1999. **94**(2): p. 281-288.

170. Pichler, T. and J. Veizer, *Precipitation of Fe(III) oxyhydroxide deposits from shallow-water hydrothermal fluids in Tutum Bay, Ambitle Island, Papua New Guinea.* Chemical Geology, 1999. **162**(1): p. 15-31.

171. Masala, O. and R. Seshadri, *SYNTHESIS ROUTES FOR LARGE VOLUMES OF NANOPARTICLES.* Annual Review of Materials Research, 2004. **34**(1): p. 41-81.

172. Rajamathi, M. and R. Seshadri, *Oxide and chalcogenide nanoparticles from hydrothermal/solvothermal reactions.* Current Opinion in Solid State and Materials Science, 2002. **6**(4): p. 337-345.

173. De Yoreo, J.J., et al., *Crystallization by particle attachment in synthetic, biogenic, and geologic environments.* Science, 2015. **349**(6247): p. aaa6760.

174. Thanh, N.T.K., N. Maclean, and S. Mahiddine, *Mechanisms of Nucleation and Growth of Nanoparticles in Solution.* Chemical Reviews, 2014. **114**(15): p. 7610-7630.

175. Hoang, V.V. and D. Ganguli, *Amorphous nanoparticles — Experiments and computer simulations.* Physics Reports, 2012. **518**(3): p. 81-140.

176. Jun, Y.-S., D. Kim, and C.W. Neil, *Heterogeneous Nucleation and Growth of Nanoparticles at Environmental Interfaces.* Accounts of Chemical Research, 2016. **49**(9): p. 1681-1690.

177. Floroiu, R.M., A.P. Davis, and A. Torrents, *Kinetics and Mechanism of As2S3(am) Dissolution under N2.* Environmental Science & Technology, 2004. **38**(4): p. 1031-1037.

178. Lengke, M.F. and R.N. Tempel, *Kinetic rates of amorphous As2S3 oxidation at 25 to 40°C and initial pH of 7.3 to 9.4.* Geochimica et Cosmochimica Acta, 2001. **65**(14): p. 2241-2255.

179. Akerman, N., et al., *Energy sources for chemolithotrophs in an arsenic- and iron-rich shallow-sea hydrothermal system.* Geobiology, 2011. **9**: p. 436-45.

180. Oremland, R.S. and J.F. Stolz, *The Ecology of Arsenic.* Science, 2003. **300**(5621): p. 939.

181. Bühring, S. and S. Sievert, *The shal-low sub-ma-ri-ne hot vent sys-tem off Mi-los (Greece) – a na-tu-ral la-bo-ra-to-ry to stu-dy hydro-ther-mal geo-mi-cro-bio-lo-gy. In Life in Extreme Environments, Life at Vents and Seeps, ed. J. Kall-mey-er*. 2017.

182. Meier, D., et al., *Microbial metal-sulfide oxidation in inactive hydrothermal vent chimneys suggested by metagenomic and metaproteomic analyses: Chemosynthetic bacteria on iron-sulfur deposits.* Environmental Microbiology, 2018. **21**.

183. Couture, R.M., et al., *Sorption of Arsenite, Arsenate, and Thioarsenates to Iron Oxides and Iron Sulfides: A Kinetic and Spectroscopic Investigation.* Environmental Science & Technology, 2013. **47**(11): p. 5652-5659.

184. Garcia-Pichel, F. and B.M. Bebout, *Penetration of ultraviolet radiation into shallow water sediments: high exposure for photosynthetic communities.* Marine Ecology Progress Series, 1996. **131**(1/3): p. 257-262.

185. Mladenov, N., et al., *Dissolved Organic Matter Sources and Consequences for Iron and Arsenic Mobilization in Bangladesh Aquifers.* Environmental Science & Technology, 2010. **44**(1): p. 123-128.

186. Manceau, A., et al., *Formation of Mercury Sulfide from Hg(II)–Thiolate Complexes in Natural Organic Matter.* Environmental Science & Technology, 2015. **49**(16): p. 9787-9796.

187. Mazrui, Nashaat M., et al., *The precipitation, growth and stability of mercury sulfide nanoparticles formed in the presence of marine dissolved organic matter.* Environmental Science: Processes & Impacts, 2018. **20**(4): p. 642-656.

188. Slowey, A.J., *Rate of formation and dissolution of mercury sulfide nanoparticles: The dual role of natural organic matter.* Geochimica et Cosmochimica Acta, 2010. **74**(16): p. 4693-4708.

189. Gebauer, D., et al., *The Multiple Roles of Additives in CaCO 3 Crystallization: A Quantitative Case Study.* Advanced Materials, 2009. **21**: p. 435.

190. Durán-Toro, V.M., et al., *Amorphous arsenic sulfide nanoparticles in a shallow water hydrothermal system.* Marine Chemistry, 2019. **211**: p. 25-36.

191. Bissen, M. and F.H. Frimmel, *Arsenic — a Review. Part I: Occurrence, Toxicity, Speciation, Mobility.* Acta hydrochimica et hydrobiologica, 2003. **31**(1): p. 9-18.

192. O'Day, P., *Chemistry and Mineralogy of Arsenic.* Elements, 2006. **2**: p. 77-83.

193. Webster, J.G. and D.K. Nordstrom, *Geothermal Arsenic*, in *Arsenic in Ground Water: Geochemistry and Occurrence*, A.H. Welch and K.G. Stollenwerk, Editors. 2003, Springer US: Boston, MA. p. 101-125.

194. Lue, J.T., *Physical properties of nanomaterials.* Encyclopedia of nanoscience and nanotechnology, 2007. **10**(1): p. 1-46.

195. Sharma, V.K. and M. Sohn, *Aquatic arsenic: toxicity, speciation, transformations, and remediation.* Environment international, 2009. **35**(4): p. 743-759.

196. Aiken, G.R., H. Hsu-Kim, and J.N. Ryan, *Influence of Dissolved Organic Matter on the Environmental Fate of Metals, Nanoparticles, and Colloids.* Environmental Science & Technology, 2011. **45**(8): p. 3196-3201.

197. Sperling, R.A. and W.J. Parak, *Surface modification, functionalization and bioconjugation of colloidal inorganic nanoparticles.* Philosophical Transactions of the Royal Society A: Mathematical, Physical and Engineering Sciences, 2010. **368**(1915): p. 1333-1383.

198. Durán-Toro, V., et al., *Quantum dot-based assay for Cu2+ quantification in bacterial cell culture.* Analytical Biochemistry, 2014. **450**: p. 30-36.

199. Yang, S., et al., *Renal Clearance and Degradation of Glutathione-Coated Copper Nanoparticles.* Bioconjugate Chemistry, 2015. **26**(3): p. 511-519.

200. Priester, J., et al., *Integrated approach to evaluating the toxicity of novel cysteine-capped silver nanoparticles to Escherichia coli and Pseudomonas aeruginosa.* The Analyst, 2013. **139**.

201. Shen, X., et al., *One-step synthesis of water-dispersible cysteine functionalized magnetic Fe3O4 nanoparticles for mercury(II) removal from aqueous solutions.* Applied Surface Science, 2014. **317**: p. 1028-1034.

202. Lokhande, C.D., *A chemical method for preparation of metal sulfide thin films.* Materials Chemistry and Physics, 1991. **28**(1): p. 145-149.

203. Peña-Méndez, Y., M.T.S. Nair, and P.K. Nair, *Thin films of arsenic sulfide by chemical deposition and formation of InAs.* Semiconductor Science and Technology, 2006. **21**(4): p. 450-461.

204. Gao, J., et al., *Colloidal Stability of Gold Nanoparticles Modified with Thiol Compounds: Bioconjugation and Application in Cancer Cell Imaging.* Langmuir, 2012. **28**(9): p. 4464-4471.

205. Evans, R.J. and H.A. Butts, *Inactivation of Amino Acids by Autoclaving.* Science, 1949. **109**(2840): p. 569.

206. Haberstroh, P.R. and D.M. Karl, *Dissolved free amino acids in hydrothermal vent habitats of the Guaymas Basin.* Geochimica et Cosmochimica Acta, 1989. **53**(11): p. 2937-2945.

207. Weiss, I.M., et al., *Thermal decomposition of the amino acids glycine, cysteine, aspartic acid, asparagine, glutamic acid, glutamine, arginine and histidine.* BMC biophysics, 2018. **11**(1): p. 2.

208. Lim, D., et al., *Oxidative stress-related PMK-1 P38 MAPK activation as a mechanism for toxicity of silver nanoparticles to reproduction in the nematode Caenorhabditis elegans.* Environmental toxicology and chemistry, 2012. **31**(3): p. 585-592.

209. Nair, P.M.G. and I.M. Chung, *Changes in the growth, redox status and expression of oxidative stress related genes in chickpea (Cicer arietinum L.) in response to copper oxide nanoparticle exposure.* Journal of Plant Growth Regulation, 2015. **34**(2): p. 350-361.

210. Shukla, R.K., et al., *ROS-mediated genotoxicity induced by titanium dioxide nanoparticles in human epidermal cells.* Toxicology in vitro, 2011. **25**(1): p. 231-241.

211. Yang, X., et al., *Mechanism of silver nanoparticle toxicity is dependent on dissolved silver and surface coating in Caenorhabditis elegans.* Environmental science & technology, 2011. **46**(2): p. 1119-1127.

212. Antelmann, H. and J.D. Helmann, *Thiol-based redox switches and gene regulation.* Antioxidants & redox signaling, 2011. **14**(6): p. 1049-1063.

213. Dhanjal, S., A.K. Singh, and S.S. Cameotra, *Global gene expression analysis of bacterial stress response to elevated concentrations of toxic metalloids—selenium and arsenic.* Geomicrobiology Journal, 2014. **31**(6): p. 480-492.

214. Hei, T.K. and M. Filipic, *Role of oxidative damage in the genotoxicity of arsenic.* Free Radical Biology and Medicine, 2004. **37**(5): p. 574-581.

215. Helmann, J.D., *Bacillithiol, a new player in bacterial redox homeostasis.* Antioxidants & redox signaling, 2011. **15**(1): p. 123-133.

216. Mishra, S., et al., *Thiol metabolism and antioxidant systems complement each other during arsenate detoxification in Ceratophyllum demersum L.* Aquatic Toxicology, 2008. **86**(2): p. 205-215.

217. Tripathi, P., et al., *Differential response of oxidative stress and thiol metabolism in contrasting rice genotypes for arsenic tolerance.* Ecotoxicology and Environmental Safety, 2012. **79**: p. 189-198.

218. Allen, T., R. Singhal, and S.V.S. Rana, *Resistance to oxidative stress in a freshwater fish Channa punctatus after exposure to inorganic arsenic.* Biological trace element research, 2004. **98**(1): p. 63-72.

219. Luo, X.P., et al., *Determination of aldehydes and other lipid peroxidation products in biological samples by gas chromatography-mass spectrometry.* Analytical biochemistry, 1995. **228**(2): p. 294-298.

220. Pérez, J.M., et al., *Escherichia coli YqhD exhibits aldehyde reductase activity and protects from the harmful effect of lipid peroxidation-derived aldehydes.* Journal of Biological Chemistry, 2008. **283**(12): p. 7346-7353.

221. Prakash, C., M. Soni, and V. Kumar, *Biochemical and molecular alterations following arsenic-induced oxidative stress and mitochondrial dysfunction in rat brain.* Biological trace element research, 2015. **167**(1): p. 121-129.

222. Ramos, O., et al., *Arsenic increased lipid peroxidation in rat tissues by a mechanism independent of glutathione levels.* Environmental health perspectives, 1995. **103**(suppl 1): p. 85-88.

223. Singh, N., et al., *Metabolic adaptations to arsenic-induced oxidative stress in Pterisvittata L and Pterisensiformis L.* Plant Science, 2006. **170**(2): p. 274-282.

224. Srivastava, S., et al., *Arsenic exacerbates atherosclerotic lesion formation and inflammation in ApoE-/-mice.* Toxicology and applied pharmacology, 2009. **241**(1): p. 90-100.

225. Wang, T.-C., et al., *Trivalent arsenicals induce lipid peroxidation, protein carbonylation, and oxidative DNA damage in human urothelial cells.* Mutation Research/Fundamental and Molecular Mechanisms of Mutagenesis, 2007. **615**(1-2): p. 75-86.

226. Rosen, B.P., *Biochemistry of arsenic detoxification.* FEBS letters, 2002. **529**(1): p. 86-92.

227. Gunsolus, I.L., et al., *Influence of nickel manganese cobalt oxide nanoparticle composition on toxicity toward Shewanella oneidensis MR-1: redesigning for reduced biological impact.* Environmental Science: Nano, 2017. **4**(3): p. 636-646.

228. Hang, M.N., et al., *Impact of nanoscale lithium nickel manganese cobalt oxide (NMC) on the bacterium Shewanella oneidensis MR-1.* Chemistry of Materials, 2016. **28**(4): p. 1092-1100.

229. Maurer-Jones, M.A., et al., *Impact of TiO2 nanoparticles on growth, biofilm formation, and flavin secretion in Shewanella oneidensis.* Analytical chemistry, 2013. **85**(12): p. 5810-5818.

230. Qiu, T.A., et al., *Gene expression as an indicator of the molecular response and toxicity in the bacterium Shewanella oneidensis and the water flea Daphnia magna exposed to functionalized gold nanoparticles.* Environmental Science: Nano, 2015. **2**(6): p. 615-629.

231. Qiu, T.A., et al., *A mechanistic study of TiO2 nanoparticle toxicity on Shewanella oneidensis MR-1 with UV-containing simulated solar irradiation: Bacterial growth, riboflavin secretion, and gene expression.* Chemosphere, 2017. **168**: p. 1158-1168.

232. Williams, D.N., et al., *Adverse Interactions of Luminescent Semiconductor Quantum Dots with Liposomes and Shewanella oneidensis.* ACS applied nano materials, 2018. **1**(9): p. 4788-4800.

233. Wu, B., et al., *Bacterial responses to Cu-doped TiO2 nanoparticles.* Science of the total environment, 2010. **408**(7): p. 1755-1758.

234. Wu, B., et al., *Comparative eco-toxicities of nano-ZnO particles under aquatic and aerosol exposure modes.* Environmental Science & Technology, 2010. **44**(4): p. 1484-1489.

235. Wu, B., et al., *Cu-doped TiO2 nanoparticles enhance survival of Shewanella oneidensis MR-1 under Ultraviolet Light (UV) exposure.* Science of the total environment, 2011. **409**(21): p. 4635-4639.

236. Atkinson, S.J., et al., *An octaheme c-type cytochrome from Shewanella oneidensis can reduce nitrite and hydroxylamine.* FEBS letters, 2007. **581**(20): p. 3805-3808.

237. Beliaev, A.S., et al., *Global transcriptome analysis of Shewanella oneidensis MR-1 exposed to different terminal electron acceptors.* Journal of Bacteriology, 2005. **187**(20): p. 7138-7145.

238. Cruz-García, C., et al., *Respiratory nitrate ammonification by Shewanella oneidensis MR-1.* Journal of bacteriology, 2007. **189**(2): p. 656-662.

239. Gralnick, J.A., et al., *Extracellular respiration of dimethyl sulfoxide by Shewanella oneidensis strain MR-1.* Proceedings of the National Academy of Sciences, 2006. **103**(12): p. 4669-4674.

240. Reardon, C.L., et al., *Role of outer-membrane cytochromes MtrC and OmcA in the biomineralization of ferrihydrite by Shewanella oneidensis MR-1.* Geobiology, 2010. **8**(1): p. 56-68.

241. Shirodkar, S., et al., *The octahaem SirA catalyses dissimilatory sulfite reduction in Shewanella oneidensis MR-1.* Environmental microbiology, 2011. **13**(1): p. 108-115.

242. Wang, J., et al., *Biotransformation and biomethylation of arsenic by Shewanella oneidensis MR-1.* Chemosphere, 2016. **145**: p. 329-335.

243. Saltikov, C.W., et al., *The ars detoxification system is advantageous but not required for As (V) respiration by the genetically tractable Shewanella species strain ANA-3.* Appl. Environ. Microbiol., 2003. **69**(5): p. 2800-2809.

244. Saltikov, C.W., R.A. Wildman, and D.K. Newman, *Expression dynamics of arsenic respiration and detoxification in Shewanella sp. strain ANA-3.* Journal of bacteriology, 2005. **187**(21): p. 7390-7396.

245. Noble, R.T. and J.A. Fuhrman, *Use of SYBR Green I for rapid epifluorescence counts of marine viruses and bacteria.* Aquatic Microbial Ecology, 1998. **14**(2): p. 113-118.

246. Bligh, E.G. and W.J. Dyer, *A rapid method of total lipid extraction and purification.* Canadian journal of biochemistry and physiology, 1959. **37**(8): p. 911-917.

247. Sturt, H.F., et al., *Intact polar membrane lipids in prokaryotes and sediments deciphered by high-performance liquid chromatography/electrospray ionization multistage mass spectrometry—new biomarkers for biogeochemistry and microbial ecology.* Rapid Communications in Mass Spectrometry, 2004. **18**(6): p. 617-628.

248. Geiger, O., et al., *Amino acid-containing membrane lipids in bacteria.* Progress in lipid research, 2010. **49**(1): p. 46-60.

249. Kim, Y.H., J.S. Yoo, and M.S. Kim, *Structural characterization of sulfoquinovosyl, monogalactosyl and digalactosyl diacylglycerols by FAB-CID-MS/MS.* Journal of mass spectrometry, 1997. **32**(9): p. 968-977.

250. Elias, D.A., et al., *The influence of cultivation methods on Shewanella oneidensis physiology and proteome expression.* Archives of Microbiology, 2008. **189**(4): p. 313-324.

251. Zhang, P., et al., *Revisiting Fragmentation Reactions of Protonated α-Amino Acids by High-Resolution Electrospray Ionization Tandem Mass Spectrometry with Collision-Induced Dissociation.* Scientific reports, 2019. **9**(1): p. 6453.

252. Mateos, L.M., et al., *Corynebacterium glutamicum as a model bacterium for the bioremediation of arsenic.* International Microbiology, 2006. **9**(3): p. 207-215.

253. Frolova, G.M., et al., *Lipid composition of novel Shewanella species isolated from Far Eastern seas.* Microbiology, 2005. **74**(6): p. 664-669.

254. Moule, A.L. and S.G. Wilkinson, *Polar lipids, fatty acids, and isoprenoid quinones of Alteromonas putrefaciens (Shewanella putrefaciens).* Systematic and applied microbiology, 1987. **9**(3): p. 192-198.

255. Hwang, Y.J., et al., *Shewanella psychromarinicola sp. nov., a psychrophilic bacterium isolated from pelagic sediment of the Ross Sea (Antarctica), and reclassification of Shewanella arctica Kim et al. 2012 as a later heterotypic synonym of Shewanella frigidimarina Bowman et al. 1997.* International journal of systematic and evolutionary microbiology, 2019. **69**(8): p. 2415-2423.

256. Park, H.Y. and C.O. Jeon, *Shewanellaaestuarii sp. nov., a marine bacterium isolated from a tidal flat.* International journal of systematic and evolutionary microbiology, 2013. **63**(12): p. 4683-4690.

257. Hidalgo, F.J., F. Nogales, and R. Zamora, *The role of amino phospholipids in the removal of the cito-and geno-toxic aldehydes produced during lipid oxidation.* Food and chemical toxicology, 2008. **46**(1): p. 43-48.

258. Heller, J.I., et al., *p-Hydroxyphenylacetaldehyde, an aldehyde generated by myeloperoxidase, modifies phospholipid amino groups of low density lipoprotein in human atherosclerotic intima.* Journal of Biological Chemistry, 2000. **275**(14): p. 9957-9962.

259. Sohlenkamp, C. and O. Geiger, *Bacterial membrane lipids: diversity in structures and pathways.* FEMS microbiology reviews, 2016. **40**(1): p. 133-159.

260. Chattopadhyay, M.K., et al., *Increase in oxidative stress at low temperature in an Antarctic bacterium.* Current microbiology, 2011. **62**(2): p. 544-546.

261. Maurer, L.M., et al., *pH regulates genes for flagellar motility, catabolism, and oxidative stress in Escherichia coli K-12.* Journal of bacteriology, 2005. **187**(1): p. 304-319.

262. Russell, N.J., *Adaptive modifications in membranes of halotolerant and halophilic microorganisms.* Journal of Bioenergetics and Biomembranes, 1989. **21**(1): p. 93-113.

263. Woolley, J.F., J. Stanicka, and T.G. Cotter, *Recent advances in reactive oxygen species measurement in biological systems.* Trends in Biochemical Sciences, 2013. **38**(11): p. 556-565.

264. Lu, P. and C. Zhu, *Arsenic Eh–pH diagrams at 25°C and 1 bar.* Environmental Earth Sciences, 2011. **62**(8): p. 1673-1683.

265. Robinson, C., et al. *In Situ Investigations Of Shallow Water Hydrothermal Vent Systems, Palaeochori Bay, Milos, Aegean Sea*. Society of Underwater Technology.

266. Matschullat, J., *Arsenic in the geosphere—a review.* Science of the Total Environment, 2000. **249**(1-3): p. 297-312.

267. Maurer, E.I., et al., *Systematic analysis of silver nanoparticle ionic dissolution by tangential flow filtration: toxicological implications.* Nanotoxicology, 2014. **8**(7): p. 718-727.

268. McAllister, M., *Dynamic Dissolution: A Step Closer to Predictive Dissolution Testing?* Molecular Pharmaceutics, 2010. **7**(5): p. 1374-1387.

Versicherung an Eides Statt / *Affirmation in lieu of an oath* gem. § 5 Abs. 5 der Promotionsordnung vom 18.06.2018 /

according to § 5 (5) of the Doctoral Degree Rules and Regulations of 18 June, 2018

Ich / I, _____
(Vorname / First *Name*, Name / *Name*, Anschrift / *Address*, ggf. Matr.-Nr. / *student ID no., if applicable)*

versichere an Eides Statt durch meine Unterschrift, dass ich die vorliegende Dissertation selbständig und ohne fremde Hilfe angefertigt und alle Stellen, die ich wörtlich dem Sinne nach aus Veröffentlichungen entnommen habe, als solche kenntlich gemacht habe, mich auch keiner anderen als der angegebenen Literatur oder sonstiger Hilfsmittel bedient habe und die zu Prüfungszwecken beigelegte elektronische Version (PDF) der Dissertation mit der abgegebenen gedruckten Version identisch ist. / *With my signature I affirm in lieu of an oath that I prepared the submitted dissertation independently and without illicit assistance from third parties, that I appropriately referenced any text or content from other sources, that I used only literature and resources listed in the dissertation, and that the electronic (PDF) and printed versions of the dissertation are identical.*

Ich versichere an Eides Statt, dass ich die vorgenannten Angaben nach bestem Wissen und Gewissen gemacht habe und dass die Angaben der Wahrheit entsprechen und ich nichts verschwiegen habe*. / I affirm in lieu of an oath that the information provided herein to the best of my knowledge is true and complete.*

Die Strafbarkeit einer falschen eidesstattlichen Versicherung ist mir bekannt, namentlich die Strafandrohung gemäß § 156 StGB bis zu drei Jahren Freiheitsstrafe oder Geldstrafe bei vorsätzlicher Begehung der Tat bzw. gemäß § 161 Abs. 1 StGB bis zu einem Jahr Freiheitsstrafe oder Geldstrafe bei fahrlässiger Begehung. / *I am aware that a false affidavit is a criminal offence which is punishable by law in accordance with § 156 of the German Criminal Code (StGB) with up to three years imprisonment or a fine in case of intention, or in accordance with § 161 (1) of the German Criminal Code with up to one year imprisonment or a fine in case of negligence.*

_____ _____

Ort / *Place*, Datum / *Date* Unterschrift / *Signature*